# Supporting Information

## Bimetallic PdCu–$Fe_3O_4$ catalyst with optimal *d*-band centre for selective *N*-methylation of aromatic amine with methanol

*Jin Hee Cho,[a] Yoonhoo Ha,[b] Ahra Cho,[a] Jihye Park,[b] Jaeyoon Choi, [a]*

*Youngdae Won [c] Hyungjun Kim,[b]* and Byeong Moon Kim[a]**

[a]Department of Chemistry, College of Natural Sciences, Seoul National University,

1 Gwanak-ro, Gwanak-gu, Seoul 08826, Republic of Korea

[b]Department of Chemistry, Korea Advanced Institute of Science and Technology (KAIST),

Daejeon 34141, Republic of Korea

[c]The Research Institute of Basic Sciences, Seoul National University, 1 Gwanak-ro,

Gwanak-gu, Seoul, 08826, Republic of Korea

Corresponding author's email address
Byeong Moon Kim: kimbm@snu.ac.kr
Hyungjun Kim: linus16@kaist.ac.kr

## Table of Contents page

# 1. Materials/Instrumentation

**Materials**

All commercially available chemicals were used as received without further purification. Palladium chloride (99% purity) and copper(II) chloride dihydrate (99.0% purity) were purchased from Alfa-Aesar. Polyvinylpyrrolidone (PVP, Mw~10,000) was purchased from Sigma-Aldrich. Iron oxide nanoparticle ($Fe_3O_4$ NP) was purchased from Beijing-DK-nano-technology.

**ESCA (Electron Spectroscopy for Chemical Analysis)**

1. Model: Axis Supra™ (Kratos, U.K.)
2. Vacuum System
   (1) The sample analysis chamber is a multiport ultra-high vacuum chamber of mu-metal construction.
   (2) Bakeout : 24hour~7day timer with thermostatically controlled, no need remove any cables and cameras before baking.
   (3) Pumping kit
   - The sample analysis chamber : TMP, TSP
     ( Base pressure in the analysis chamber is < 5x10 –10 torr )
   - The load lock chamber : TMP, oil free dry scroll pump.
     ( Base pressure in the analysis chamber is < 5x10-8 torr )

3. Electron energy analyser
   (1) 165mm mean radius concentric hemispherical analyser for spectroscopy and a spherical mirror analyser for imaging.
   (2) 128 channel delay line detector (DLD) be used for both spectroscopy and parallel imaging modes.
   (3) In spectroscopy mode should have greater than 100 discrete data channels improving the sensitivity in spectroscopy mode.
   (4) X-ray photoelectron spectroscopy
   - Ultimate energy resolution : ≤ 0.48eV($Ag3d_{5/2}$ peak)
   (5) X-ray photoelectron imaging
   - Lateral resolution of the parallel imaging : ≤1 ㎛
4. Automated monochromatic X-ray source
   (1) 500 mm Rowland circle geometry, controlled by data system.
   (2) Auto arrangement provides easy control, optimisation and calibration of the mirror position and ensures that the X-ray illuminated area is correctly aligned with the analysis position.

**Transmission Electron Microscope II (ccd camera type)**

1. Model: JEM 3010 (JEOL, JAPAN)
2. Specification
   a. EDS (INCA, Oxford)
   b. GATAN UltraScan CCD Camara
   c. Accelerating Voltage: 300 kV
   d. Vacuum System: 10-5 pa order (specimen chamber)
   e. Resolution: Point image: 0.17 nm Lattice image: 0.14 nm

**Cs-TEM (Cs corrected TEM with Cold FEG)**

1. Model: JEM-ARM200F (Cold Field Emission Type)
2. Specifications:
   a. HT: 60, 80, 120, 200 kV
   b. Magnification: 50 to 2,000,000 X (TEM), 200 to 1,500,000 X (STEM)
   c. Resolution
      - TEM mode: Lattice 0.07 nm/ Point 0.11 nm - STEM mode: 0.136 nm
   d. Sample tilting
      - X / Y: ± 25° / ± 25°
3. Analysis functions:
   a. CCD Camera: UltraScan 1000XP (2,048 x 2,048 pixel) b. EDS: SDD Type (Active area 1 00 $mm^2$/ Solid angle 0.7 str)

**Cs-STEM (Cs corrected STEM with Cold FEG)**

1. Model: JEM-ARM200F (Cold Field Emission Type, JEOL)
2. Specifications
   a. HT: 60, 80, 120, 200 kV
   b. Magnification: 50 to 2,000,000 X (TEM), 200 to 1,500,000 X (STEM)
   c. Resolution - STEM mode: HAADF 0.1 nm/ BF 0.136 nm - TEM mode: Point 0.23 nm
   d. Sample tilting - X / Y: ±35° / ±30°

3. Analysis functions
   a. CCD Camera: UltraScan 1000XP (2,048 x 2,048 pixel)
   b. EDS: SDD Type (Active area 100 $mm^2$/ Solid angle 0.9 str)
   c. EELS: Model 965 GIF Quantum ER

**FE-SEM (Field Emission Scanning Electron Microscope)**

1. Model: JSM-7600F (FE-SEM)
2. Specification
   a. Resolution: 1) 1.0 nm at 15 kV 2) 1.5 nm at 1 kV
   b. Voltage range: 0.1 ~ 30 kV
   c. Maximum image size: 5,120 x 3,840 pixels
   d. Probe current: 1pA ~ 200 nA
   e. Tilt: -5 ~ 70°
   f. Rotation: 360°
   g. Working Distance: 1.5 ~ 25 mm

* PdCu–$Fe_3O_4$ samples were analyzed on Cs-STEM (Cs corrected STEM with Cold FEG), Cs-TEM (Cs corrected TEM with Cold FEG) and High resolution Transmission Electron Microscope (ccd camera type), and ESCA installed at the National Center for Inter-university Research Facilities (NCIRF) at Seoul National University.

*SEM images of PdCu–$Fe_3O_4$ were obtained with a JSM7600F at a voltage of 15 kV installed at Seoul National University Research Institute of Advanced Materials.

**XRD (Powder X-Ray Diffractometry)**

1. Model: D8 ADVANCE with DAVINCI (BRUKER, German)2.
2. Specification
   a. Detector: LYNXEYE XE
   b. Generator: 40 kV, 40 mA
   c. 2 theta range: 5-100 degree
   d. Step: 0.02
   f. Scanspeed: 0.5 sec/step
   g. Savelength(λ): Cu kα1 - 1.541

*XRD data of PdCu–$Fe_3O_4$ were obtained from institution The National Instrumentation Center for Environmental Management(NICEM) at Seoul National University.

## 2. Experimental Details

**Synthesis of $Pd_1Cu_{0.6}$–$Fe_3O_4$ NPs**

Palladium chloride ($PdCl_2$, 0.102 g) and polyvinylpyrrolidone (PVP, Mw ~10,000, 1.20 g) were placed in 12.0 mL ethylene glycol (EG) in a 50.0 mL round-bottom flask. The mixture was sonicated for 10 min and heated for 1 h at 100 °C. Simultaneously, copper(II) chloride dihydrate ($CuCl_2$•$2H_2O$, 0.074 g) and PVP (Mw ~10,000, 0.460 g) were dissolved in 9.00 mL water in a 50.0 mL round-bottom flask. This copper mixture was sonicated for 10 min and heated for 30 min at 70 °C in an oil bath. Meanwhile, 0.300 g of $Fe_3O_4$ NPs (100 nm, DK nano) was placed in 80.0 mL of EG. The heated palladium mixture was firstly added dropwise to $Fe_3O_4$ NP solution via a syringe pump. Next, the heated copper precursor was secondly added dropwise. Lastly, an aqueous sodium borohydride ($NaBH_4$, 0.030g) solution in water (6.00 mL) was added dropwise twice to the resulting mixture using syringe pump. The mixture was stirred for 3 h at 100 °C. The nanoparticles were than washed with ethanol. $Pd_1Cu_{0.6}$–$Fe_3O_4$NPs (0.310 g) was obtained from drying in a rotary evaporator for 20 min at 50 °C.

**Synthesis of $Pd_xCu_y$–$Fe_3O_4$ NPs**

$Pd_xCu_y$–$Fe_3O_4$NPs were prepared using the same method as that of $Pd_1Cu_{0.6}$–$Fe_3O_4$NPs but with different Pd and Cu quantities. In common, $Fe_3O_4$ NPs (0.100 g) with EG (30.0 mL) and sodium borohydride (0.020 g) in water (4.00 mL) were used. The precursor quantities in each composition were as follows: (1) $Pd_1Cu_{0.3}$–$Fe_3O_4$ NPs: $PdCl_2$ (0.034 g), PVP (0.400 g), and EG (4.00 mL) for the Pd precursor and $CuCl_2$•$2H_2O$ (0.012 g), PVP (0.076 g) and water (1.50 mL) for the Cu precursor. (2) $Pd_1Cu_1$–$Fe_3O_4$ NPs: $PdCl_2$ (0.017 g), PVP (0.200 g) and EG (2.00 mL) for the Pd precursor and $CuCl_2$•$2H_2O$ (0.020 g), PVP (0.130 g) and water (2.60 mL) for the Cu precursor. (3) $Pd_{0.5}Cu_1$–$Fe_3O_4$ NPs: $PdCl_2$ (0.010 g), PVP (0.120 g), and EG (1.20 mL) for the Pd precursor, and $CuCl_2$•$2H_2O$ (0.033 g), PVP (0.200 g) and water (4.00 mL) for the Cu precursor. (4) $Pd_{0.2}Cu_1$–$Fe_3O_4$ NPs: $PdCl_2$ (0.008 g), PVP (0.100 g), and EG (1.00 mL) for the Pd precursor and $CuCl_2$•$2H_2O$ (0.041g), PVP (0.245 g) and water (4.00 mL) for the Cu precursor.

**Synthesis of Pd–$Fe_3O_4$ NPs**

$PdCl_2$ (0.102 g) and PVP (1.20 g) in ethylene glycol (26.0 mL) were placed in a 100 mL round-bottom flask. The mixture was sonicated until complete dissolution and then stirred at 100 °C for 1 h. $Fe_3O_4$ support was prepared by mixing. The Pd precursor solution was then added dropwise to $Fe_3O_4$ (0.300 g) in EG (90.0 mL) in a 250 mL round-bottom flask via a syringe pump. The solution was stirred at 110 °C for 23 h and the resulting Pd–$Fe_3O_4$ were washed as in the preparation of PdCu–$Fe_3O_4$ NPs. After drying, 0.280 g of Pd–$Fe_3O_4$ NPs were obtained.

**Synthesis of Cu–$Fe_3O_4$ NPs**

$CuCl_2$•$2H_2O$ (0.025 g) and PVP (0.150 g) in deionized water (3.00 mL) were placed in 50.0 mL round-bottom flask. This copper precursor was sonicated for 5 min. The mixture was stirred at 70 °C for 30 min. The copper mixture was then added dropwise to an aqueous $Fe_3O_4$ (0.100g) solution in 30.0 mL water. After the addition is complete, an aqueous sodium borohydride ($NaBH_4$, 0.020 g) solution in water (4.00 mL) was added dropwise to the resulting solution via a syringe pump. The resulting Cu–$Fe_3O_4$ nanoparticle was washed in the same way as in the preparation of PdCu–$Fe_3O_4$ NPs. Lastly, Cu–$Fe_3O_4$ NPs (0.090 g) was obtained.

**Synthesis of PdCu NPs on different supports**

Bimetallic PdCu on $TiO_2$, $CeO_2$ and $Al_2O_3$ were prepared following the same procedure as used for the PdCu–$Fe_3O_4$ synthesis, with each oxide as a replacement of $Fe_3O_4$. Each 0.100 g of titanium(IV) oxide (nanopowder, <100 nm particle size), cerium(IV) oxide (nanopowder, <50 nm particle size), and aluminum oxide (nanopowder, <50 nm particle size) was placed in EG (30 mL). $PdCl_2$ (0.034 g), PVP(0.400 g), and EG (4.00 mL) were used to prepare the Pd precursor, and $CuCl_2$•$2H_2O$ (0.025 g), PVP (0.015 g), and water (3.00 mL) were used for the Cu precursor. Sodium borohydride (0.020 g) of and water (4.00 mL) were used as reductants.

**A general procedure for *N*-methylation of amine using methanol**

$Pd_1Cu_{0.6}$–$Fe_3O_4$NPs (5 mol% catalyst based on Pd), amine (0.500 mmol), $K_2CO_3$ (0.500 mmol, 0.069 g), and methanol (5.00 mL) were placed in a 35.0 mL pressured tube. The mixture was then stirred at 140 °C in an oil bath. After cooling to room temperature, the catalyst was separated using an external magnet. Subsequently, the solvent was removed using a rotary evaporator and the residue was purified by column chromatography to furnish the desired amine. The product was analyzed by GC and NMR spectroscopy.

**Deuterium labeling test**

Reactions using $CH_3OH$, $CD_3OD$ and $CH_3OD$ for the *N*-methylation were explored under the same conditions following the general procedure. The resulting products were confirmed by $^1H$ NMR and GC.

**Procedure for gram-scale synthesis**

$Pd_1Cu_{0.6}$–$Fe_3O_4$NPs (5 mol% catalyst based on Pd), aniline (10.0 mmol), $K_2CO_3$ (10.0 mmol) and methanol (50.0 mL) were placed in a 500 mL round-bottom pressure flask with a magnetic stirrer bar. The mixture was sonicated for 1 min. The reaction was stirred for 24 h at 140 °C in an oil bath. After completion of reaction, the catalyst was separated by an external magnet. Methanol was removed with a rotary evaporator. The crude product was then purified using column chromatography over silica gel to furnish the *N*-methyl aniline in 0.916 g (85% yield)

## 3. Catalyst Characterization

| Catalyst | Pd (wt%) | Cu (wt%) | Metal ratio of Pd:Cu |
|---|---|---|---|
| $Pd–Fe_3O_4$ | **8.80** | **-** | **-** |
| $Pd_1Cu_{0.3}–Fe_3O_4$ | **8.89** | **1.58** | 1.00 : 0.29 |
| $Pd_1Cu_{0.6}–Fe_3O_4$ | **8.37** | **3.02** | 1:00 : 0.60 |
| $Pd_1Cu_1–Fe_3O_4$ | **4.94** | **3.21** | 1.00 : 1.08 |
| $Pd_{0.5}Cu_1–Fe_3O_4$ | **3.39** | **4.24** | 0.47 : 1.00 |
| $Pd_{0.2}Cu_1–Fe_3O_4$ | **3.17** | **8.78** | 0.21 : 1.00 |
| $Cu–Fe_3O_4$ | **-** | **7.07** | - |

**Figure S1.** ICP-AES data of $Pd_xCu_y–Fe_3O_4$ NPs.

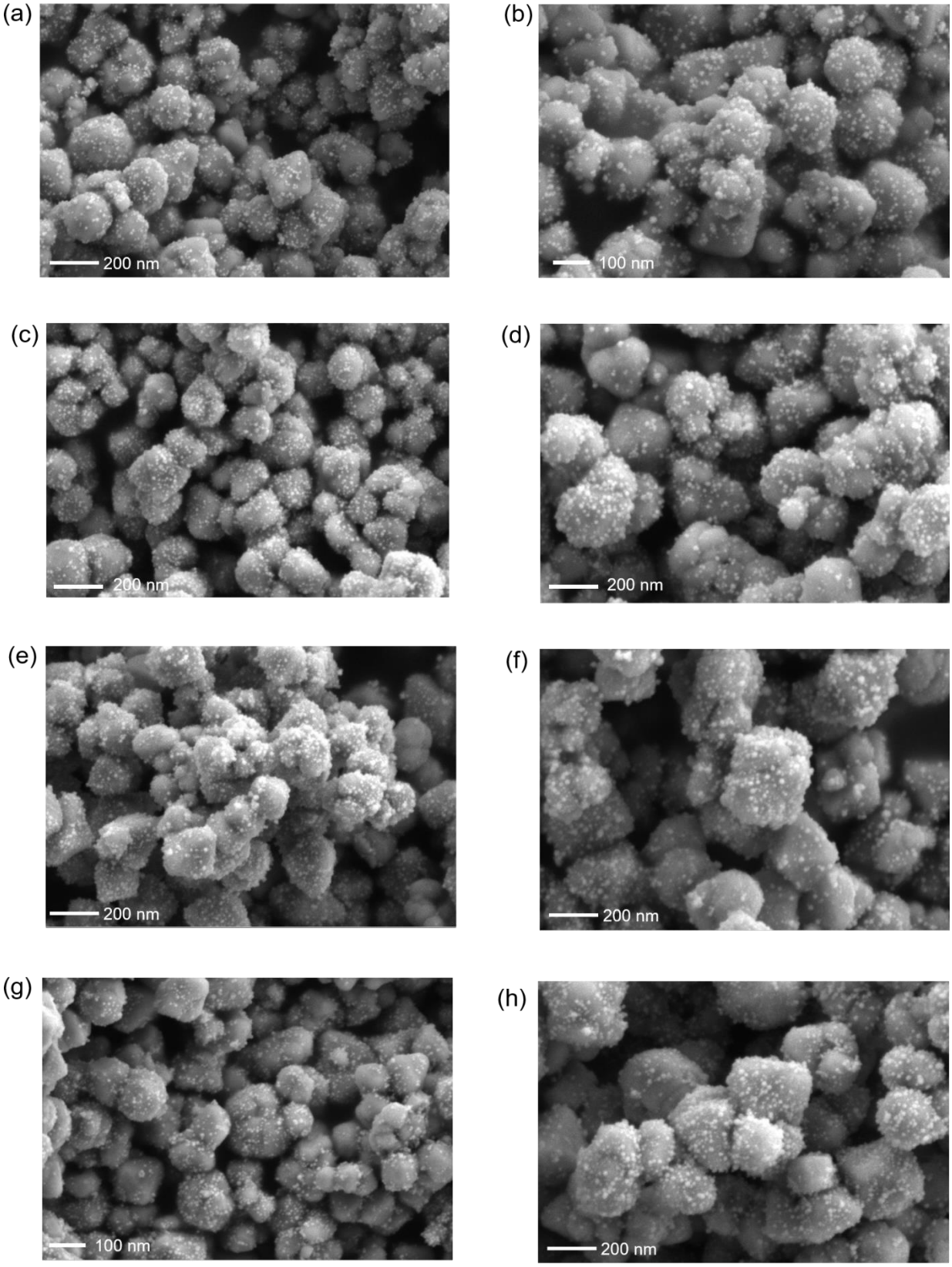
(a)
200 nm
(b)
100 nm
(c)
200 nm
(d)
200 nm
(e)
200 nm
(f)
200 nm
(g)
100 nm
(h)
200 nm

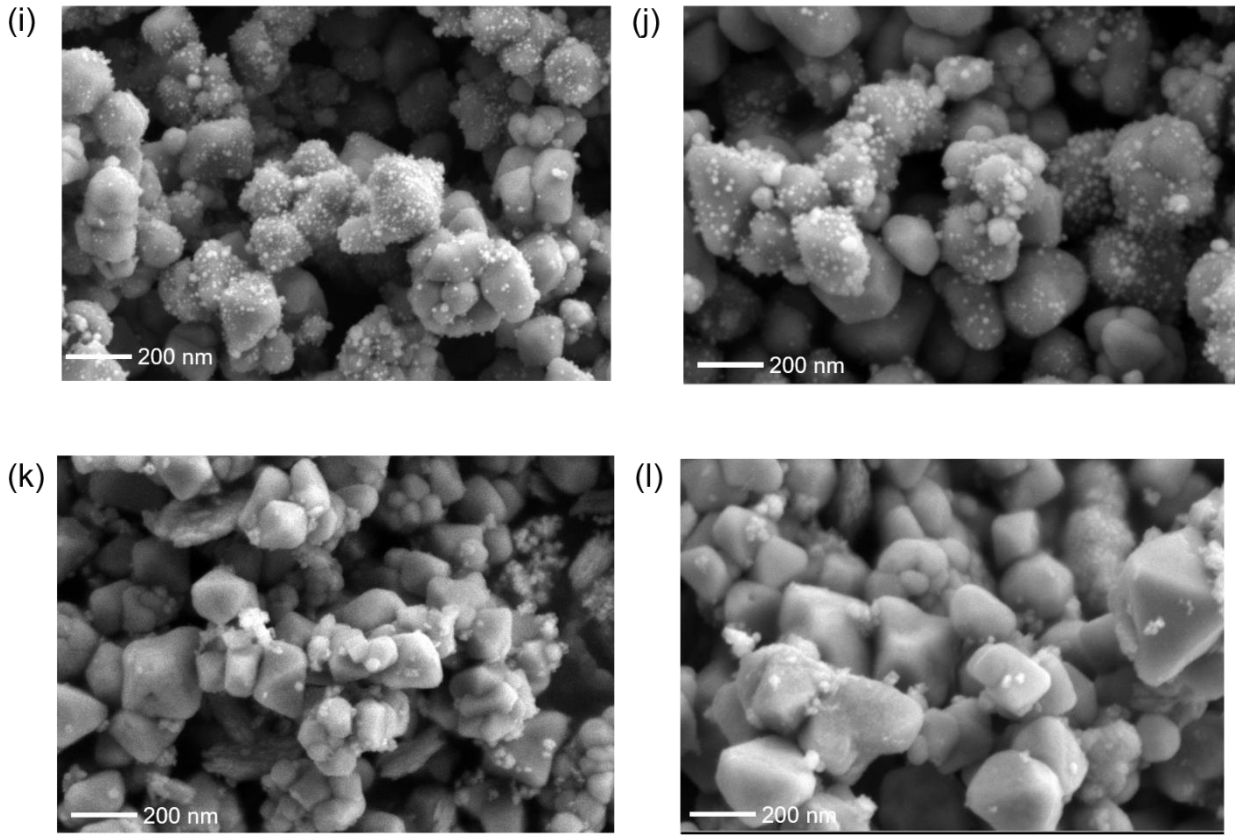


**Figure S2.** FE-SEM images of (a) and (b) Pd–$Fe_3O_4$ NPs; (c) and (d) $Pd_1Cu_{0.3}$–$Fe_3O_4$ NPs; (e) and (f) $Pd_1Cu_1$–$Fe_3O_4$ NPs; (g) and (h) $Pd_{0.5}Cu_1$–$Fe_3O_4$ NPs; (i) and (j) $Pd_{0.2}Cu_1$–$Fe_3O_4$ NPs; (k) and (l) Cu–$Fe_3O_4$ NPs.

(a)

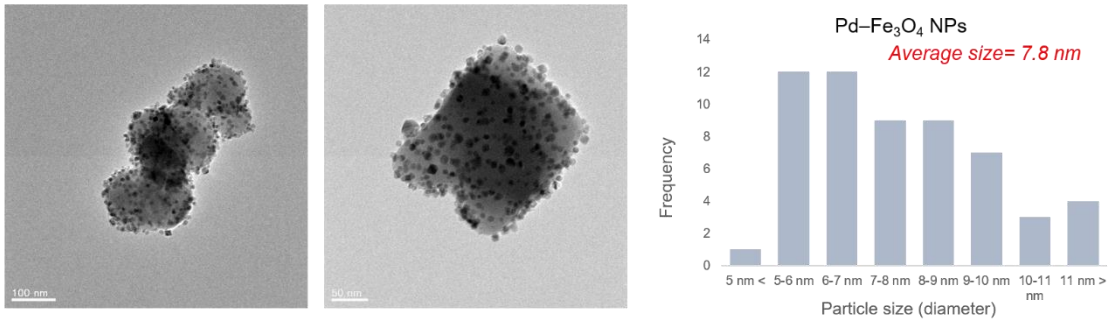
100 nm
50 nm
Pd–Fe3O4 NPs
Average size= 7.8 nm
Frequency
0
2
4
6
8
10
12
14
5 nm <
5-6 nm
6-7 nm
7-8 nm
8-9 nm
9-10 nm
10-11 nm
11 nm >
Particle size (diameter)

(b)

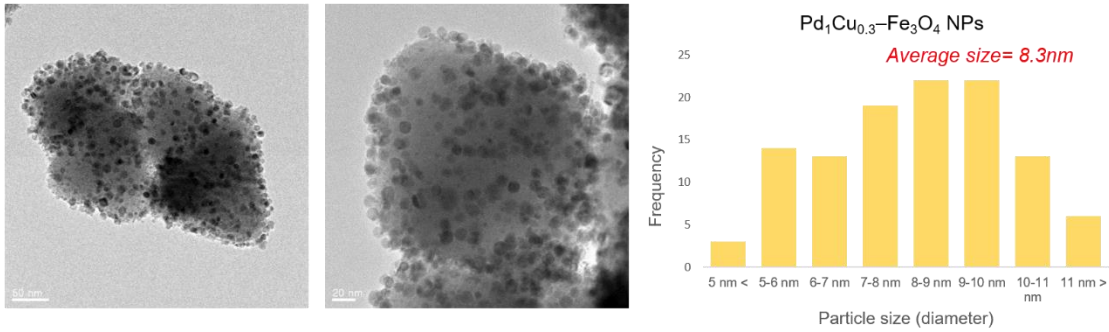
50 nm
20 nm
Pd1Cu0.3–Fe3O4 NPs
Average size= 8.3nm
Frequency
0
5
10
15
20
25
5 nm <
5-6 nm
6-7 nm
7-8 nm
8-9 nm
9-10 nm
10-11 nm
11 nm >
Particle size (diameter)

(c)

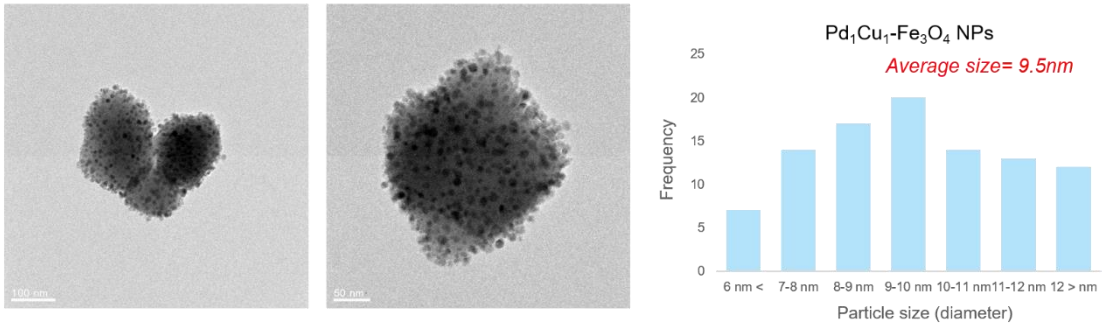
100 nm
50 nm
Pd1Cu1-Fe3O4 NPs
Average size= 9.5nm
Frequency
0
5
10
15
20
25
6 nm <
7-8 nm
8-9 nm
9-10 nm
10-11 nm
11-12 nm
12 > nm
Particle size (diameter)

(d)

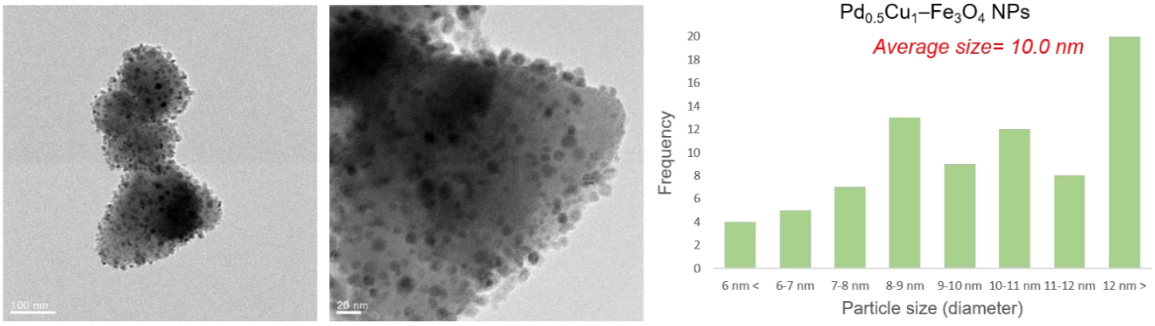
100 nm
20 nm
Pd0.5Cu1–Fe3O4 NPs
Average size= 10.0 nm
Frequency
0
2
4
6
8
10
12
14
16
18
20
6 nm <
6-7 nm
7-8 nm
8-9 nm
9-10 nm
10-11 nm
11-12 nm
12 nm >
Particle size (diameter)

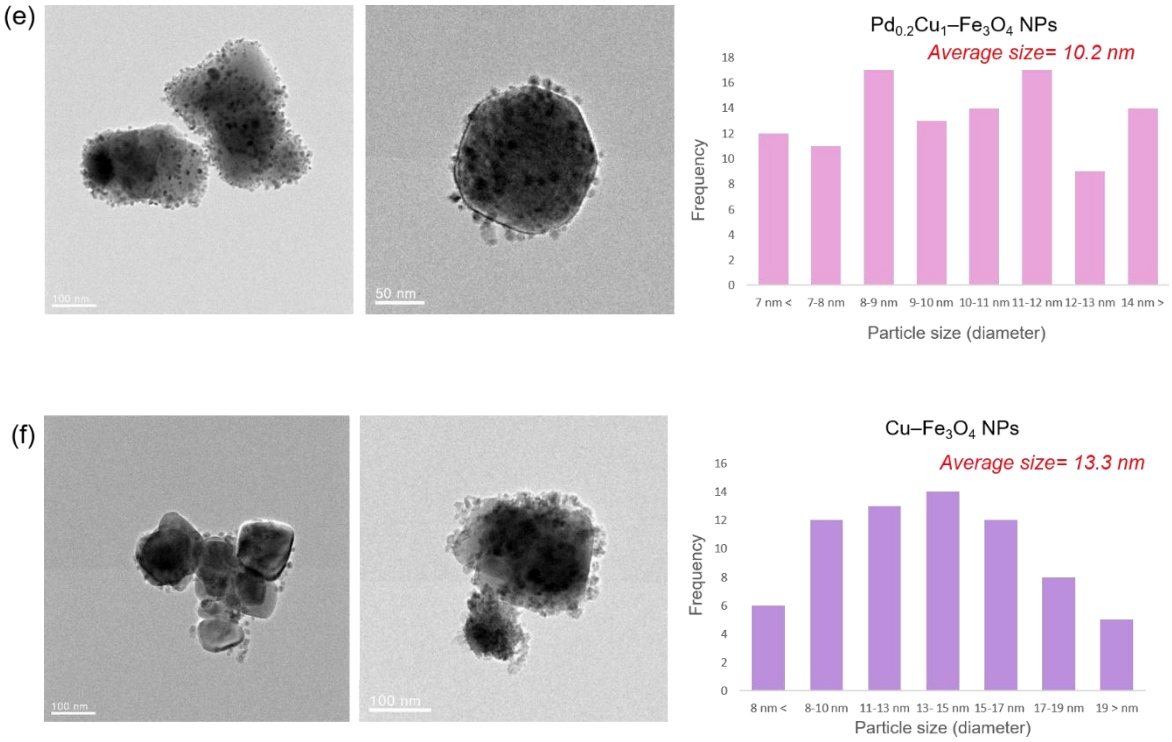


**Figure S3.** HR-TEM images and the particle size distributions of (a) Pd–$Fe_3O_4$ NPs; (b) $Pd_1Cu_{0.3}$–$Fe_3O_4$ NPs; (c) $Pd_1Cu_1$–$Fe_3O_4$ NPs; (d) $Pd_{0.5}Cu_1$–$Fe_3O_4$ NPs; (e) $Pd_{0.2}Cu_1$–$Fe_3O_4$ NPs; (f) Cu–$Fe_3O_4$ NPs.

| Catalyst (on $Fe_3O_4$) | Average particle size | Volume mean diameter ($D_{43}$) |
|---|---|---|
| Pd | 7.8 nm | 9.7 nm |
| $Pd_1Cu_{0.3}$ | 8.3 nm | 9.8 nm |
| $Pd_1Cu_{0.6}$ | 8.9 nm | 10.2 nm |
| $Pd_1Cu_1$ | 9.5 nm | 10.7 nm |
| $Pd_{0.5}Cu_1$ | 10.0 nm | 11.7 nm |
| $Pd_{0.2}Cu_1$ | 10.2 nm | 17.0 nm |
| Cu | 13.3 nm | 21.8 nm |

**Figure S4.** Average particle distribution of $Pd_xCu_y$–$Fe_3O_4$ NPs.

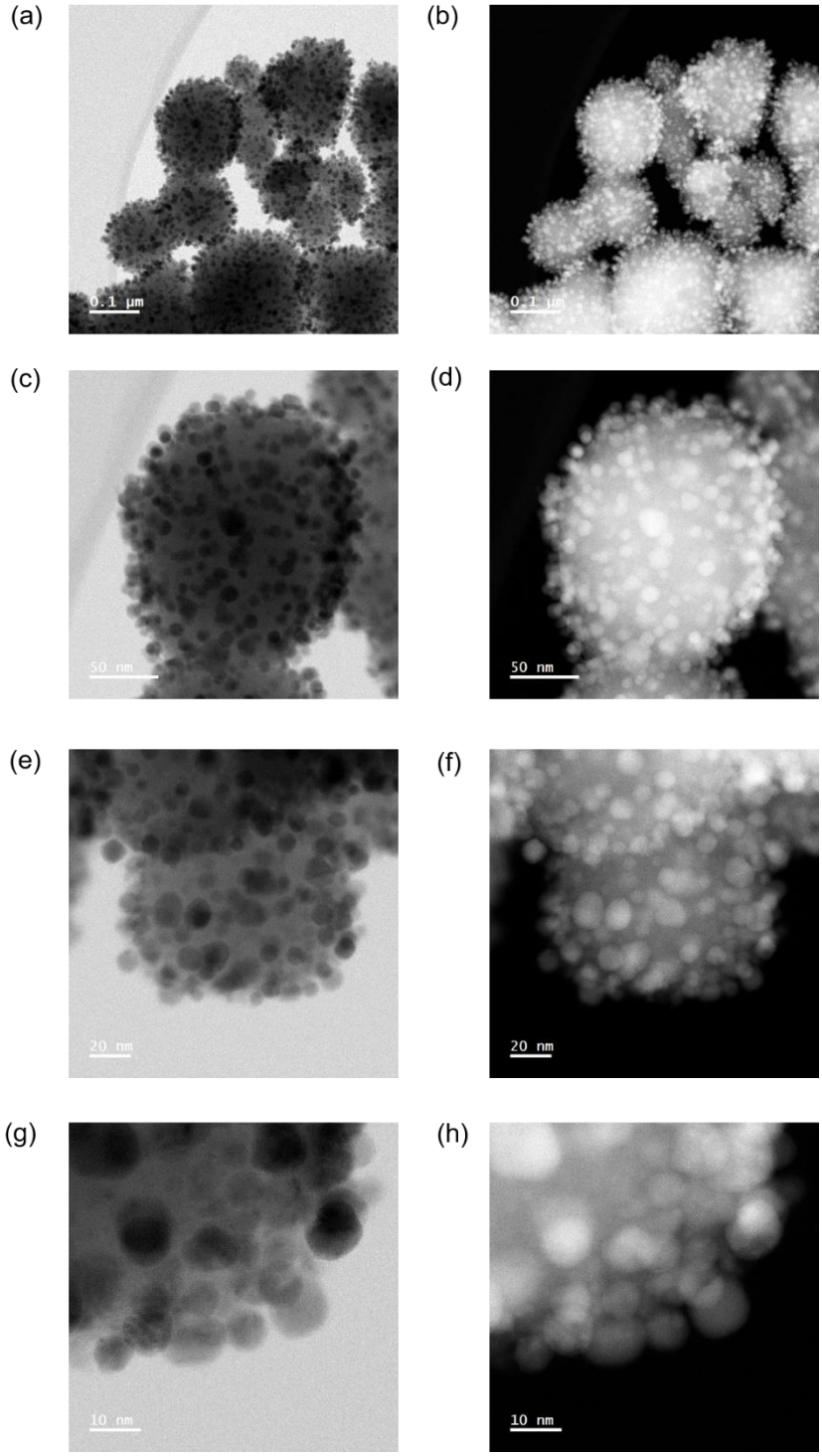


**Figure S5**. (a), (c), (e), and (g) HADDF-STEM images of $Pd_1Cu_{0.6}$–$Fe_3O_4$ NPs; (b), (d), (e), and (h) BF-STEM images of $Pd_1Cu_{0.6}$–$Fe_3O_4$ NPs.

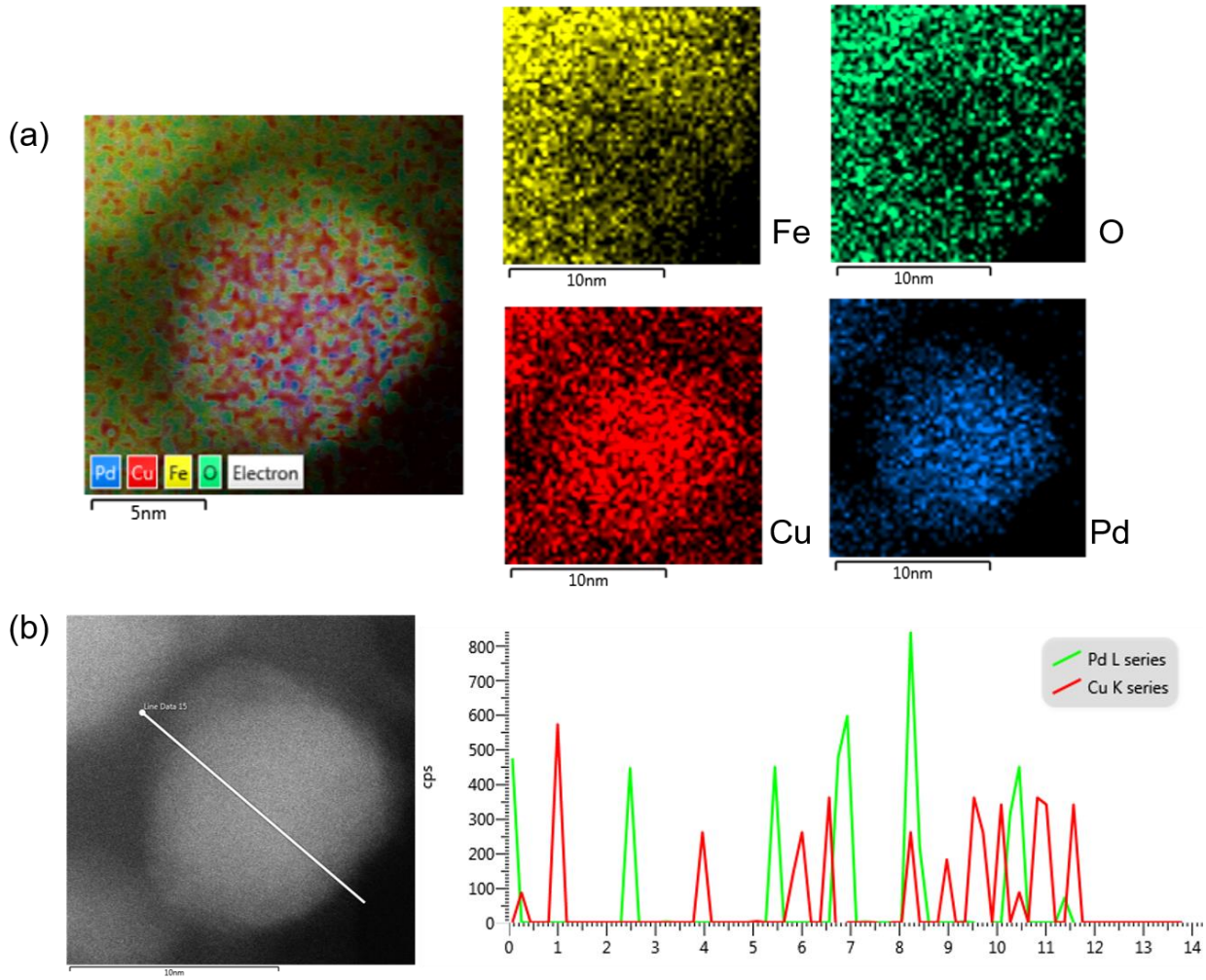


**Figure S6**. EDS and line scanning of $Pd_1Cu_{0.6}$–$Fe_3O_4$ NPs; (a) EDS images, (b) line scanning spectrum.

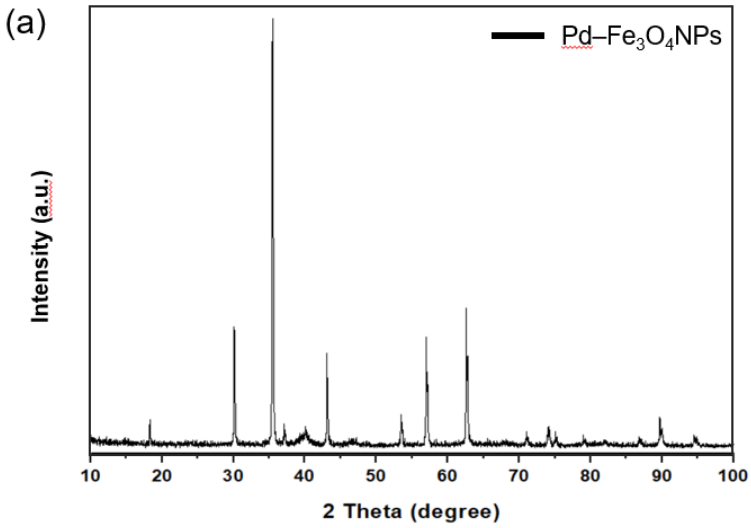
(a)
Pd–Fe3O4NPs
Intensity (a.u.)
10
20
30
40
50
60
70
80
90
100
2 Theta (degree)

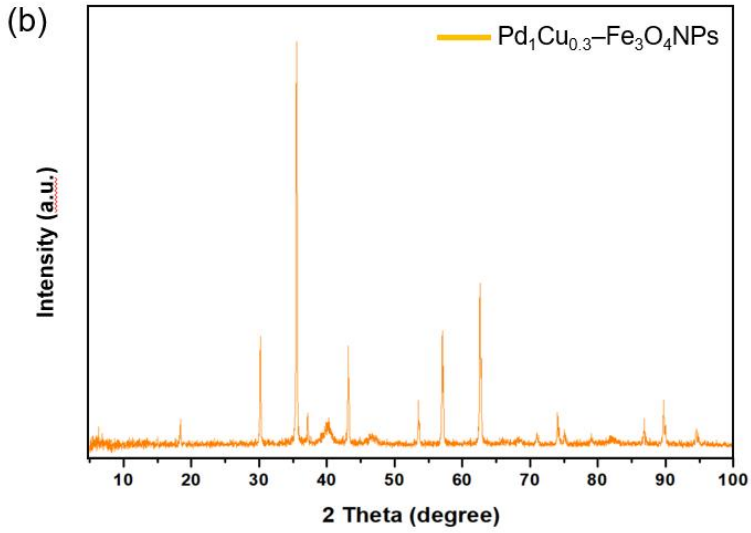
(b)
Pd1Cu0.3–Fe3O4NPs
Intensity (a.u.)
10
20
30
40
50
60
70
80
90
100
2 Theta (degree)

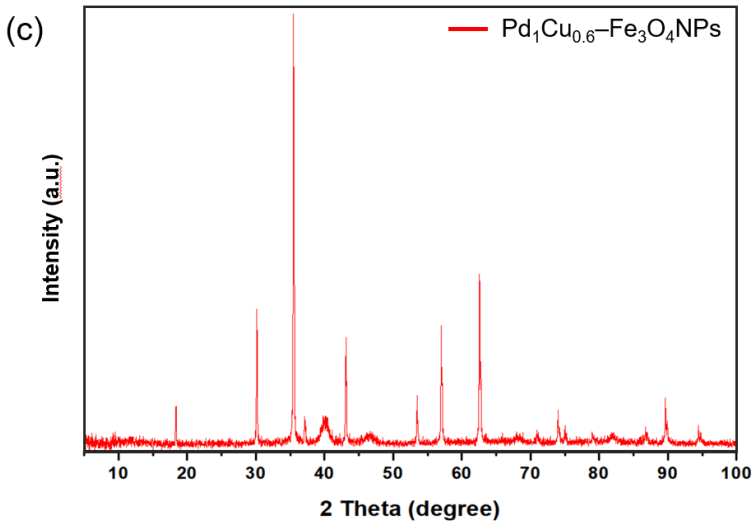
(c)
Pd1Cu0.6–Fe3O4NPs
Intensity (a.u.)
10
20
30
40
50
60
70
80
90
100
2 Theta (degree)

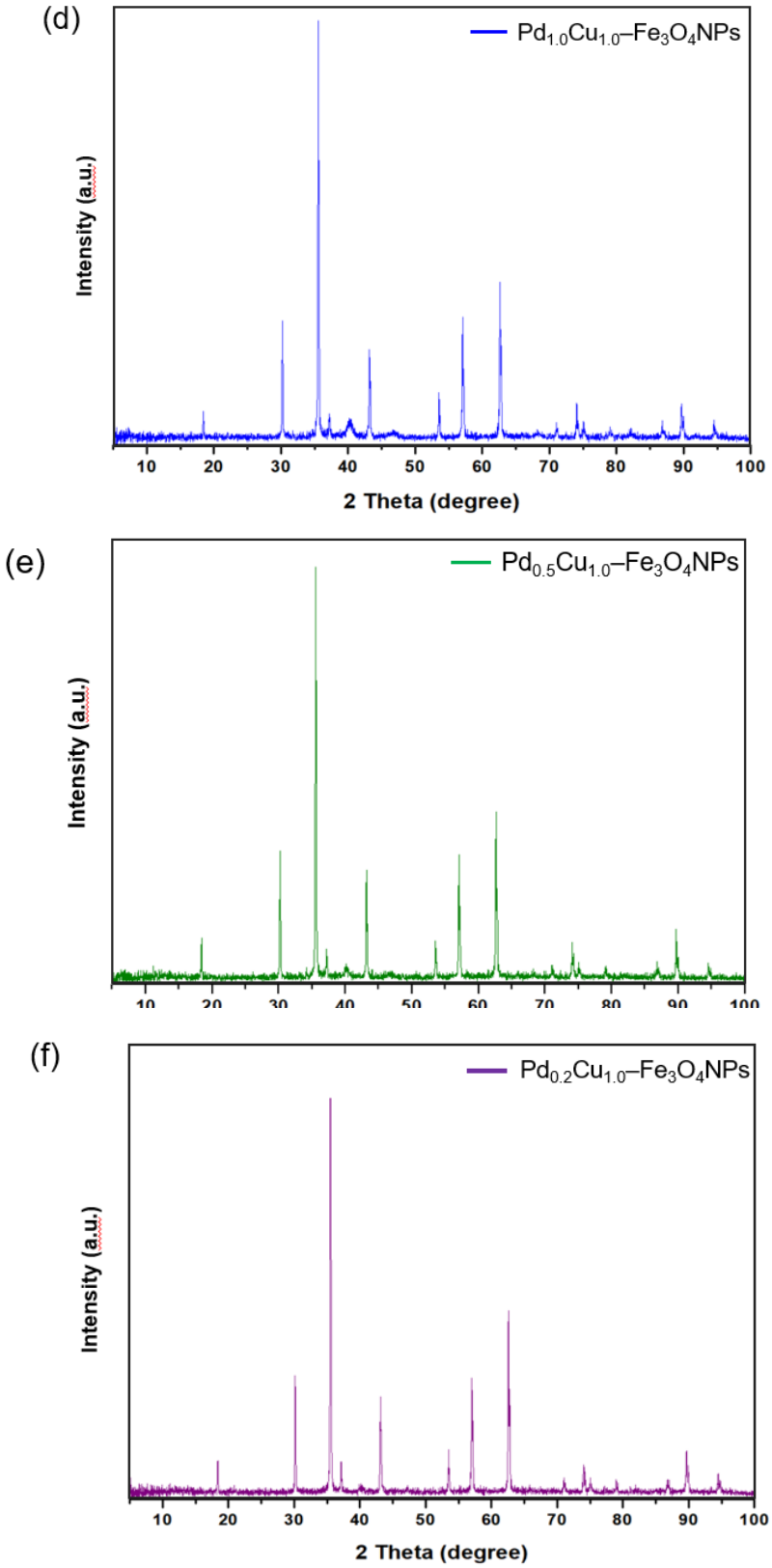
(d)
Pd1.0Cu1.0–Fe3O4NPs
Intensity (a.u.)
10 20 30 40 50 60 70 80 90 100
2 Theta (degree)
(e)
Pd0.5Cu1.0–Fe3O4NPs
Intensity (a.u.)
(f)
Pd0.2Cu1.0–Fe3O4NPs
Intensity (a.u.)
10 20 30 40 50 60 70 80 90 100
2 Theta (degree)

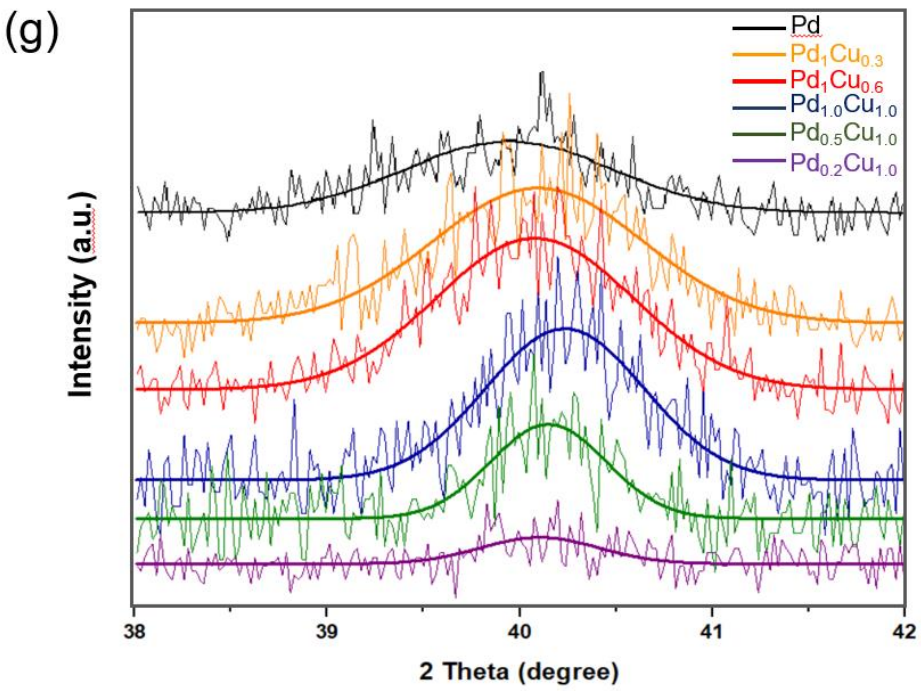


**Figure S7**. XRD patterns of (a) Pd–$Fe_3O_4$ NPs; (b) $Pd_1Cu_{0.3}$–$Fe_3O_4$ NPs; (c) $Pd_1Cu_{0.6}$–$Fe_3O_4$ NPs; (d) $Pd_1Cu_1$–$Fe_3O_4$ NPs; (e) $Pd_{0.5}Cu_1$–$Fe_3O_4$ NPs; (f) $Pd_{0.2}Cu_1$–$Fe_3O_4$ NPs; (g) the diffraction peaks of Pd (111) plane and $Pd_xCu_y$ (111) plane NPs on $Fe_3O_4$.

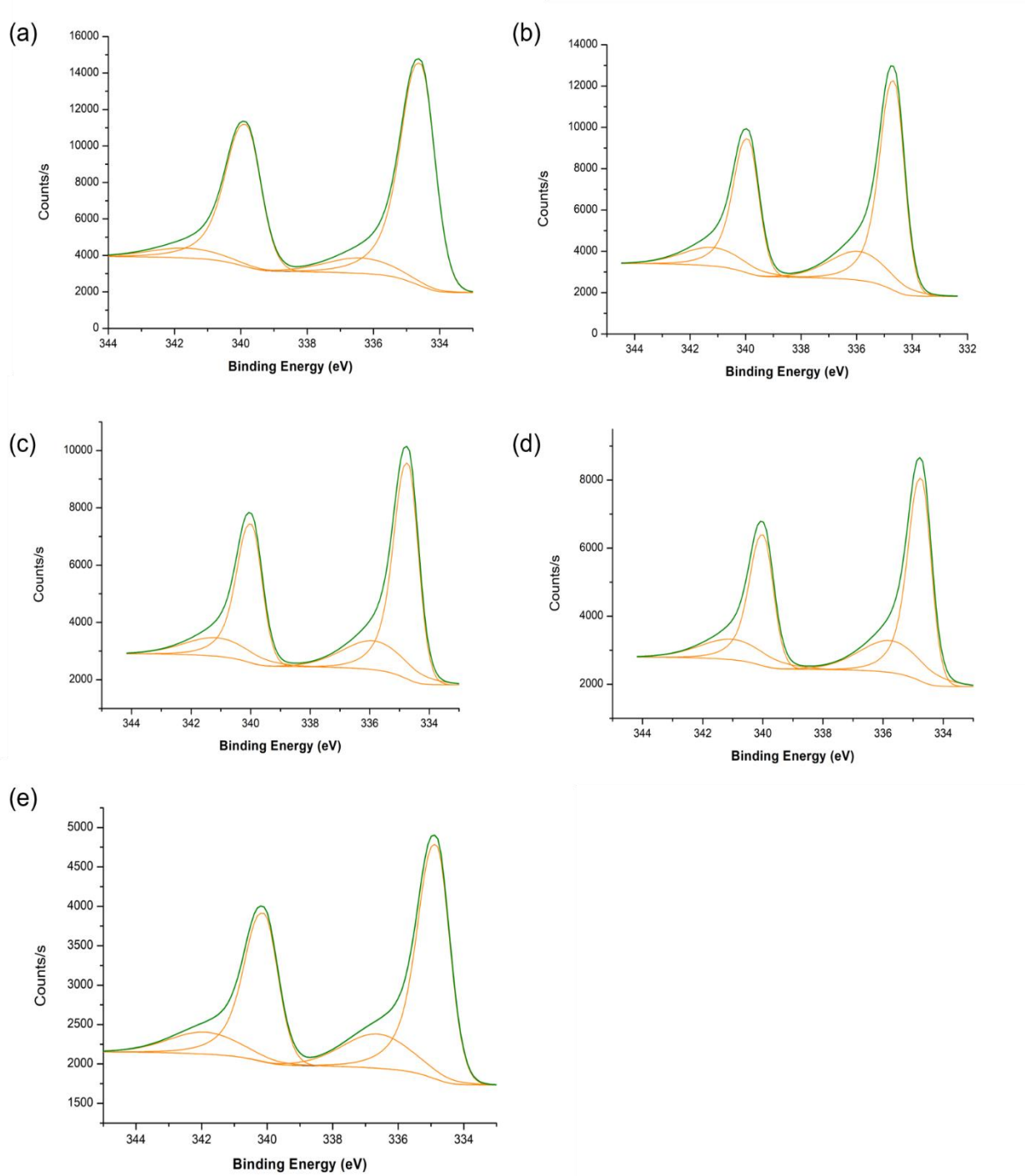


**Figure S8.** Pd 3d XPS spectra of (a) Pd–$Fe_3O_4$ NPs; (b) $Pd_1Cu_{0.3}$–$Fe_3O_4$ NPs; (c) $Pd_1Cu_1$–$Fe_3O_4$ NPs; (d) $Pd_{0.5}Cu_1$–$Fe_3O_4$ NPs; (e) $Pd_{0.2}Cu_1$–$Fe_3O_4$ NPs.

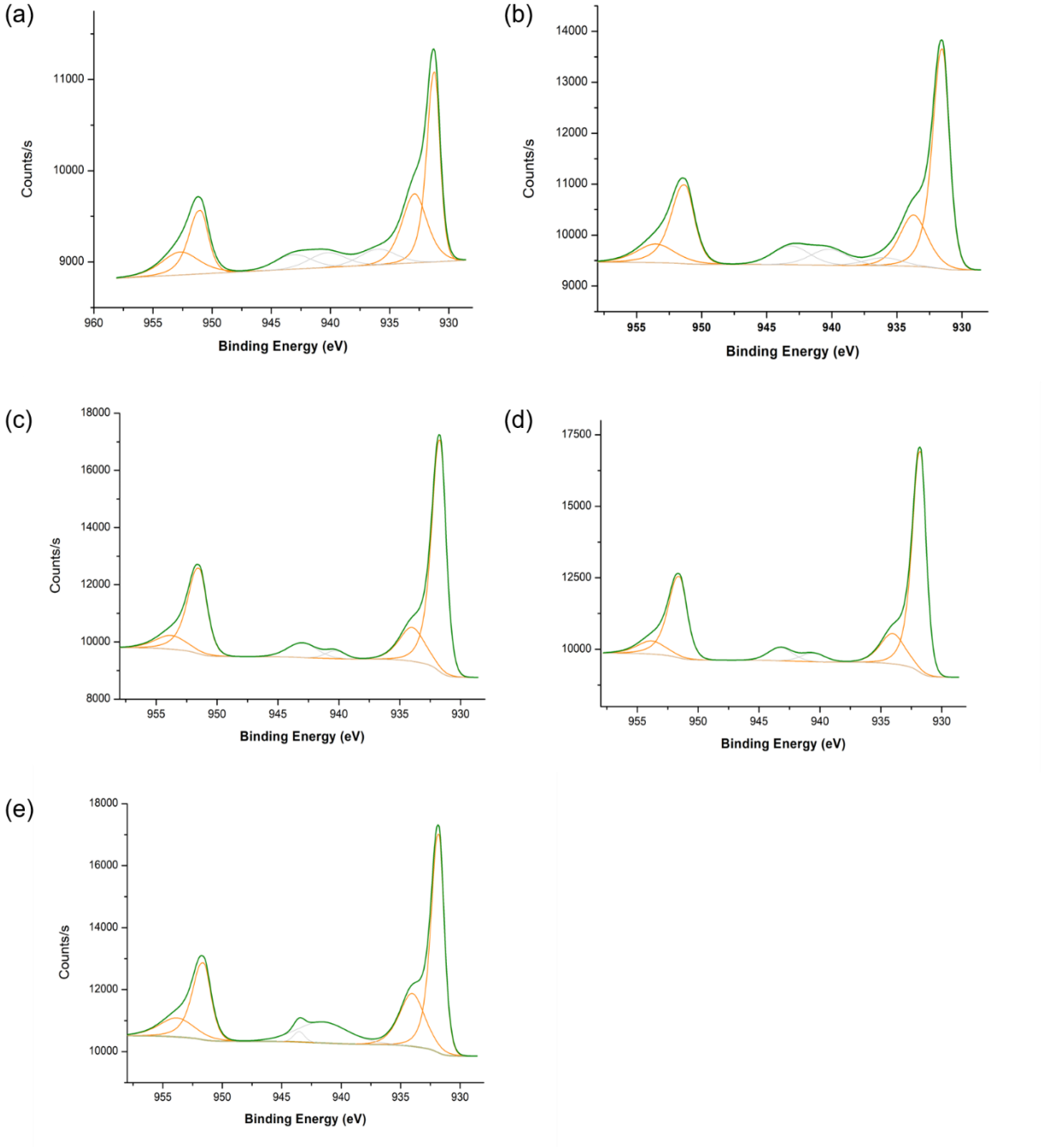


**Figure S9**. Cu 2p XPS spectra of (a) $Pd_1Cu_{0.3}$–$Fe_3O_4$ NPs; (b) $Pd_1Cu_1$–$Fe_3O_4$ NPs; (c) $Pd_{0.5}Cu_1$–$Fe_3O_4$ NPs; (d) $Pd_{0.2}Cu_1$–$Fe_3O_4$ NPs; (e) Cu–$Fe_3O_4$ NPs.

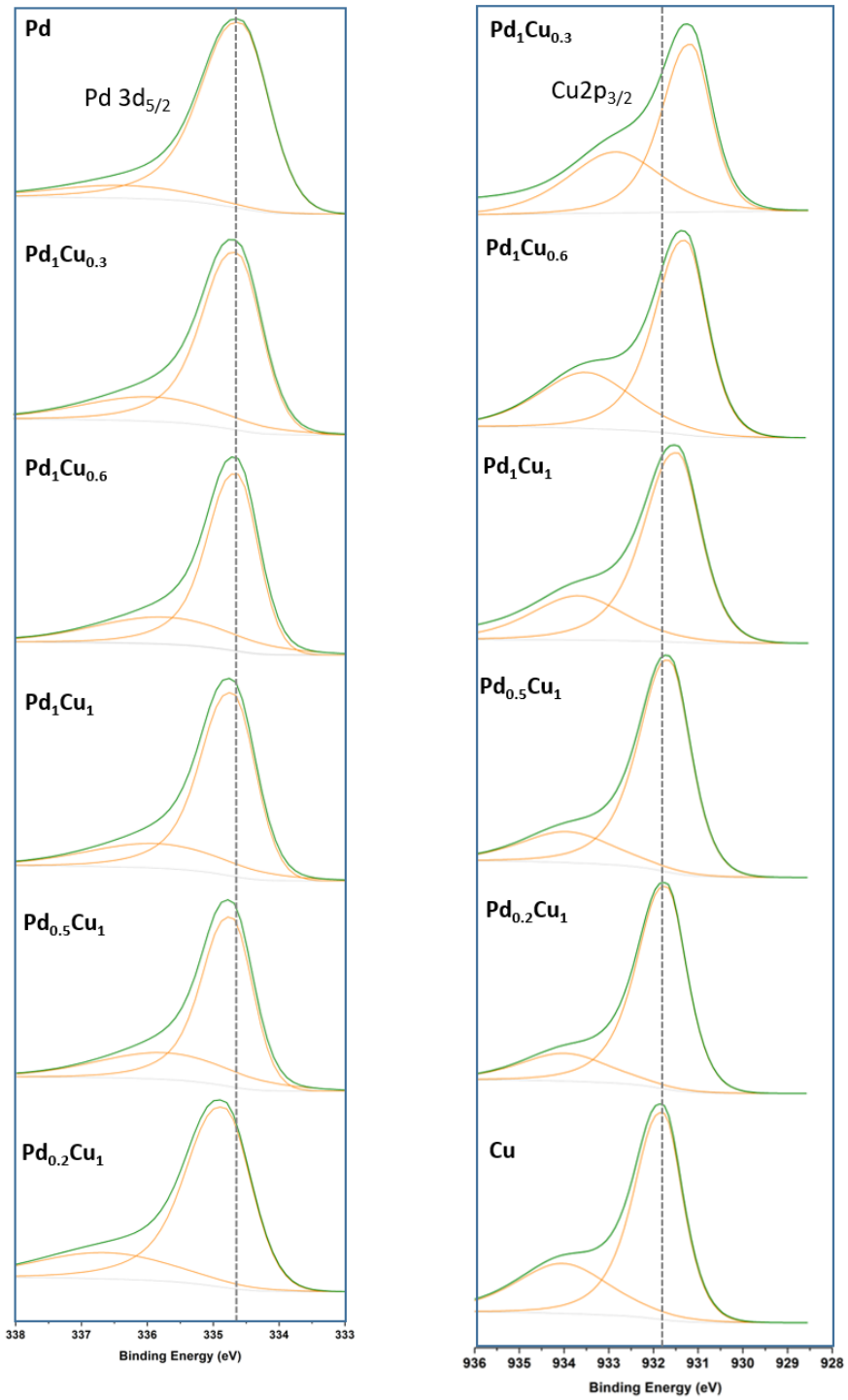


**Figure S10**. XPS spectra of the Pd $3d_{5/2}$ (left) and Cu $2p_{3/2}$ (right) regions of $Pd_xCu_y$–$Fe_3O_4$ NPs.

## 4. Supplementary figures and tables

**Table S1.** Comparison of catalytic activity of $Pd_1Cu_{0.6}$–$Fe_3O_4$ NPs with other reported heterogeneous catalytic systems for *N*-methylation using methanol

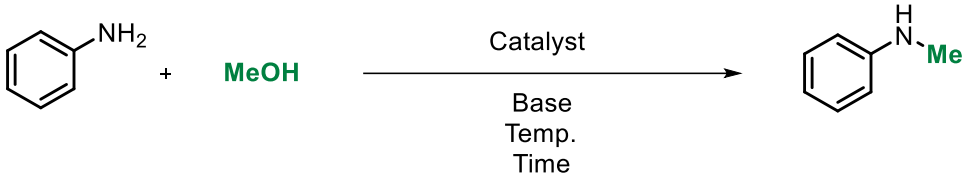


| Entry | Catalyst | Base | Temperatrue | Time | Yield (%) |
|---|---|---|---|---|---|
| 1 | Soild Molecular NHC-Ir[1] | KO*t*Bu | 130 °C | 12 h | 99 |
| 2 | Pt/C[2] | NaOH | 140 °C | 15 h | 92 |
| 3 | Pd/C[3] | $CH_3ONa$ | 150 °C | 12 h | 99 |
| 4 | Cp*Ir@CTF[4] | $Cs_2CO_3$ | 125 °C | 12 h | 95 |
| 5 | Pd@*s*PS-$NMe_2$[5] | $CH_3ONa$ | 150 °C | 10 h | 97 |
| 6 | $Pd_1Cu_{0.6}$–$Fe_3O_4$ (This work) | $K_2CO_3$ | 140 °C | 24 h | 99 |

**Table S2.** Comparison catalytic activity of PdCu nanoparticles on different supports.

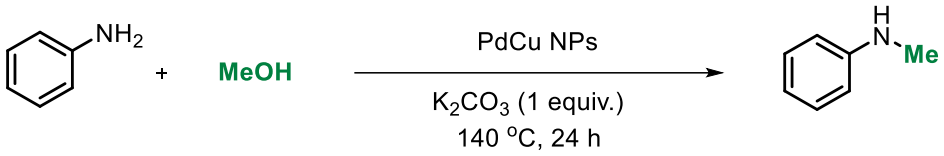


| Entry | Supports (PdCu NPs) | Conversion (%) | Yield (%) | Pd:Cu ratio |
|---|---|---|---|---|
| 1 | $Fe_3O_4$ | 93 | 93 | 1 :0.6 |
| 2 | $TiO_2$ | 82 | 82 | 1: 0.5 |
| 3 | $CeO_2$ | 85 | 85 | 1: 0.7 |
| 4 | $Al_2O_3$ | 84 | 84 | 1: 0.6 |

Reaction conditions : 6.4 mol% of total metal contents, aniline (0.2 mmol), $K_2CO_3$ (0.2 mmol), MeOH (2 mL),140 °C, 24 h, GC yield

| Catalyst | Pd (wt%) | Cu (wt%) |
|---|---|---|
| $Pd_1Cu_{0.5}$–$TiO_2$ | 6.98 | 2.25 |
| $Pd_1Cu_{0.7}$–$CeO_2$ | 3.13 | 1.35 |
| $Pd_1Cu_{0.6}$–$Al_2O_3$ | 9.05 | 3.36 |

**Figure S11.** ICP-AES data of PdCu NPs with different supports.

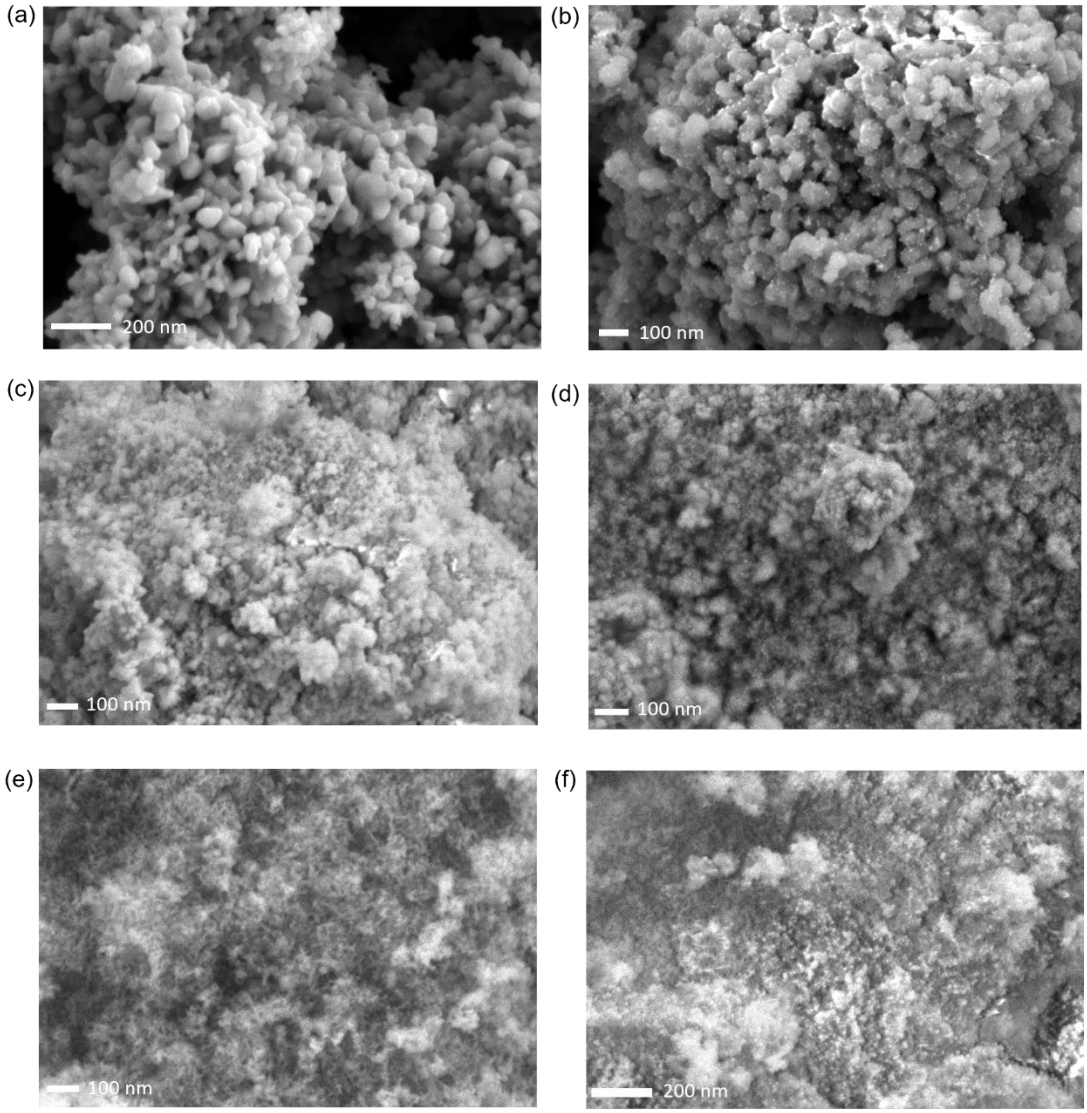


**Figure S12**. SEM images of (a) $TiO_2$ NPs; (b) PdCu–$TiO_2$ NPs; (c) $CeO_2$ NPs; (d) PdCu–$CeO_2$ NPs; (e) $Al_2O_3$ NPs; (f) PdCu–$Al_2O_3$ NPs.

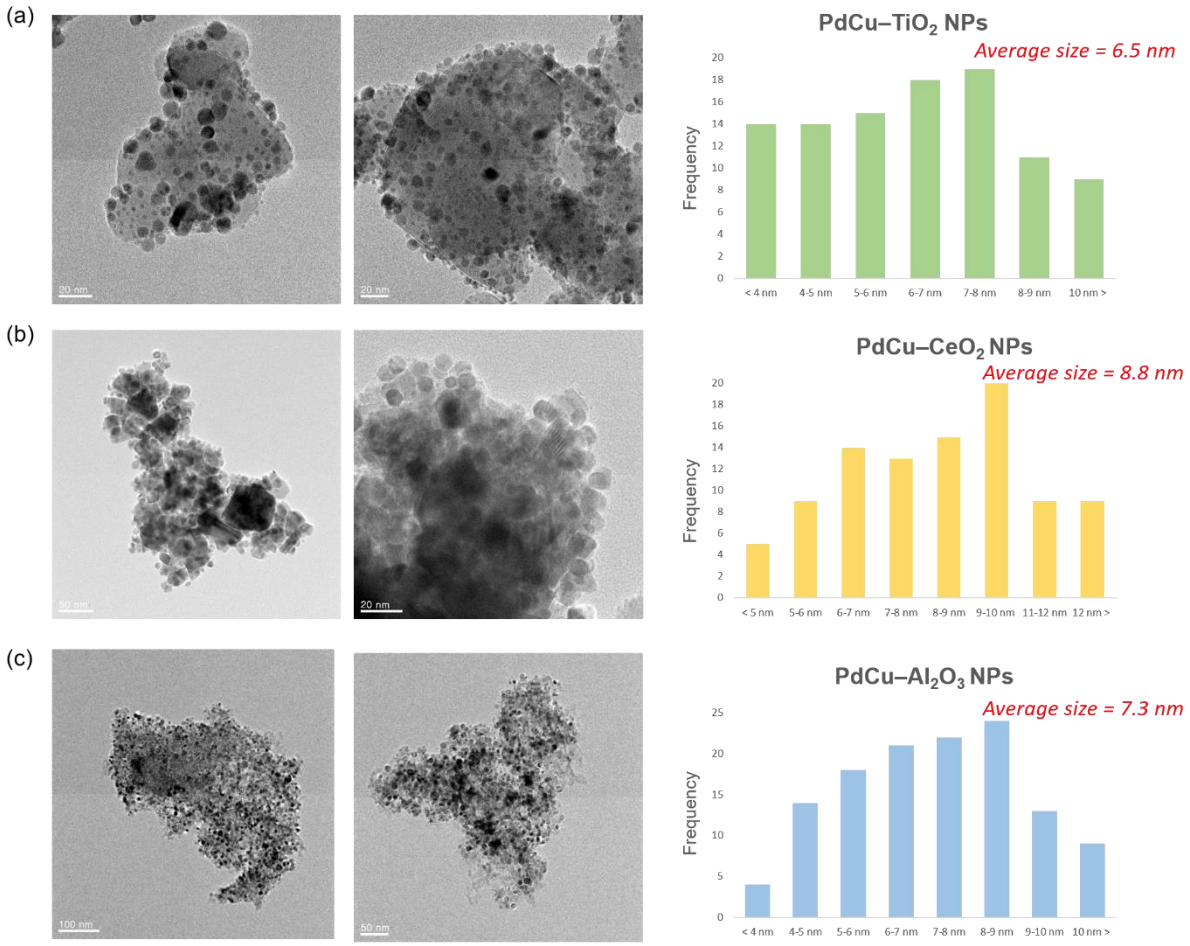


**Figure S13**. HR-TEM images of (a) PdCu–$TiO_2$ NPs; (b) PdCu–$CeO_2$ NPs; (c) PdCu–$Al_2O_3$ NPs.

## 5. Kinetic Experiment

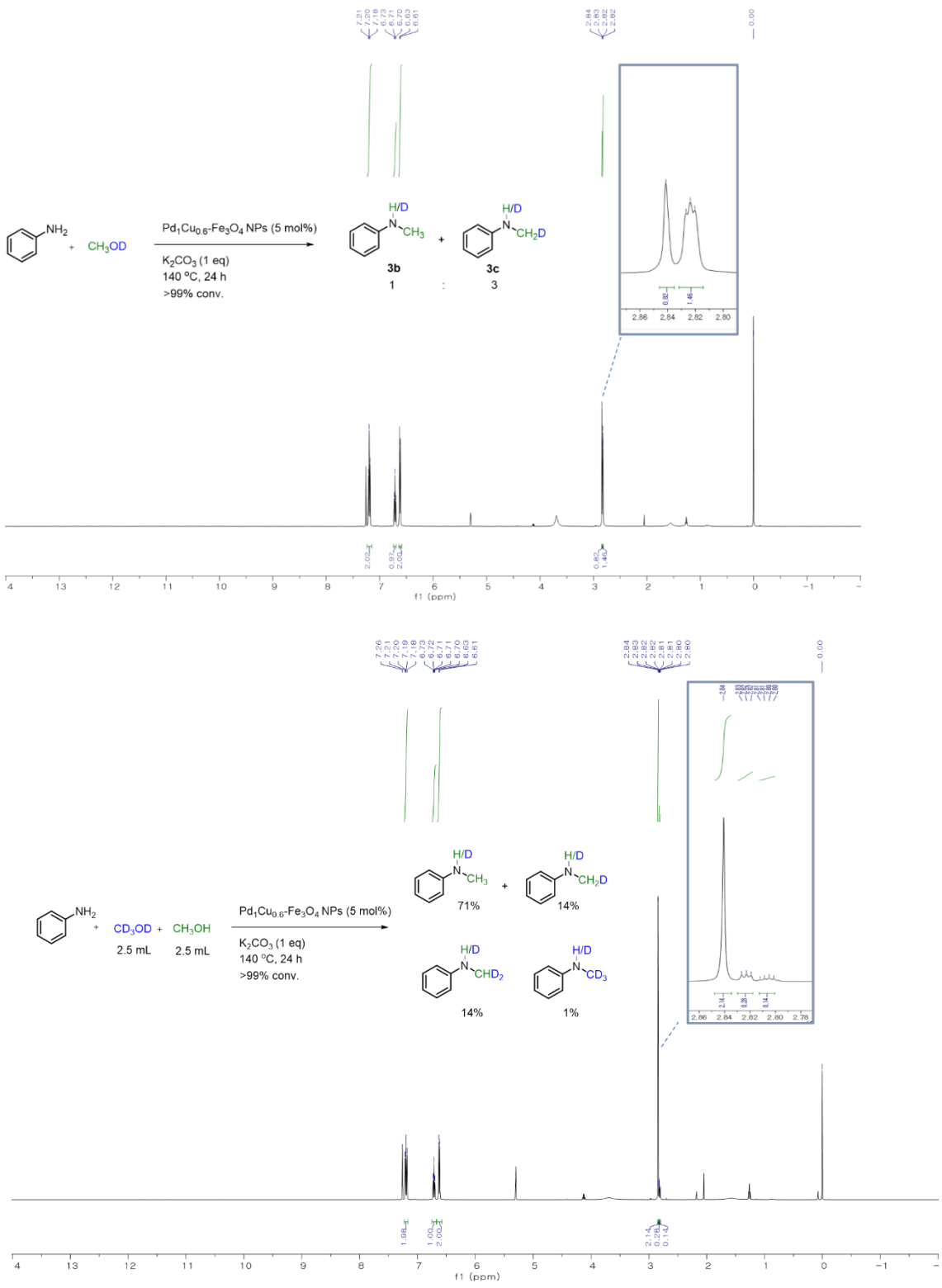


**Figure S14.** $^{1}$H NMR data analysis of deuterium labeling test.

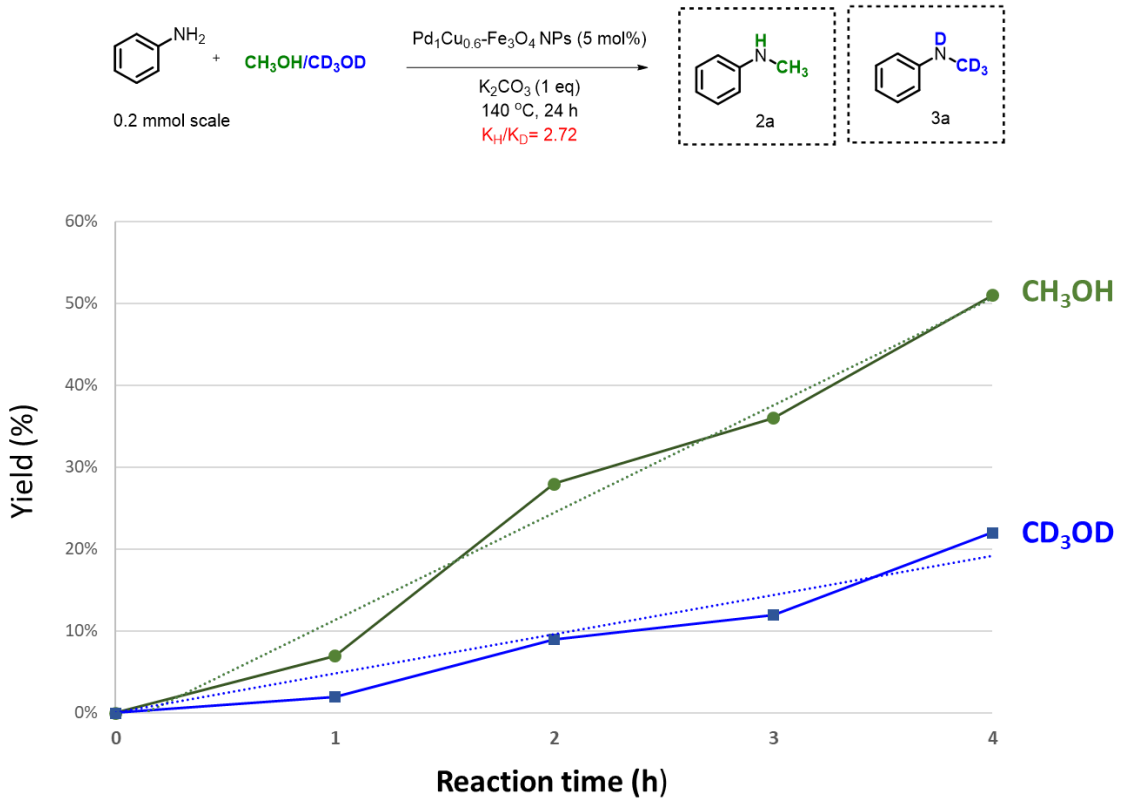


**Figure S15.** The ratio of non-deuterated (**2a**) and deuterated (**3a**) products from the reactions employing $CH_3OH$ and $CD_3OD$

## 6. Computational Details

Density functional theory (DFT) calculations were performed using the Vienna *ab initio* simulation package (VASP)[6] with employing the projector augmented wave (PAW) method[7] and the plane-wave cutoff energy of 500 eV. The exchange-correlation energy was described using the revised Perdew–Burke–Ernzerhof (RPBE) functional.[8] Convergence thresholds for the electronic and ionic self-consistency were set as $10^{-5}$ and $10^{-4}$ eV, respectively, and the dimensions of *k*-point grids and lattice parameters of corresponding simulation cells are listed in **Table S3**.

Using the fully optimized bulk structures of $Pd_xCu_y$, four layer of 4 × 4 (111) slab models were constructed with including an additional 25 Å vacuum space along the z-direction (**Figure S17a**). During the optimization of slab models, two bottommost layers were fixed, and the dipole correction was applied along the z-direction. Reciprocal spaces were sampled using $\Gamma$-centered (6 × 6 × 1) *k*-point meshes. Using the most stable surface slab model among the two possible surface geometries (**Table S4**), we calculated the hydrogen binding energies ($\Delta E_{\mathrm{H}}$) of all possible 3-fold hollow sites on the surface (**Figure S17b and Table S5**). For the calculation of the projected density of states (PDOS) of surface atoms, we employed the Blochl tetrahedron method.[9]

To calculate $Fe_3O_4$ and $Fe_3O_4$-supported catalyst models (Pd–$Fe_3O_4$ and Cu–$Fe_3O_4$), we performed spin-polarized DFT calculations by applying the Hubbard correction on Fe *d* states using $U$ = 4.50 and $J$ = 0.89 eV.[10] Averaged magnetic moment of Fe was 4.03 $\mu_{\mathrm{B}}$, in agreement with the experimental value of 4.05 $\mu_{\mathrm{B}}$.[11]

$Fe_3O_4$ (111) surface slab models were constructed using the fully optimized bulk structure of $Fe_3O_4$ with including an additional 25 Å of vacuum layer along the z-direction. During the geometry optimization of the slab models of $Fe_3O_4$, the bottommost three layers were kept fixed. Then, two layer of (12 × 12) Cu (111) slab or two layer of (11 × 11) Pd (111) slab was interfaced with the $Fe_3O_4$ (111) surface slab (**Figure S18**). We modified the in-plane lattice parameters of Cu or Pd to be matched with those of $Fe_3O_4$, applying a small lattice strain of +0.148 % to Cu and -0.449 % to Pd (**Figure S18**). We examined possible stacking configurations of interfacial models, among which the most stable one was chosen for the analyses. (**Table S6**) Reciprocal space of these Cu–$Fe_3O_4$ and Pd–$Fe_3O_4$ slab models was sampled only at the $\Gamma$-point. Due to the large computational cost of employing the Blochl tetrahedron method, we employed the Gaussian smearing of 0.05 eV to calculate the PDOS of the Cu–$Fe_3O_4$ and Pd–$Fe_3O_4$ slab models.

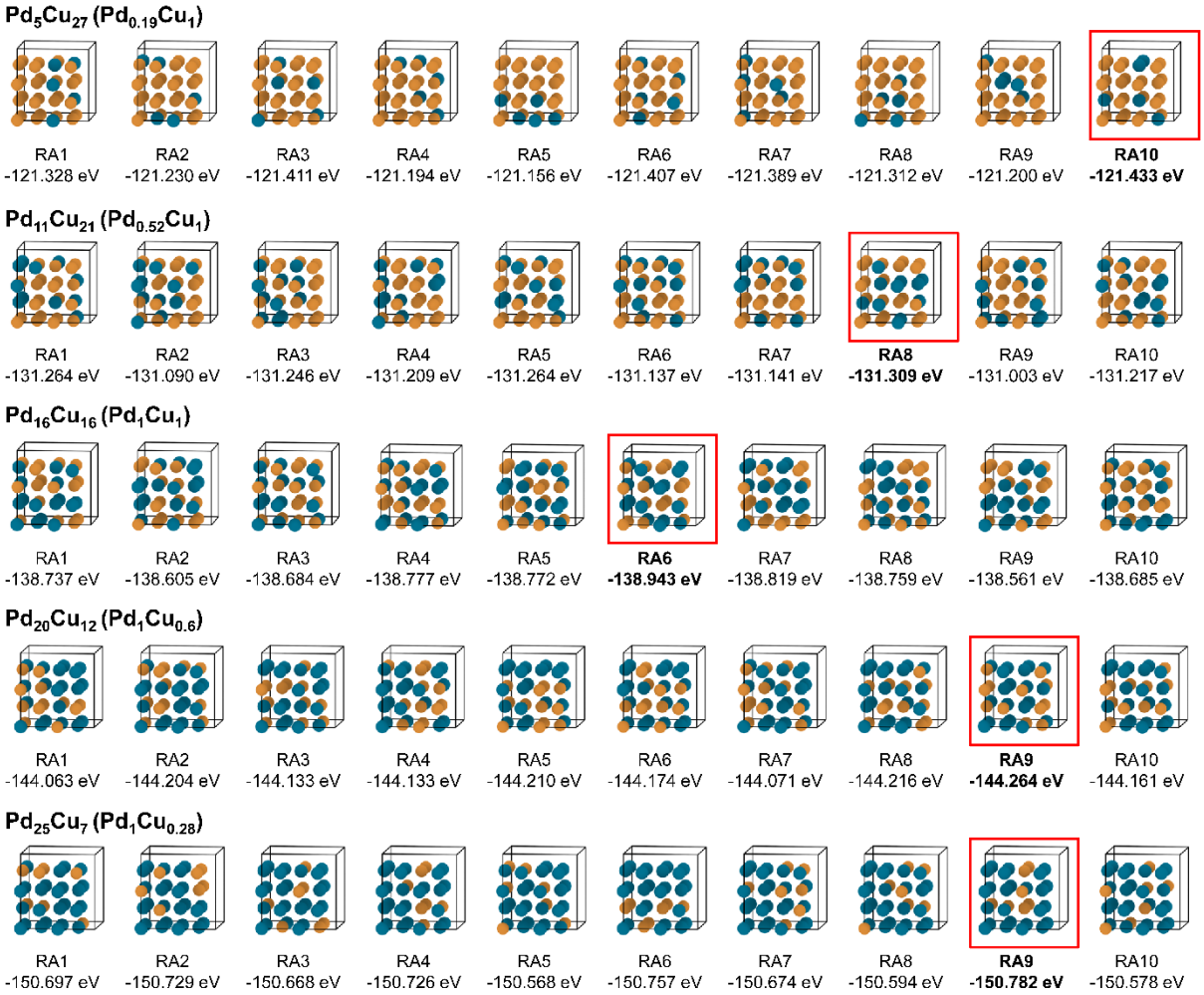


**Figure S16.** Ten atomic structures of fcc PdCu random alloy (RA) models with their optimized energies using the density functional theory (DFT) calculation. The most stable structure at each composition is indicated using a red box.

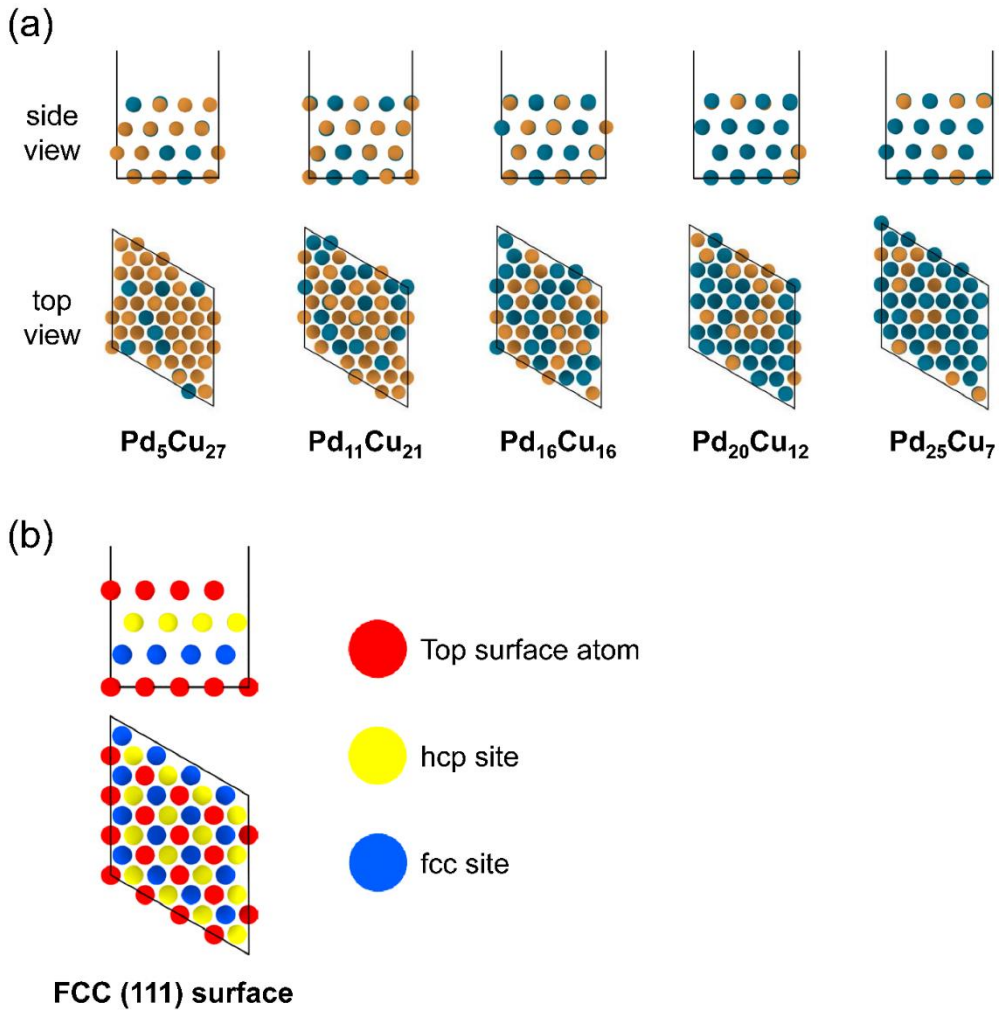


**Figure S17.** (a) DFT-optimized fcc (111) slab models of $Pd_xCu_y$ alloy. (b) On the fcc (111) surface, there are 32 different 3-fold sites consisting of 16 hcp sites and 16 fcc sites.

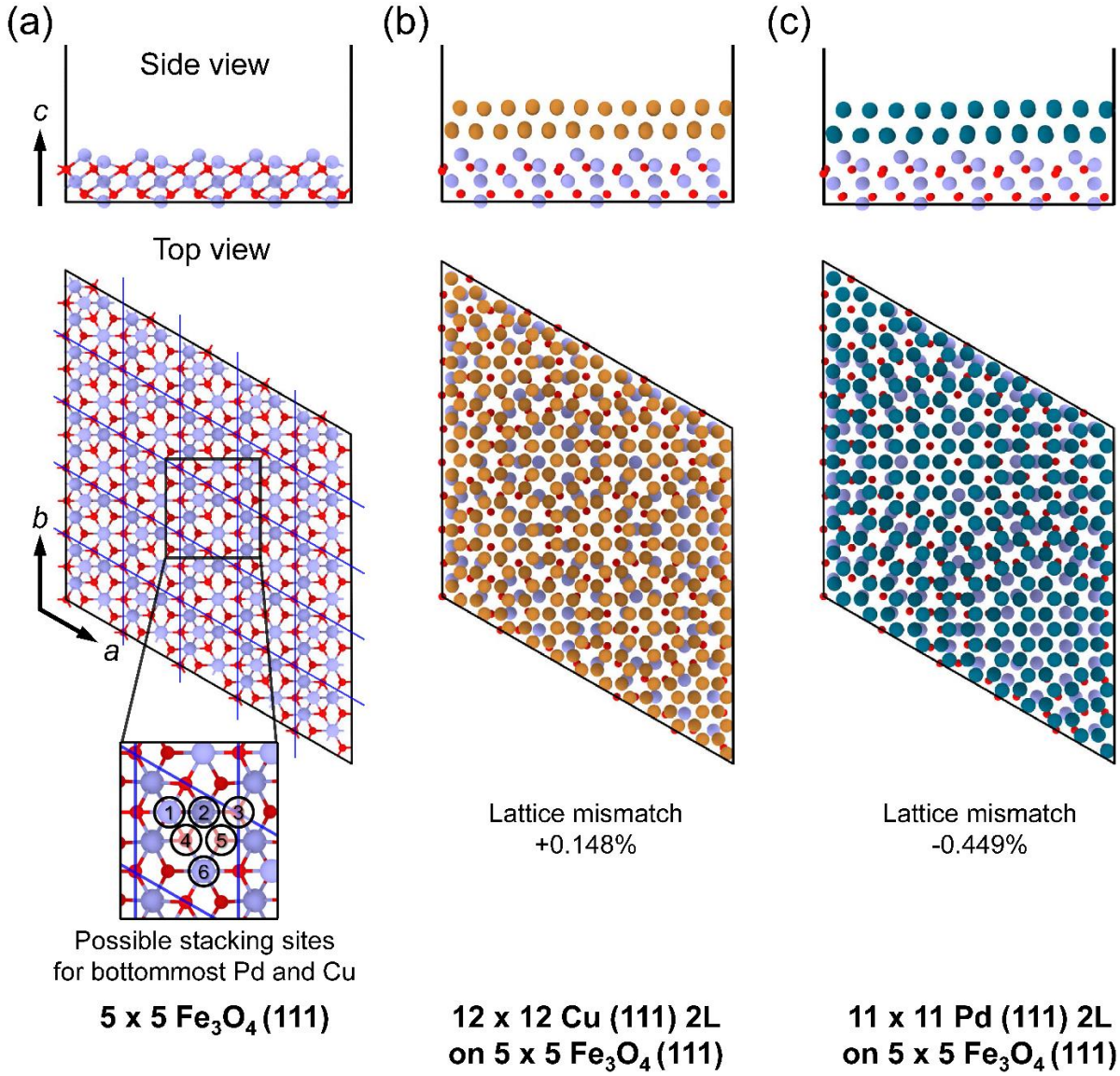


**Figure S18.** DFT-optimized (111) slab models of (a) $Fe_3O_4$, (b) Cu–$Fe_3O_4$, and (c) Pd–$Fe_3O_4$. In the top view of $Fe_3O_4$, blue line denotes the surface unit cell of $Fe_3O_4$ (111) slab.

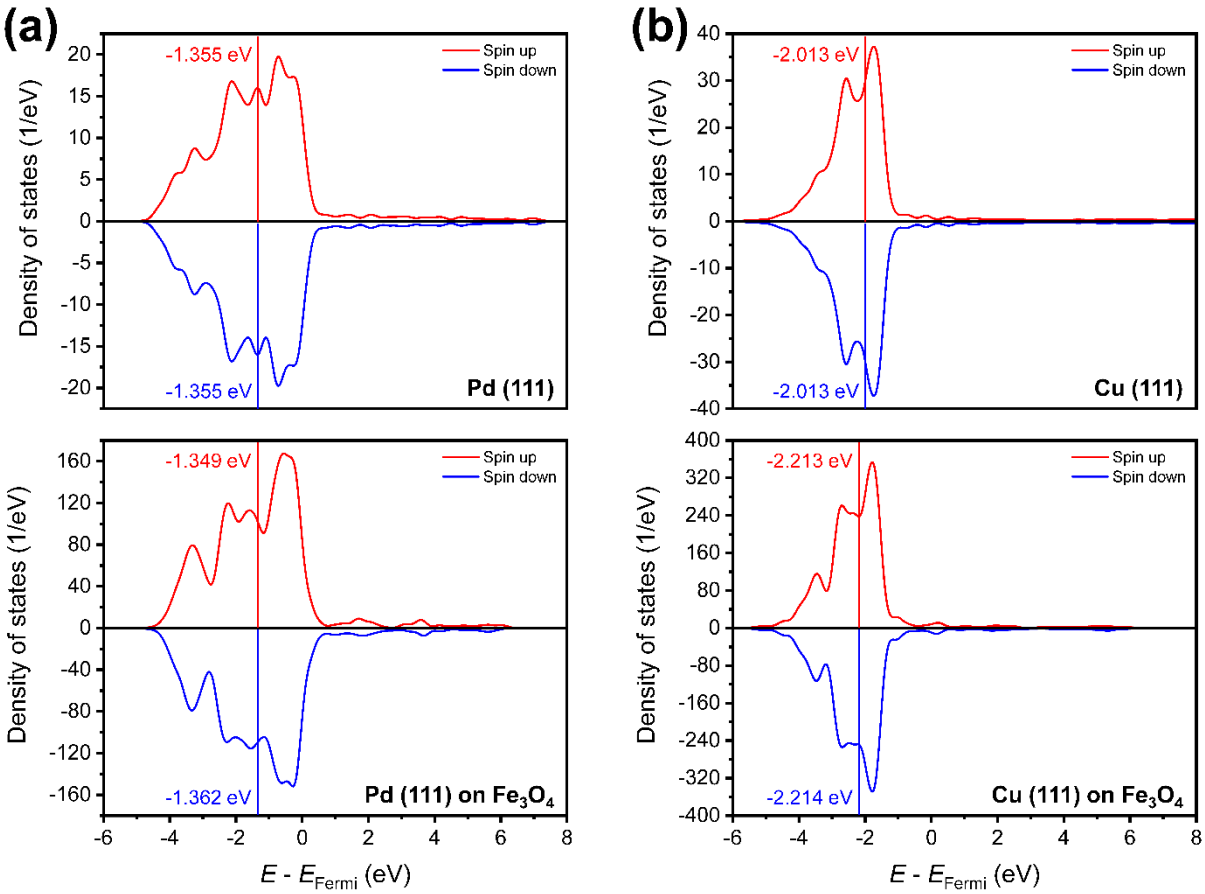


**Figure S19.** Projected density of states (PDOS) of *d*-electrons of (a) Pd and (b) Cu. Solid vertical line denotes the weight-averaged value of the PDOS, i.e., the location of the d-band center. Bottom panels are PDOS of Pd and Cu, supported on the $Fe_3O_4$.

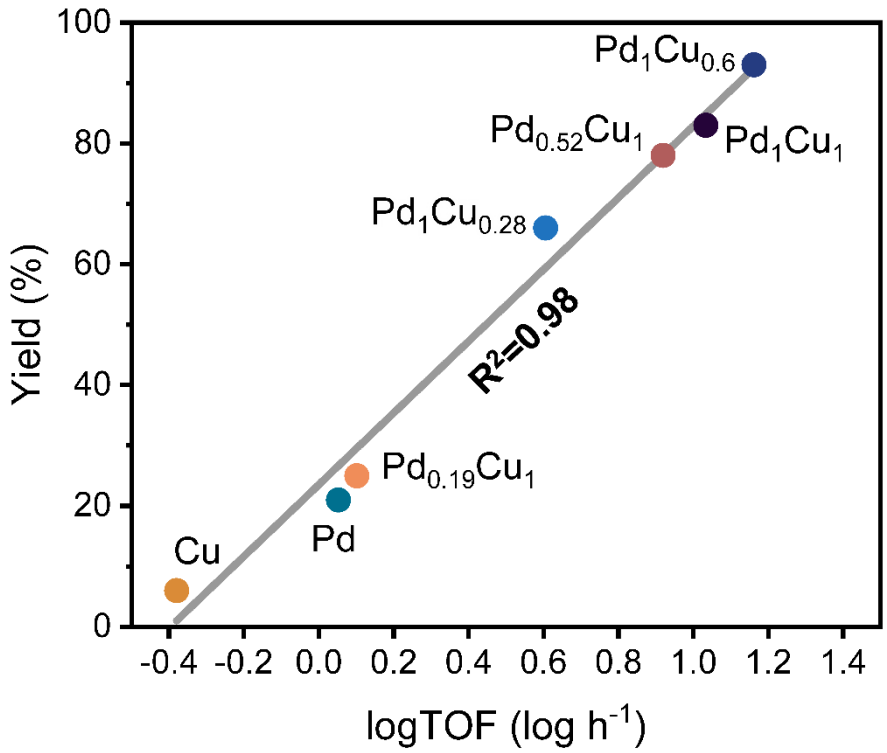


**Figure S20.** Correlation between the estimated turnover frequency (TOF) and the reaction yield of *N*-methylation produce with varying the composition of $Pd_xCu_y$.

**Table S3**. Dimensions of *k*-point meshes and corresponding lattice parameters of the simulation cell.

| Alloy | Lattice parameter | *k*-point meshes |
|---|---|---|
| Pd | *a*,*b*,*c* = 3.991 Å<br>*α*=*β*=*γ*= 90° | Monkhorst-Pack (16 × 16 × 16) |
| Cu | *a*,*b*,*c* = 3.680 Å<br>*α*=*β*=*γ*= 90° | |
| $Pd_5Cu_{27}$ ($Pd_{0.19}Cu_1$) | *a*,*b*,*c* = 7.457 Å<br>*α*=*β*=*γ*= 90° | Monkhorst-Pack (8 × 8 × 8) |
| $Pd_{11}Cu_{21}$ ($Pd_{0.52}Cu_1$) | *a*,*b*,*c* = 7.574 Å<br>*α*=*β*=*γ*= 90° | |
| $Pd_{16}Cu_{16}$ ($Pd_1Cu_1$) | *a*,*b*,*c* = 7.671 Å<br>*α*=*β*=*γ*= 90° | |
| $Pd_{20}Cu_{12}$ ($Pd_1Cu_{0.6}$) | *a*,*b*,*c* = 7.748 Å<br>*α*=*β*=*γ*= 90° | |
| $Pd_{25}Cu_7$ ($Pd_1Cu_{0.28}$) | *a*,*b*,*c* = 7.845 Å<br>*α*=*β*=*γ*= 90° | |
| $Fe_3O_4$ | *a*,*b*,*c* = 8.789 Å<br>*α*=*β*=*γ*= 90.396° | |

**Table S4**. DFT-calculated total energy of the DFT-optimized $Pd_xCu_y$ (111) surfaces.

| Alloy | Surfaces | Area (Å$^2$) | DFT energy (eV) |
|---|---|---|---|
| $Pd_5Cu_{27}$ ($Pd_{0.19}Cu_1$) | **Surface 1** | 96.318 | **-229.618 (stable)** |
| | Surface 2 | | -229.611 |
| $Pd_{11}Cu_{21}$ ($Pd_{0.52}Cu_1$) | Surface 1 | 99.350 | -249.159 |
| | **Surface 2** | | **-249.178 (stable)** |
| $Pd_{16}Cu_{16}$ ($Pd_1Cu_1$) | **Surface 1** | 101.913 | **-264.000 (stable)** |
| | Surface 2 | | -263.945 |
| $Pd_{20}Cu_{12}$ ($Pd_1Cu_{0.6}$) | **Surface 1** | 103.987 | **-274.132 (stable)** |
| | Surface 2 | | -274.034 |
| $Pd_{25}Cu_7$ ($Pd_1Cu_{0.28}$) | **Surface 1** | 106.609 | **-286.732 (stable)** |
| | Surface 2 | | -286.638 |

**Table S5**. Computed 3-fold binding energies of $Pd_xCu_y$.

| Alloy surface | | $\Delta E_H$ (eV) |
|---|---|---|
| $Pd_5Cu_{27}$ ($Pd_{0.19}Cu_1$) | fcc1 | -0.027 |
| | fcc2 | -0.036 |
| | fcc3 | 0.027 |
| | fcc4 | -0.027 |
| | fcc5 | -0.026 |
| | fcc6 | -0.124 |
| | fcc7 | -0.146 |
| | fcc8 | 0.019 |
| | fcc9 | -0.059 |
| | fcc10 | -0.010 |
| | fcc11 | -0.059 |
| | fcc12 | 0.030 |
| | fcc13 | -0.053 |
| | fcc14 | -0.047 |
| | fcc15 | -0.079 |
| | fcc16 | 1.592 |
| | hcp1 | -0.081 |
| | **hcp2** | **-0.160 (stable)** |
| | hcp3 | 0.014 |
| | hcp4 | -0.051 |
| | hcp5 | -0.085 |
| | hcp6 | 0.036 |
| | hcp7 | -0.114 |
| | hcp8 | 0.097 |
| | hcp9 | -0.069 |
| | hcp10 | -0.077 |
| | hcp11 | -0.008 |
| | hcp12 | -0.107 |
| | hcp13 | -0.107 |
| | hcp14 | 0.122 |
| | hcp15 | -0.035 |
| | hcp16 | 0.188 |
| $Pd_{11}Cu_{21}$ ($Pd_{0.52}Cu_1$) | fcc1 | -0.180 |
| | **fcc2** | **-0.292 (stable)** |
| | fcc3 | -0.172 |
| | fcc4 | -0.061 |
| | fcc5 | -0.090 |
| | fcc6 | -0.040 |
| | fcc7 | -0.092 |
| | fcc8 | -0.142 |

| | | |
|---|---|---|
| | fcc9 | -0.155 |
| | fcc10 | -0.024 |
| | fcc11 | -0.125 |
| | fcc12 | 0.039 |
| | fcc13 | -0.193 |
| | fcc14 | -0.070 |
| | fcc15 | 0.080 |
| | fcc16 | -0.094 |
| | hcp1 | -0.238 |
| | hcp2 | -0.154 |
| | hcp3 | -0.061 |
| | hcp4 | -0.053 |
| | hcp5 | -0.032 |
| | hcp6 | -0.179 |
| | hcp7 | -0.163 |
| | hcp8 | -0.170 |
| | hcp9 | -0.193 |
| | hcp10 | 0.002 |
| | hcp11 | -0.014 |
| | hcp12 | -0.102 |
| | hcp13 | -0.092 |
| | hcp14 | 0.123 |
| | hcp15 | 0.000 |
| | hcp16 | -0.067 |
| | | |
| $Pd_{16}Cu_{16}$ ($Pd_1Cu_1$) | fcc1 | -0.250 |
| | fcc2 | -0.181 |
| | **fcc3** | **-0.316 (stable)** |
| | fcc4 | -0.124 |
| | fcc5 | -0.235 |
| | fcc6 | -0.192 |
| | fcc7 | 0.069 |
| | fcc8 | -0.248 |
| | fcc9 | -0.217 |
| | fcc10 | -0.168 |
| | fcc11 | -0.287 |
| | fcc12 | -0.272 |
| | fcc13 | -0.269 |
| | fcc14 | -0.143 |
| | fcc15 | -0.207 |
| | fcc16 | -0.194 |
| | hcp1 | -0.088 |
| | hcp2 | -0.266 |
| | hcp3 | -0.191 |

| | | |
|---|---|---|
| | hcp4 | -0.228 |
| | hcp5 | -0.207 |
| | hcp6 | -0.171 |
| | hcp7 | -0.085 |
| | hcp8 | -0.110 |
| | hcp9 | -0.227 |
| | hcp10 | -0.168 |
| | hcp11 | -0.188 |
| | hcp12 | -0.154 |
| | hcp13 | -0.293 |
| | hcp14 | -0.085 |
| | hcp15 | -0.187 |
| | hcp16 | -0.211 |
| | | |
| $Pd_{20}Cu_{12}$ ($Pd_1Cu_{0.6}$) | fcc1 | -0.185 |
| | fcc2 | -0.242 |
| | fcc3 | -0.373 |
| | fcc4 | -0.295 |
| | fcc5 | -0.351 |
| | fcc6 | -0.179 |
| | fcc7 | -0.339 |
| | **fcc8** | **-0.402 (stable)** |
| | fcc9 | -0.209 |
| | fcc10 | -0.172 |
| | fcc11 | -0.066 |
| | fcc12 | -0.270 |
| | fcc13 | -0.253 |
| | fcc14 | -0.258 |
| | fcc15 | -0.336 |
| | fcc16 | -0.392 |
| | hcp1 | -0.267 |
| | hcp2 | -0.191 |
| | hcp3 | -0.328 |
| | hcp4 | -0.344 |
| | hcp5 | -0.262 |
| | hcp6 | -0.157 |
| | hcp7 | -0.211 |
| | hcp8 | -0.351 |
| | hcp9 | -0.284 |
| | hcp10 | -0.316 |
| | hcp11 | -0.104 |
| | hcp12 | -0.206 |
| | hcp13 | -0.262 |
| | hcp14 | 0.047 |

| | | |
|---|---|---|
| | hcp15 | -0.222 |
| | hcp16 | -0.223 |
| | | |
| $Pd_{25}Cu_7$ ($Pd_1Cu_{0.28}$) | fcc1 | -0.367 |
| | fcc2 | -0.319 |
| | fcc3 | -0.408 |
| | fcc4 | -0.369 |
| | fcc5 | -0.357 |
| | fcc6 | -0.300 |
| | fcc7 | -0.416 |
| | fcc8 | -0.433 |
| | fcc9 | -0.382 |
| | fcc10 | -0.205 |
| | fcc11 | -0.422 |
| | **fcc12** | **-0.444 (stable)** |
| | fcc13 | -0.247 |
| | fcc14 | -0.204 |
| | fcc15 | -0.291 |
| | fcc16 | -0.241 |
| | hcp1 | -0.185 |
| | hcp2 | -0.302 |
| | hcp3 | -0.295 |
| | hcp4 | -0.181 |
| | hcp5 | -0.298 |
| | hcp6 | -0.312 |
| | hcp7 | -0.365 |
| | hcp8 | -0.386 |
| | hcp9 | -0.199 |
| | hcp10 | -0.307 |
| | hcp11 | -0.397 |
| | hcp12 | -0.415 |
| | hcp13 | -0.210 |
| | hcp14 | -0.265 |
| | hcp15 | -0.306 |
| | hcp16 | -0.321 |

$\Delta E_H = E(^*H) - E(^*) - 0.5E(H_2)$, * denotes bare surface slab.

**Table S6**. Computed total energies of possible stacking configurations of the interfacial supercells.

| Alloy | Strain on M (%) | Stacking configuration | DFT energy (eV) |
|---|---|---|---|
| [11 x 11] Pd (111) | -0.449 | 1 | -3433.613 |
| on [5 x 5] Fe3O4 (111) | | 2 | -3433.608 |
| | | **3** | **-3433.621 (stable)** |
| | | 4 | -3433.616 |
| | | 5 | -3433.609 |
| | | 6 | -3433.615 |
| [12 x 12] Cu (111) | +0.148 | 1 | -3215.509 |
| on [5 x 5] Fe3O4 (111) | | 2 | -3215.494 |
| | | 3 | -3215.509 |
| | | 4 | -3215.489 |
| | | **5** | **-3215.519 (stable)** |
| | | 6 | -3211.589 |

## 7. Recycle Experiment

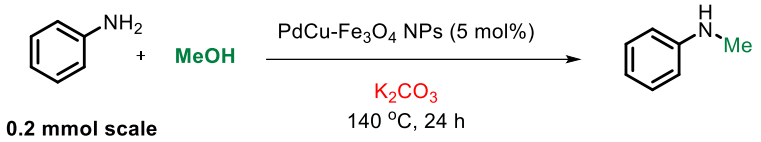


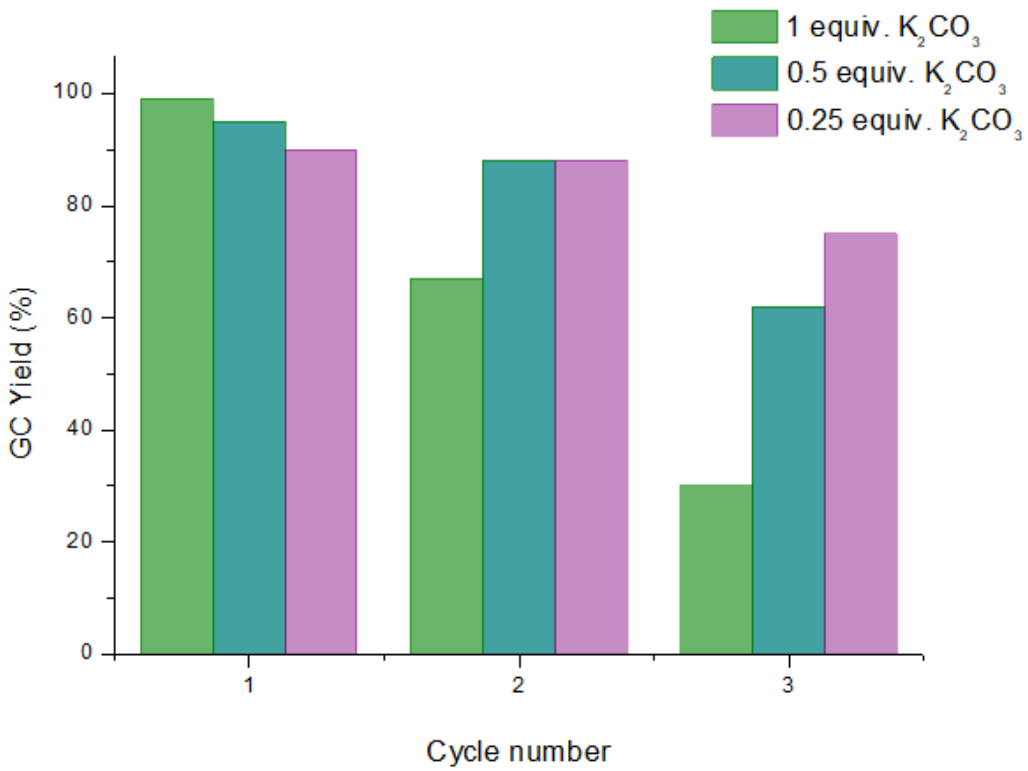


**Figure S21.** Recyclability of $Pd_1Cu_{0.6}$–$Fe_3O_4$ NPs for *N*-methylation of aniline.

(a) After 1 catalytic cycle

(1) $K_2CO_3$ 1 equiv.

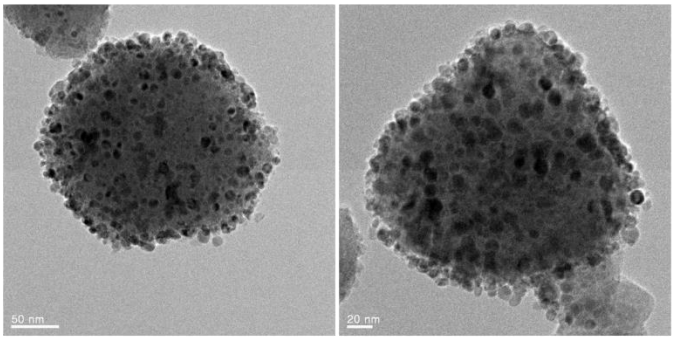


(2) $K_2CO_3$ 0.5 equiv.

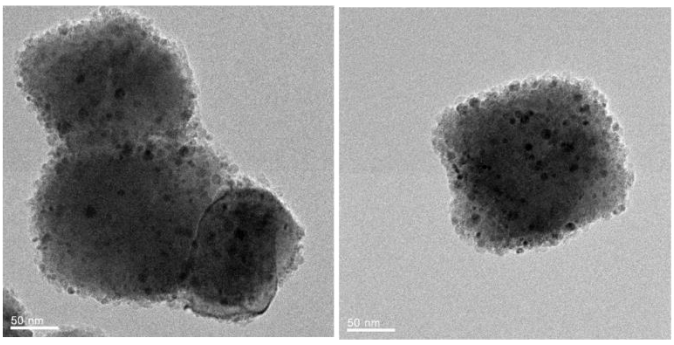


(3) $K_2CO_3$ 0.25 equiv.

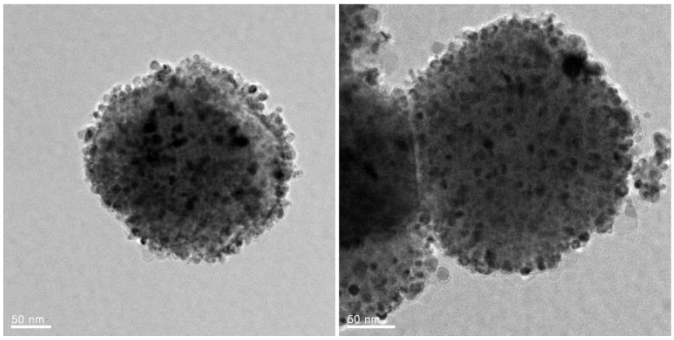

(b) After 3 catalytic cycle

(1) $K_2CO_3$ 1 equiv.

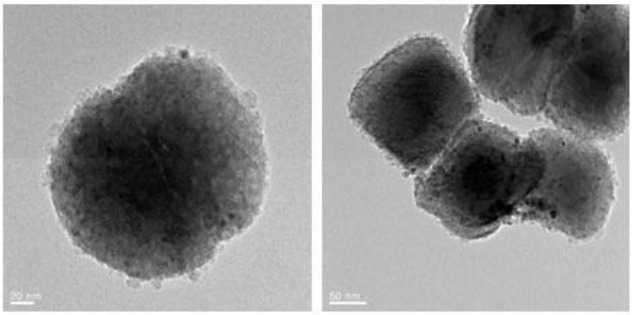

(2) $K_2CO_3$ 0.5 equiv.

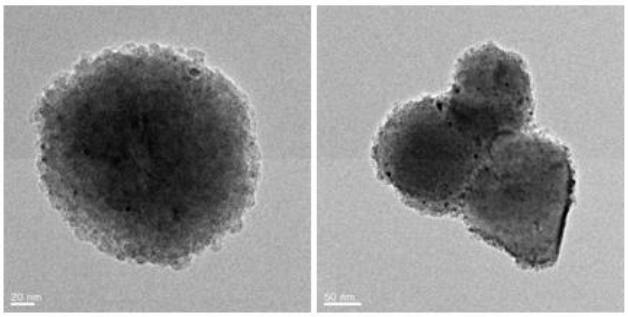

(3) $K_2CO_3$ 0.25 equiv.

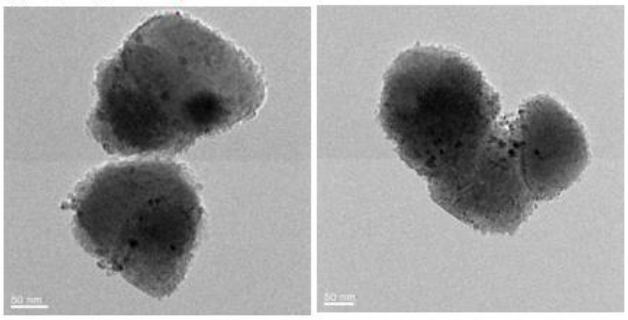

**Figure S22.** HR-TEM images of NPs; (a) $Pd_1Cu_{0.6}$–$Fe_3O_4$ NPs after 1 catalytic cycle; (b) $Pd_1Cu_{0.6}$–$Fe_3O_4$ NPs after 3 catalytic cycle.

| | Pd (wt%) | Cu (wt%) |
|---|---|---|
| Fresh catalyst | 8.42 | 2.71 |

| | Recycle 1 | | Recycle 3 | |
|---|---|---|---|---|
| Base ($K_2CO_3$) | Pd (wt%) | Cu (wt%) | Pd (wt%) | Cu (wt%) |
| 0.25 equiv. | 8.22 | 2.55 | 8.00 | 2.54 |
| 0.5 equiv. | 7.76 | 2.49 | 7.83 | 2.51 |
| 1 equiv. | 7.38 | 2.35 | 6.35 | 2.03 |

**Figure S23.** ICP-AES data of PdCu-$Fe_3O_4$ NPs after catalytic cycle.

## 8. NMR spectra

### *N*-Methylaniline,[2] 2a

A yellow oil. $^{1}$H NMR (400 MHz, Chloroform-*d*) δ 7.20 (t, *J* = 7.8 Hz, 2H), 6.71 (t, *J* = 7.5 Hz, 1H), 6.62 (d, *J* = 7.9 Hz, 2H), 3.75–3.60 (br, 1H), 2.84 (s, 3H).$^{13}$C NMR (101 MHz, Chloroform-*d*) δ 149.30, 129.18, 117.24, 112.41, 30.71.

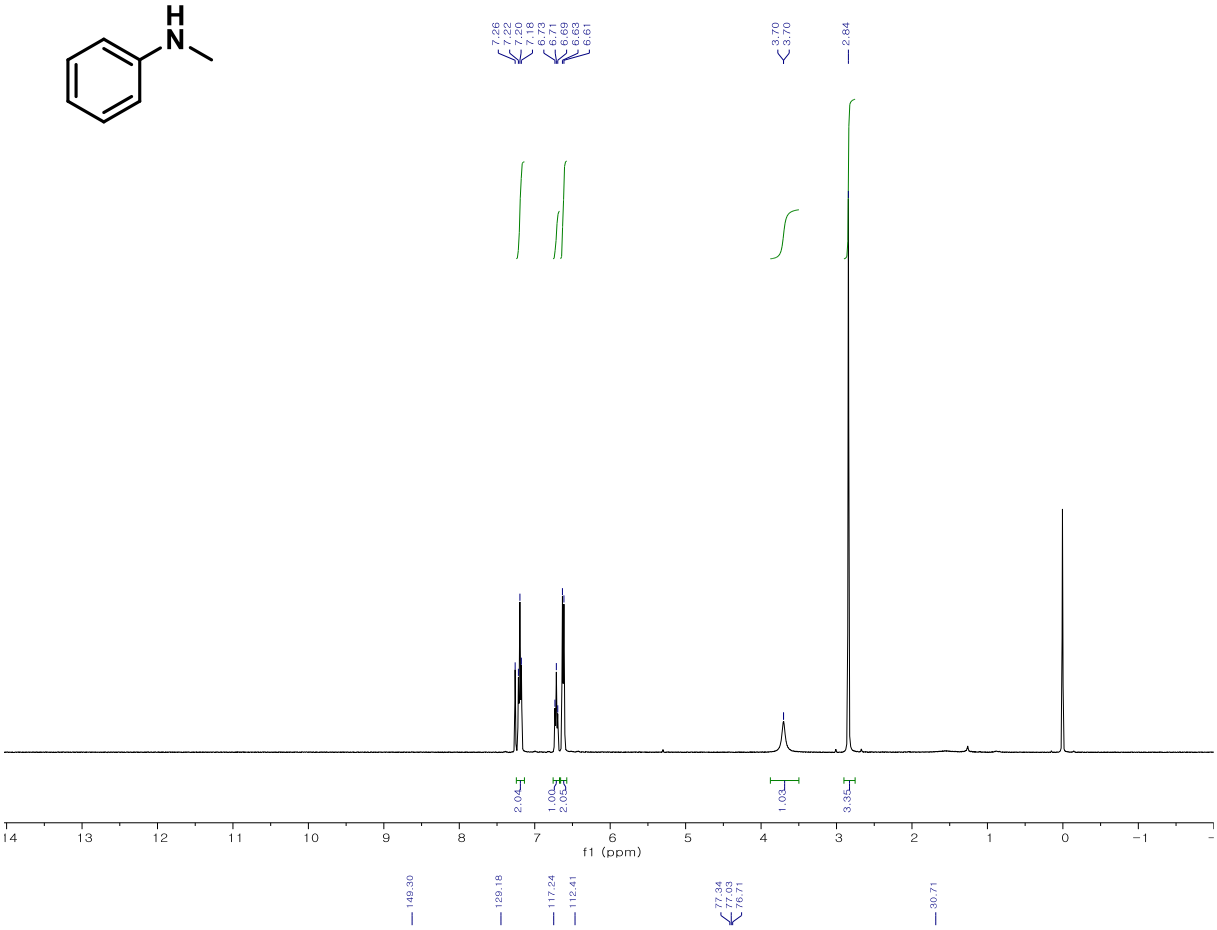


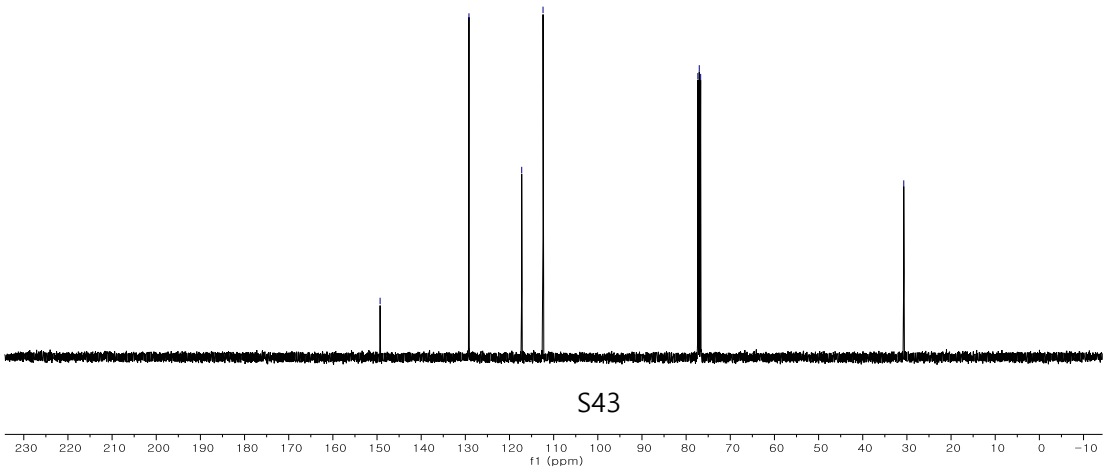

## *N*-Methylanisidine,[3] 2b

A colorless oil. $^{1}$H NMR (400 MHz, Chloroform-*d*) δ 6.79 (d, *J* = 8.9 Hz, 2H), 6.58 (d, *J* = 8.8 Hz, 2H), 3.74 (s, 3H), 2.79 (s, 3H). $^{13}$C NMR (126 MHz, Chloroform-d) δ 152.08, 143.72, 114.91, 113.65, 55.87, 31.63.

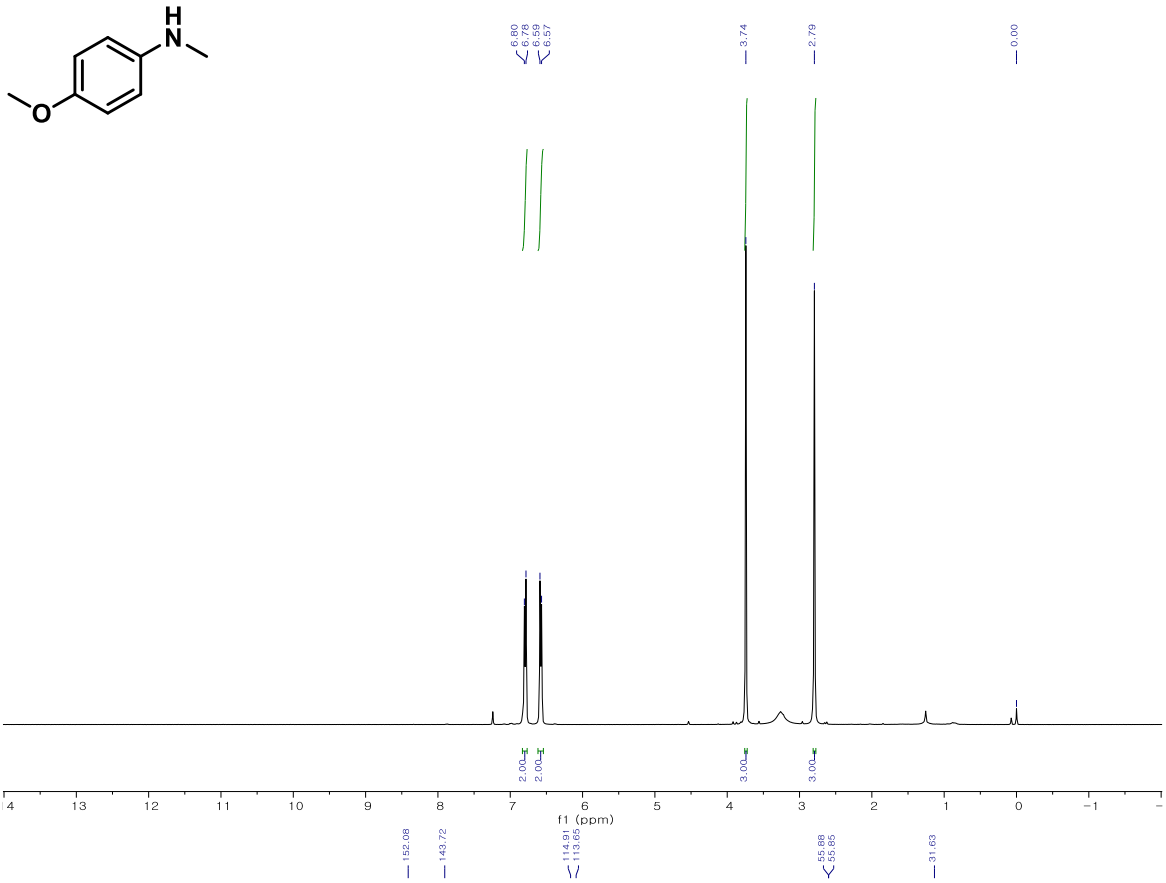


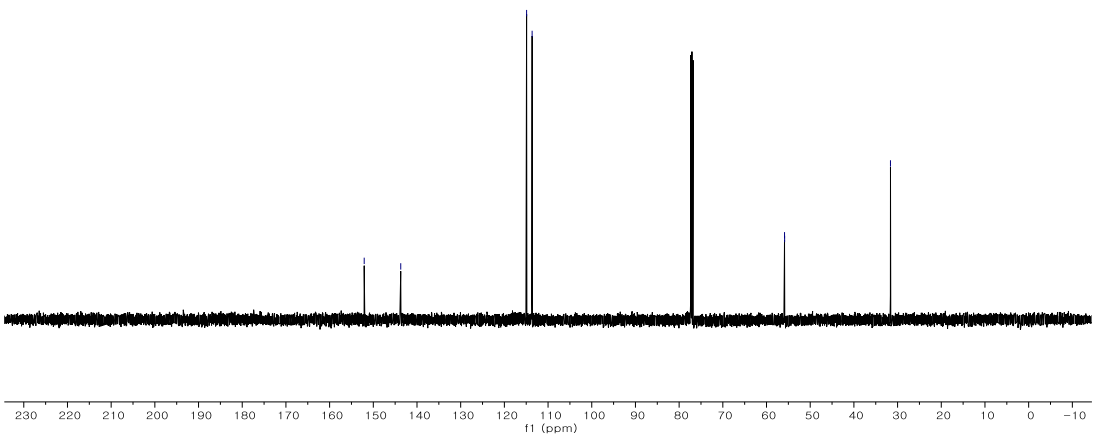

## *N*-Methyl-[1,1'-biphenyl]-4-amine,[12] 2c

A pale yellow solid. $^{1}$H NMR (400 MHz, Chloroform-*d*) δ 7.54 (d, *J* = 7.7 Hz, 2H), 7.46 (d, *J* = 8.3 Hz, 2H), 7.39 (t, *J* = 7.7 Hz, 2H), 7.24 (m, 1H), 6.69 (d, *J* = 8.5 Hz, 2H), 3.79 (s, 1H), 2.89 (s, 3H).$^{13}$C NMR (126 MHz, Chloroform-*d*) δ 148.79, 141.35, 130.16, 128.69, 127.94, 126.33, 126.06, 112.69, 30.79.

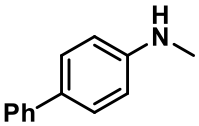


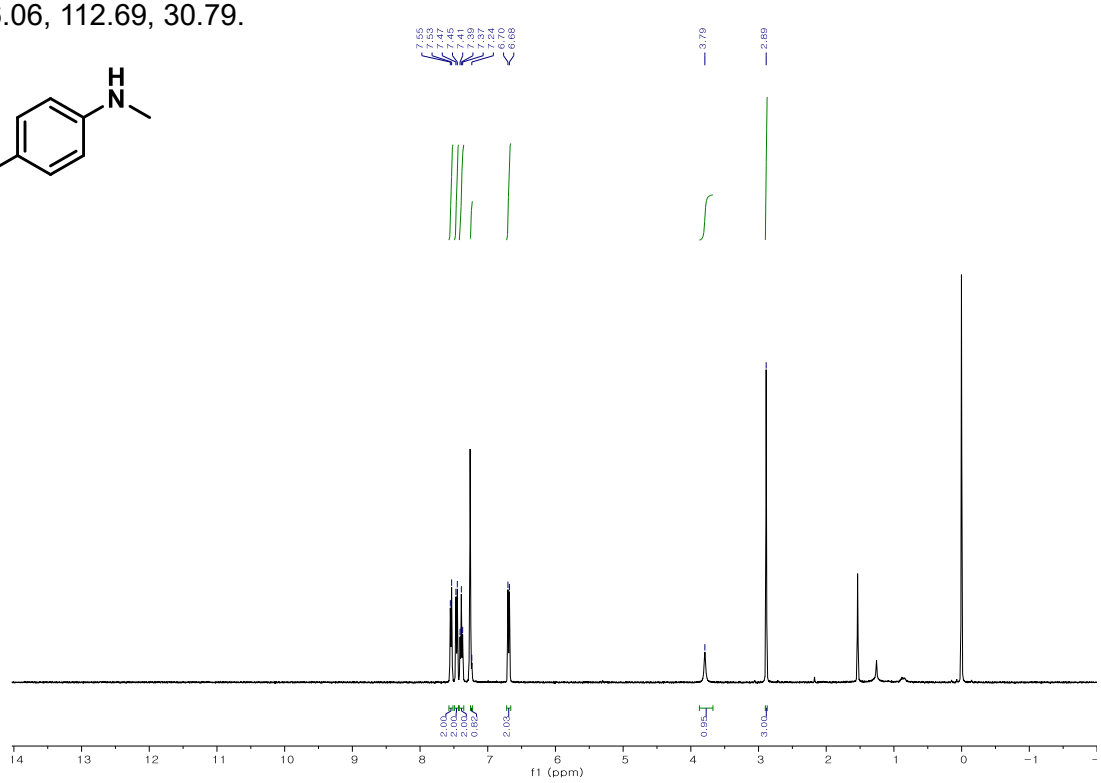


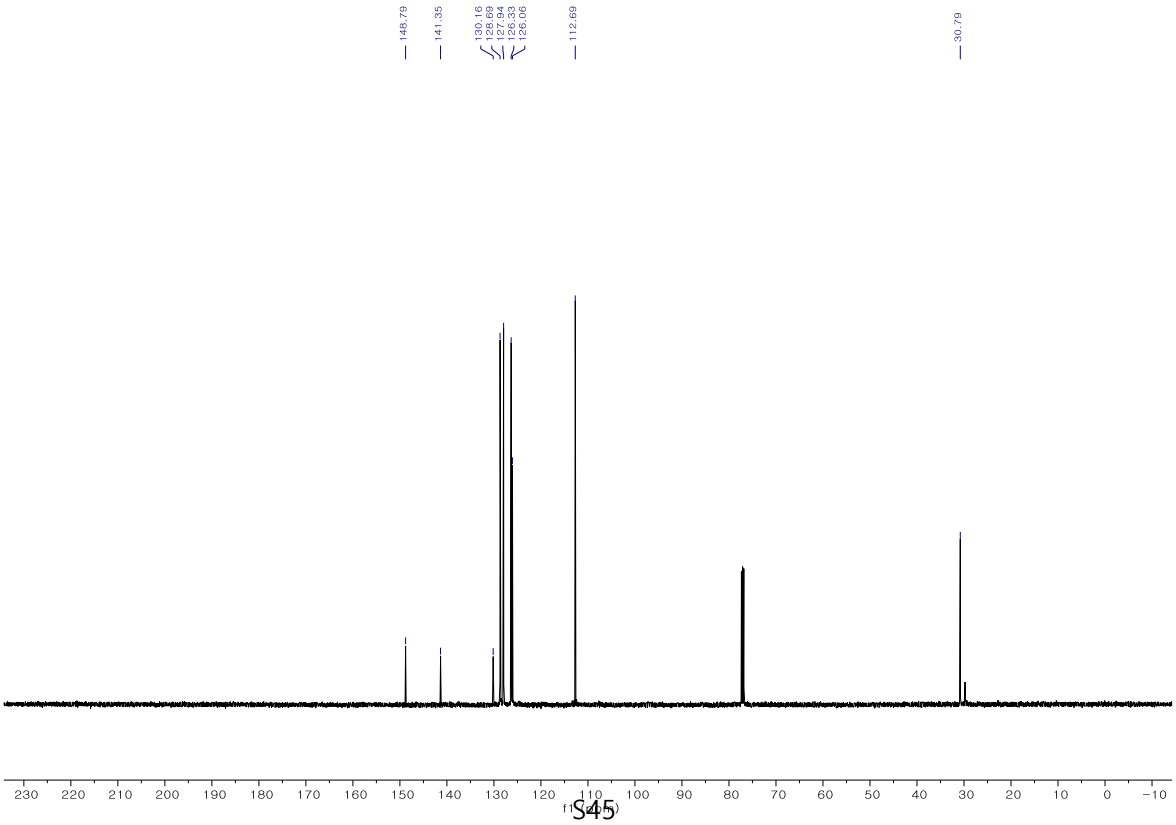

**4-Fluoro-*N*-methylaniline,[2] 2d**

A yellow liquid. $^{1}$H NMR (400 MHz, Chloroform-*d*) δ 7.02–6.81 (m, 2H), 6.64–6.40 (m, 2H), 3.59 (s, 1H), 2.81 (s, 3H). $^{13}$C NMR (101 MHz, Chloroform-*d*) δ 155.78 (d, *J* = 234.3 Hz), 145.70, 115.56 (d, *J* = 22.3 Hz), 113.09 (d, *J* = 7.4 Hz), 31.29.

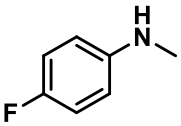

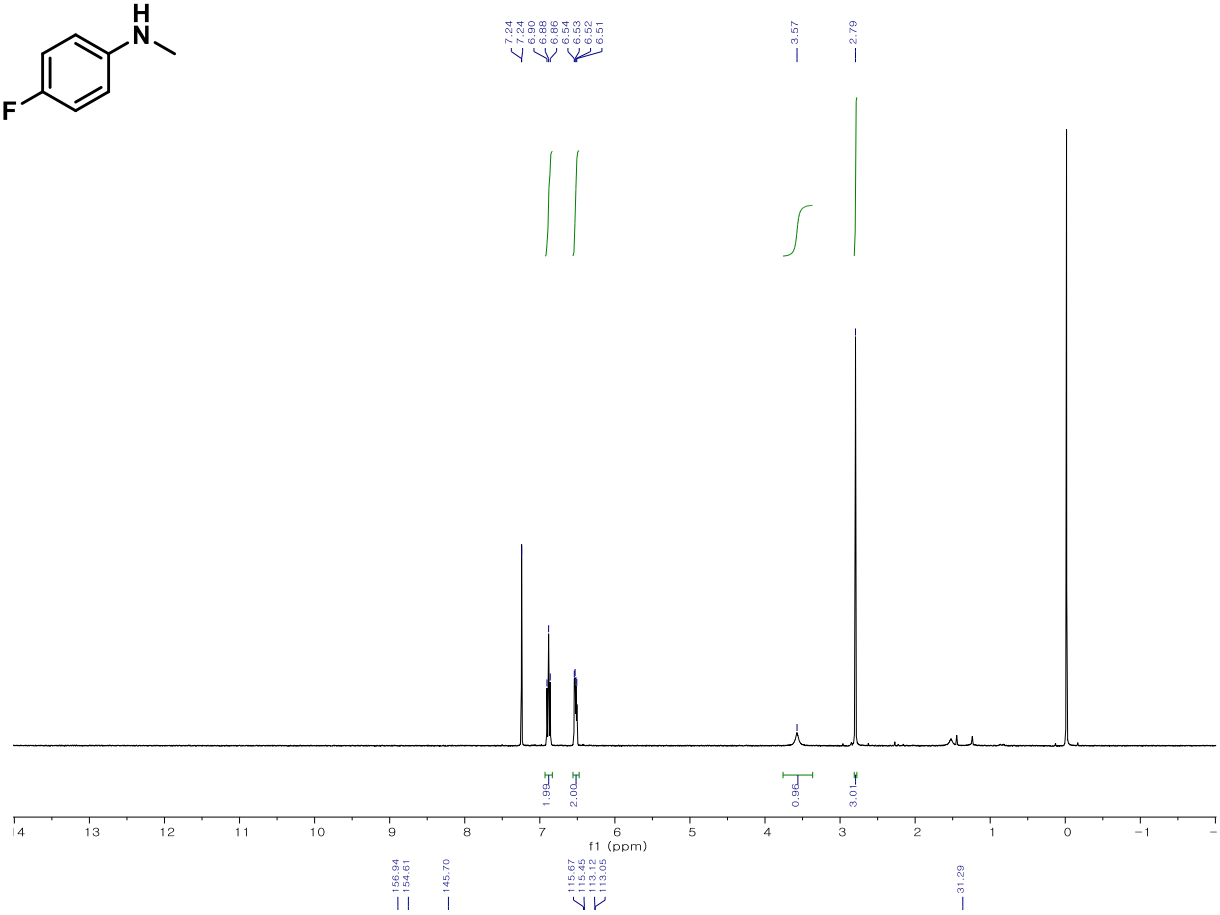


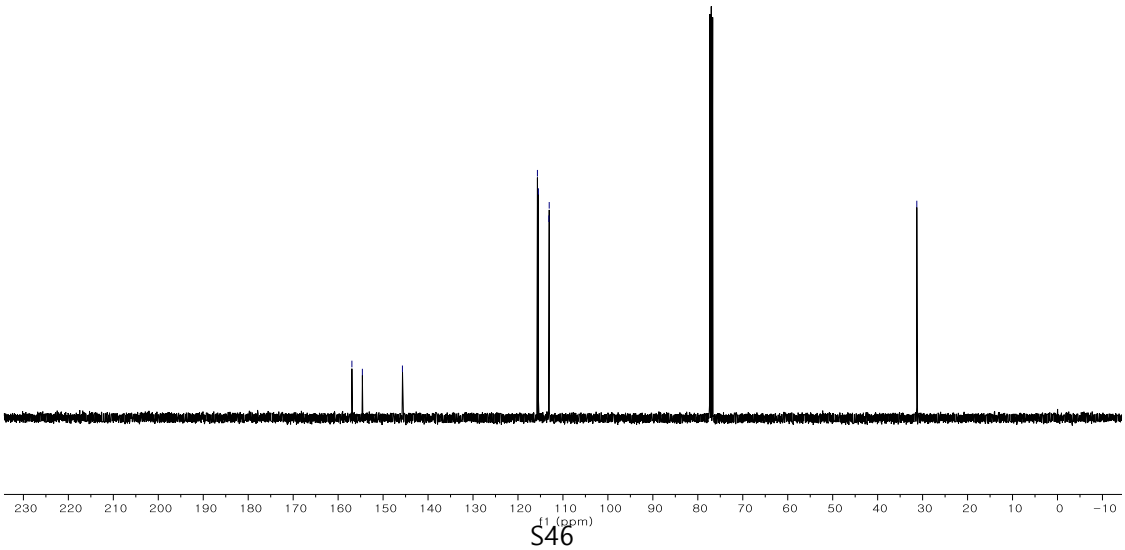

## *N*,4-Dimethylaniline,[1] 2e

A yellow liquid, $^{1}$H NMR (400 MHz, Chloroform-*d*) δ 7.00 (d, *J* = 8.0 Hz, 2H), 6.55 (d, *J* = 8.0 Hz, 2H), 3.60 (br, 1H), 2.82 (s, 3H), 2.24 (s, 3H). $^{13}$C NMR (101 MHz, Chloroform-*d*) δ 147.16, 129.69, 126.45, 112.60, 31.09, 20.38.

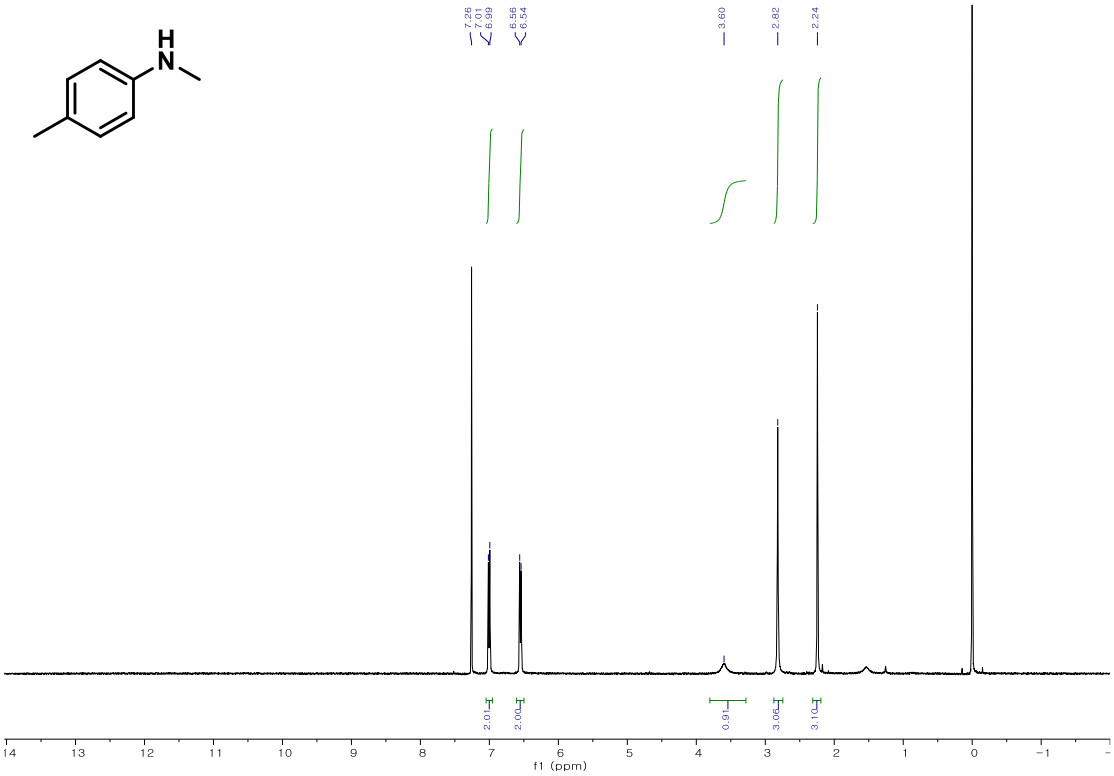


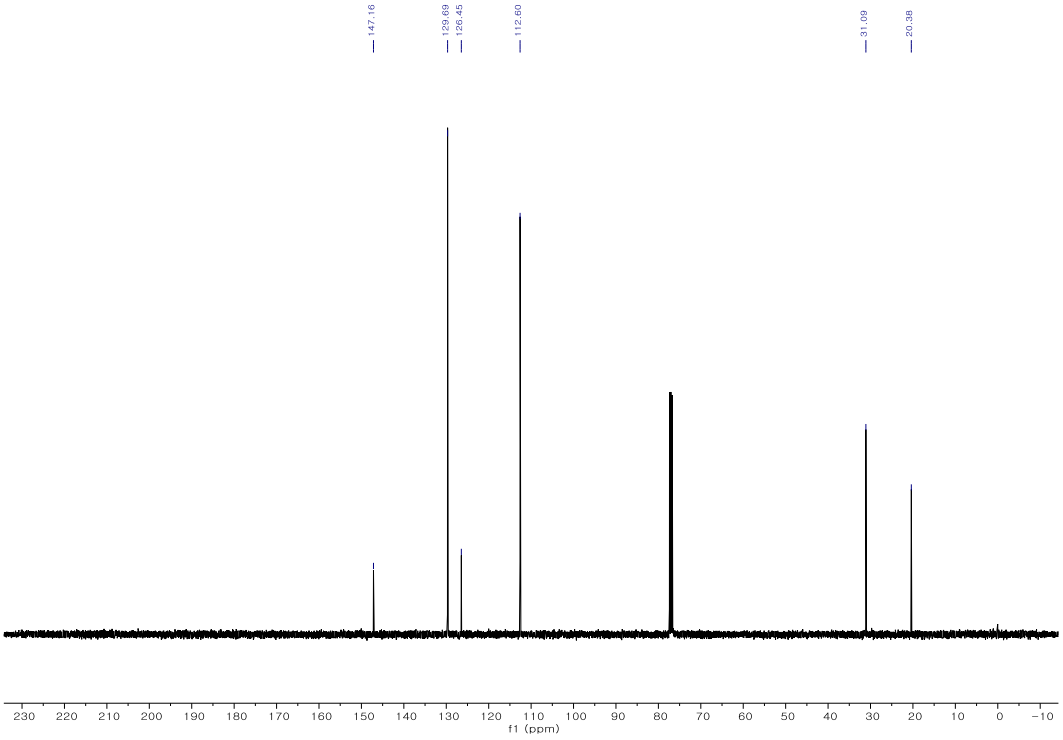

**4-*tert*-Butyl-*N*-methylaniline,[2] 2f**

A yellow oil. $^{1}$H NMR (400 MHz, Chloroform-*d*) δ 7.22 (d, *J* = 8.0 Hz, 2H), 6.58 (s, 2H), 3.45 (s, 1H), 2.81 (s, 3H), 1.28 (s, 9H). $^{13}$C NMR (126 MHz, Chloroform-*d*) δ 147.02, 140.11, 125.99, 112.26, 33.86, 31.58, 31.01.

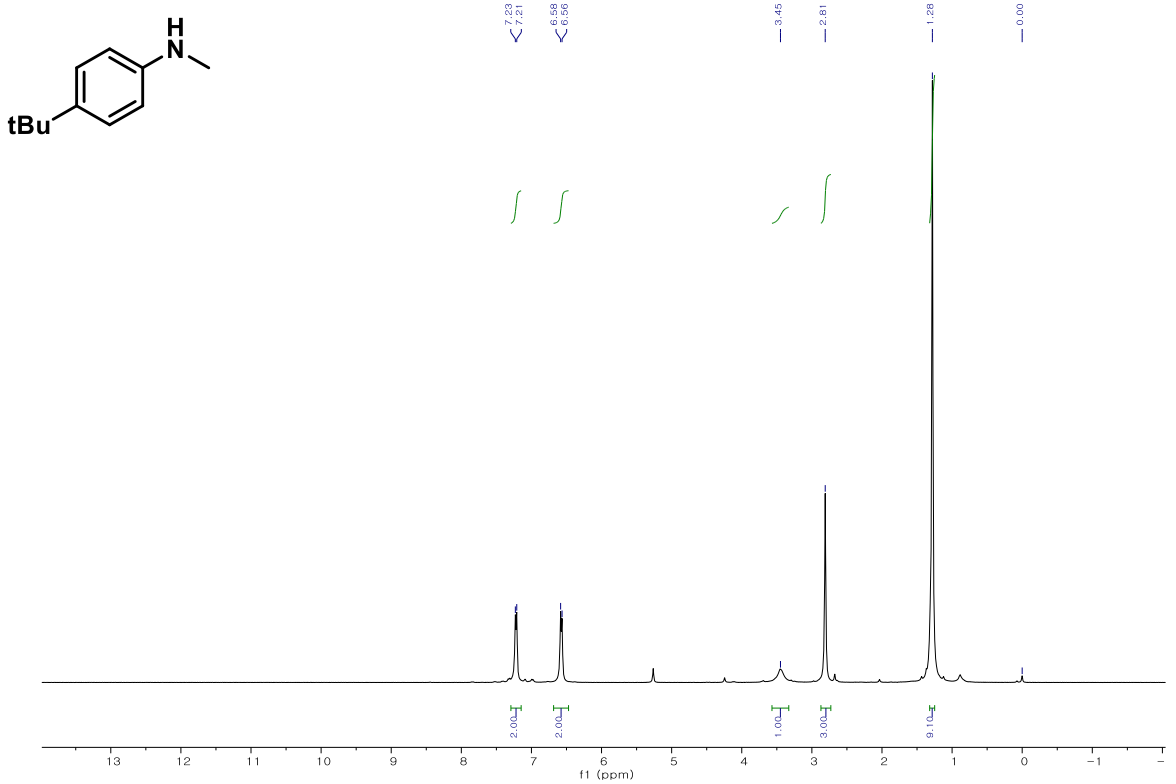


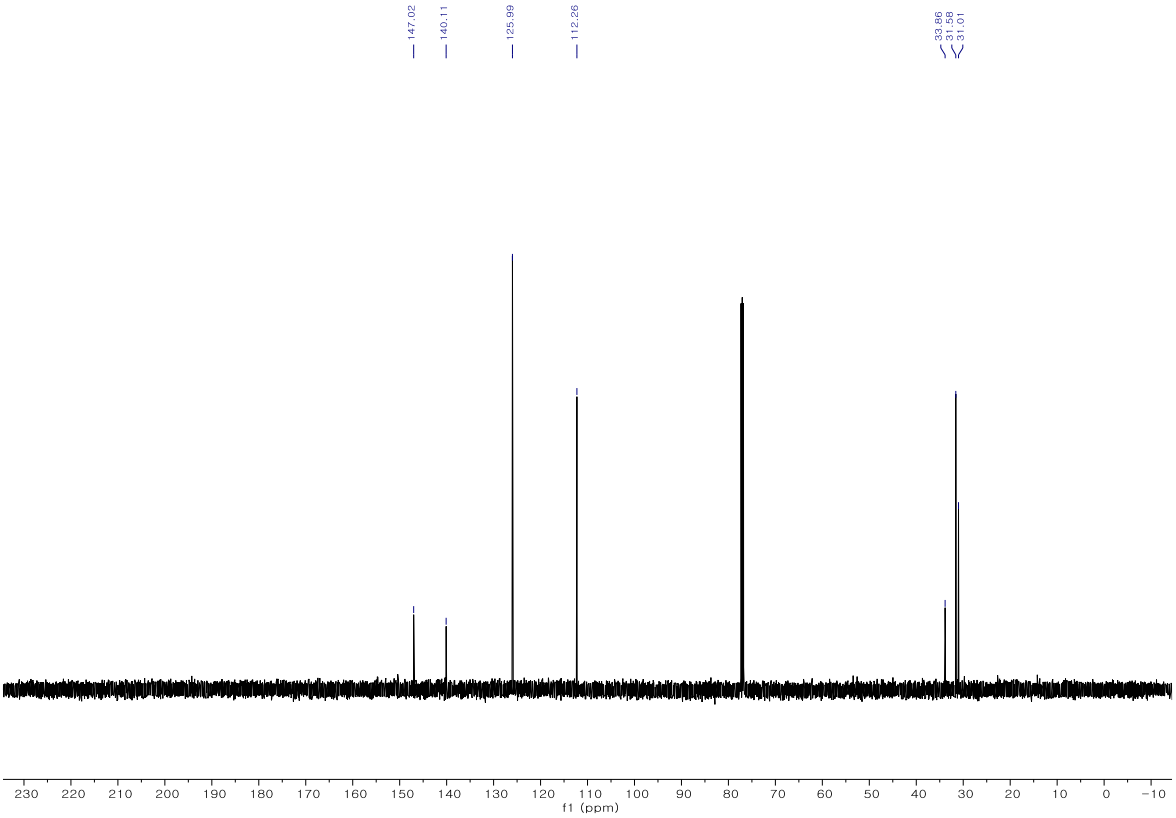

## *N*,3-Dimethylaniline,[1] 2g

A colorless liquid. $^{1}$H NMR (400 MHz, Chloroform-*d*) δ 7.08 (t, *J* = 7.8 Hz, 1H), 6.54 (d, *J* = 7.5 Hz, 1H), 6.44–6.43 (m, 2H), 3.66 (s, 1H), 2.83 (s, 3H), 2.29 (s, 3H). $^{13}$C NMR (101 MHz, Chloroform-*d*) δ 149.40, 138.96, 129.06, 118.19, 113.16, 109.62, 30.76, 21.62.

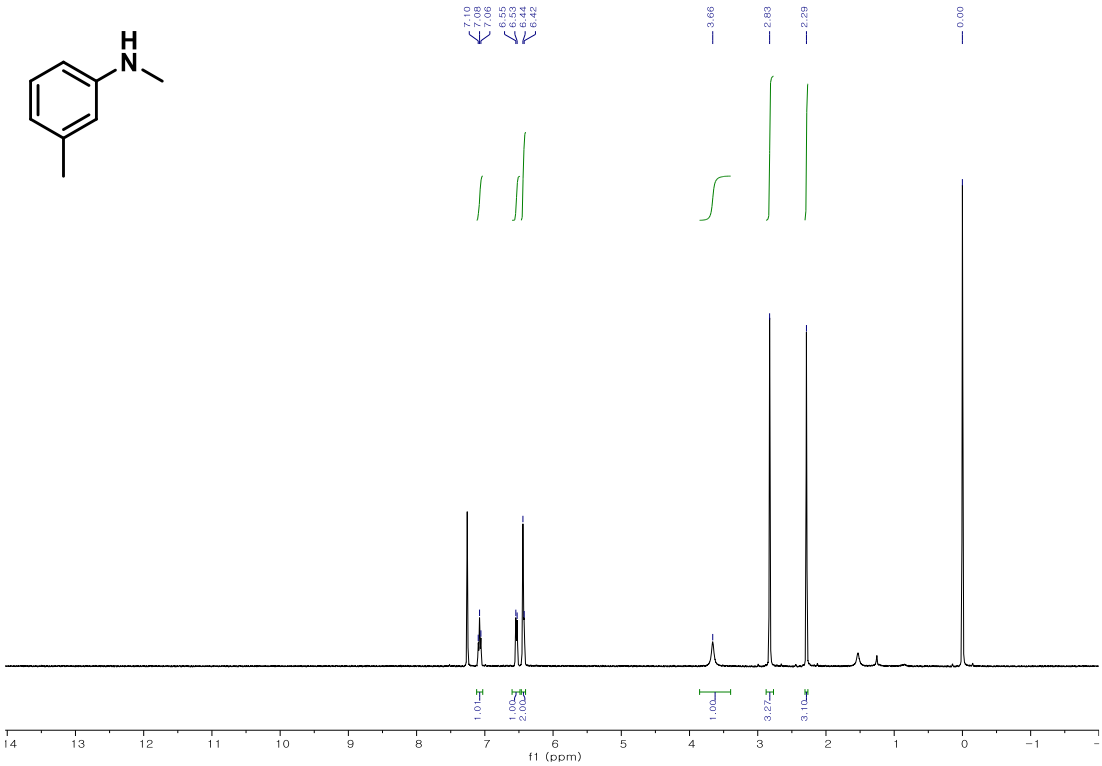


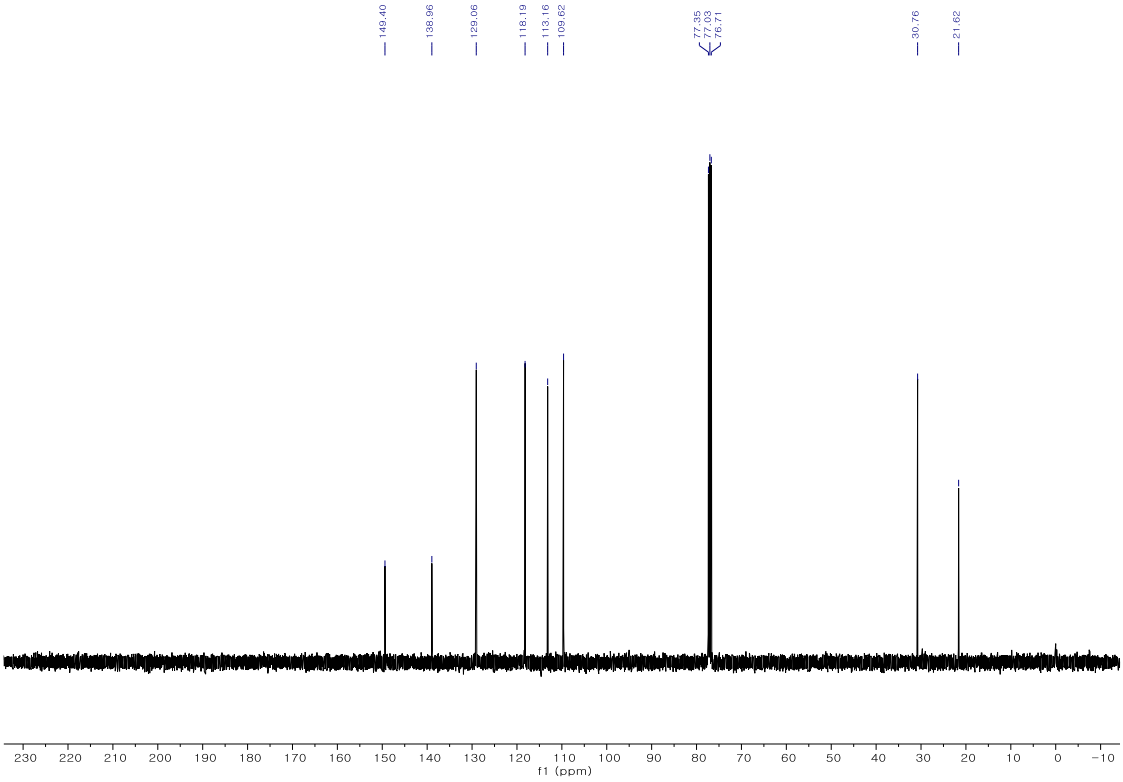

## *N*,2-Dimethylaniline,[1] 2h

A colorless liquid. $^{1}$H NMR (400 MHz, Chloroform-*d*) δ 7.16 (t, *J* = 7.9 Hz, 1H), 7.06 (d, *J* = 7.3 Hz, 1H), 6.75–6.50 (m, 2H), 3.57 (s, 1H), 2.90 (s, 3H), 2.14 (s, 3H). $^{13}$C NMR (101 MHz, Chloroform-*d*) δ 147.22, 129.88, 127.17, 121.88, 116.84, 109.12, 30.75, 17.36.

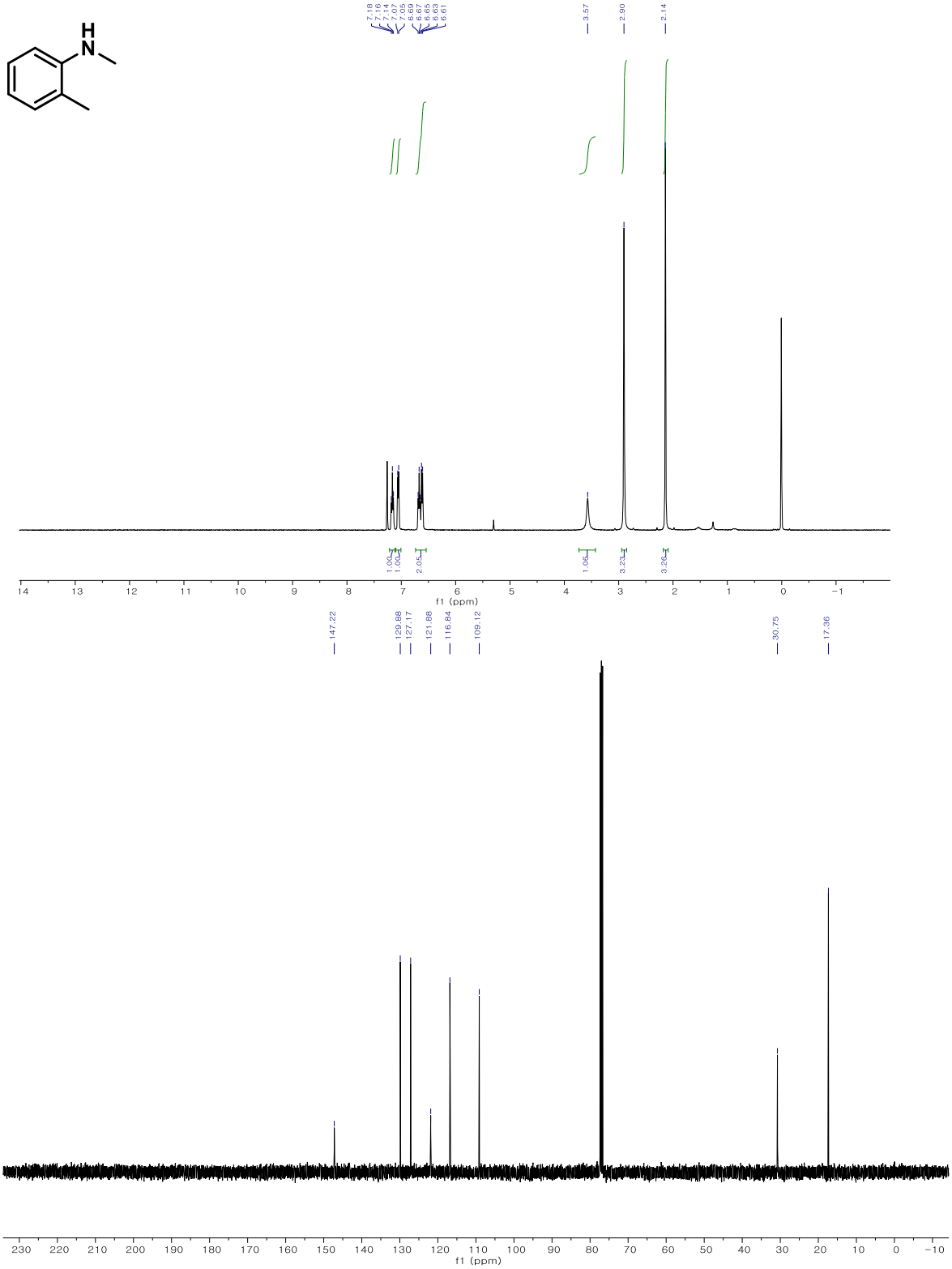

**N,3,5-Trimethylaniline,[1] 2i**

A yellow liquid. $^{1}$H NMR (400 MHz, Chloroform-*d*) δ 6.38 (s, 1H), 6.26 (s, 2H), 3.53 (s, 1H), 2.81 (s, 3H), 2.25 (s, 6H). $^{13}$C NMR (126 MHz, Chloroform-*d*) δ 149.53, 138.88, 119.32, 110.44, 30.85, 21.54.

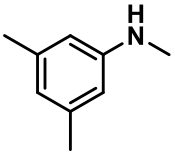

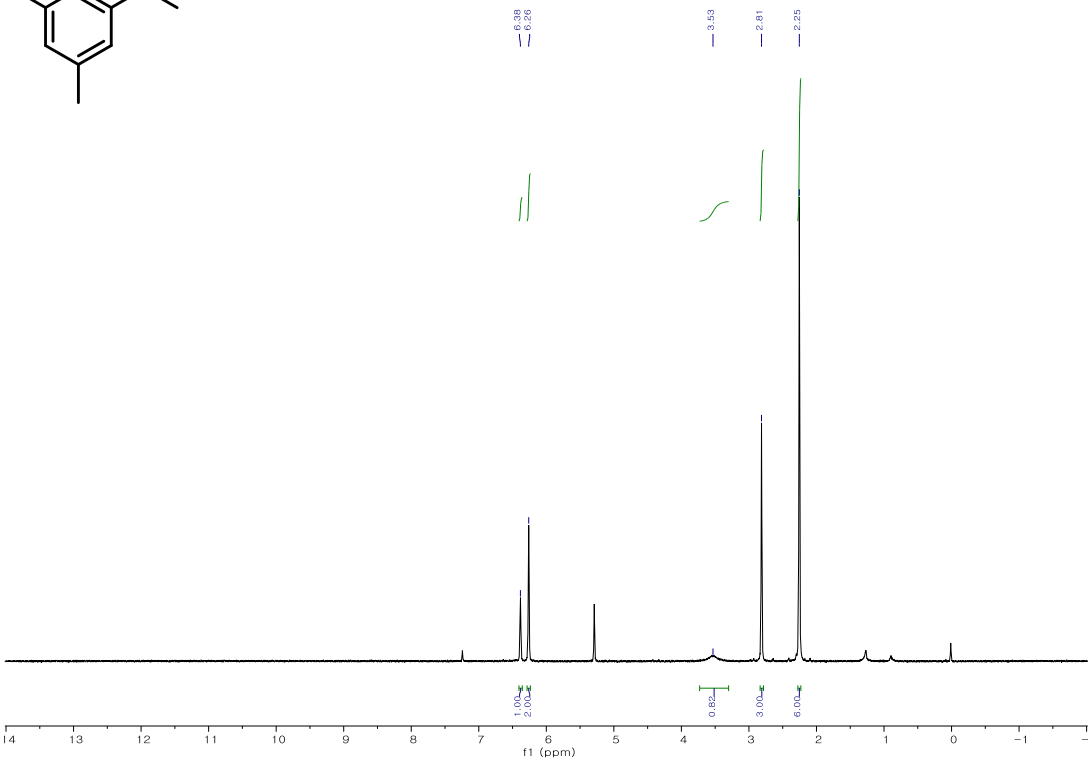


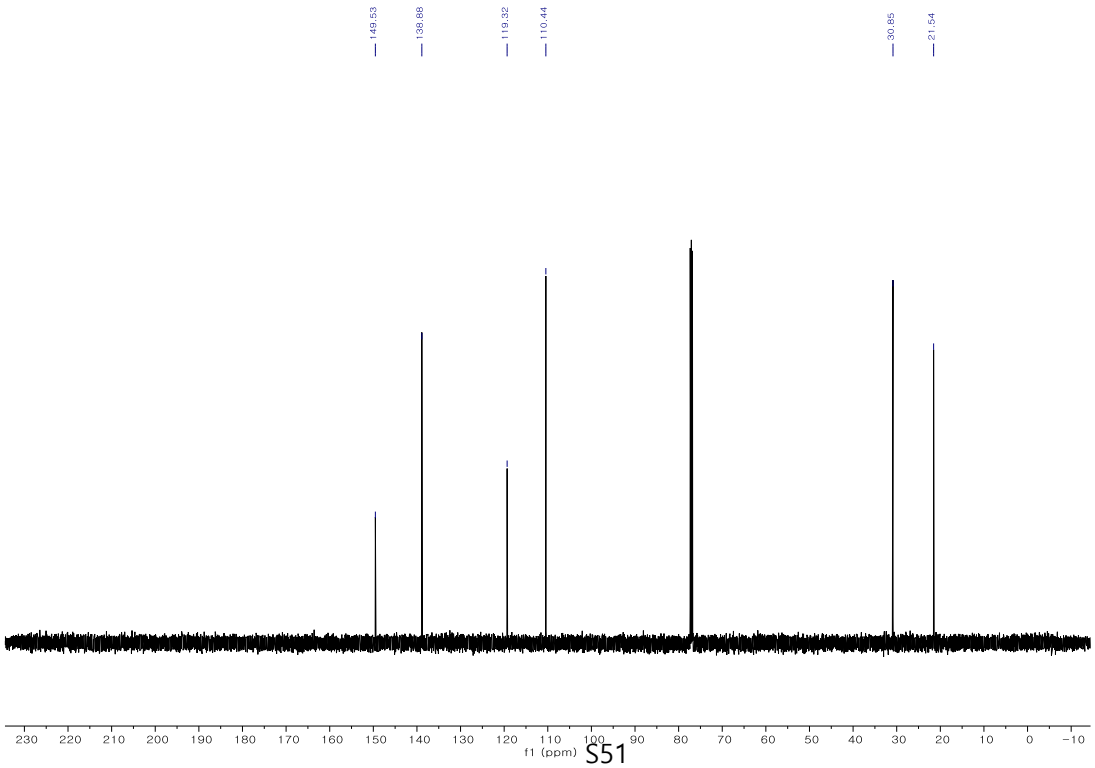

**4-Ethyl-*N*-methylaniline,[3] 2j**

A yellow oil. $^{1}$H NMR (400 MHz, Chloroform-*d*) δ 7.03 (d, *J* = 8.0 Hz, 2H), 6.57 (d, *J* = 8.0 Hz, 2H), 3.57 (br, 1H), 2.82 (s, 3H), 2.55 (q, *J* = 7.6 Hz, 2H), 1.19 (t, *J* = 7.3 Hz, 3H). $^{13}$C NMR (101 MHz, Chloroform-*d*) δ 147.35, 133.15, 128.52, 112.59, 31.05, 27.94, 16.03.

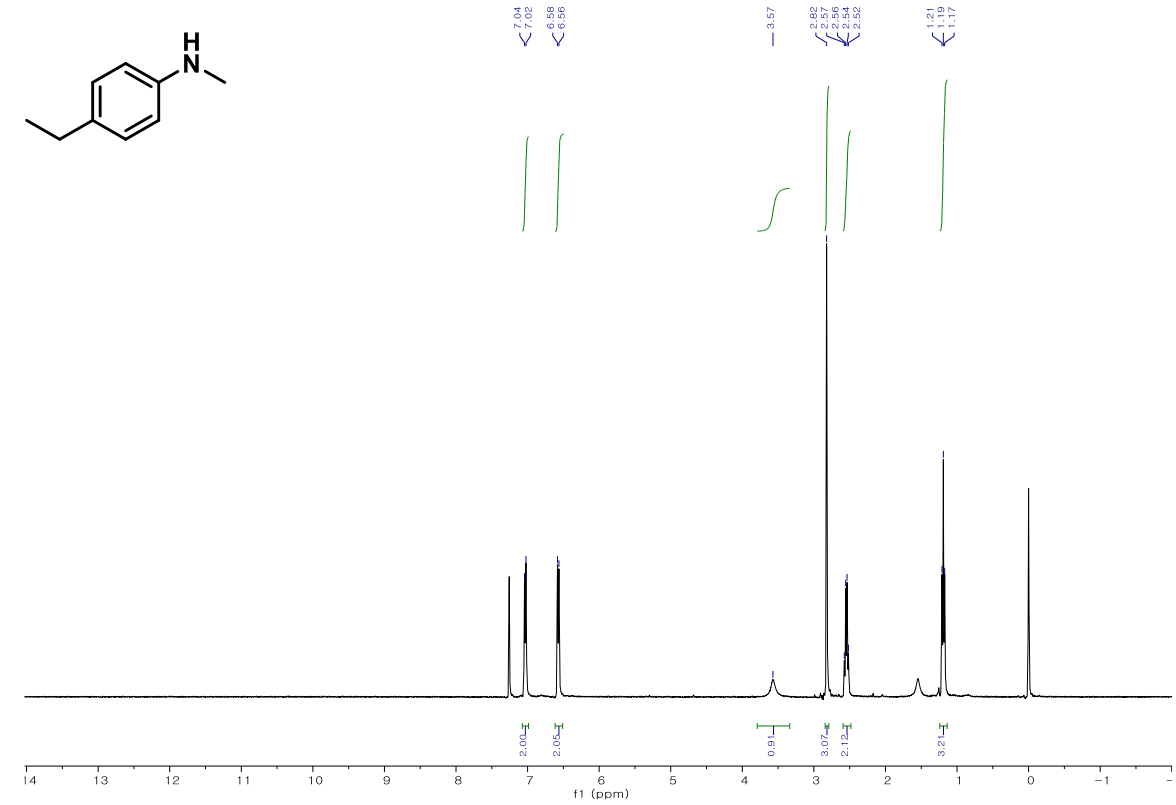


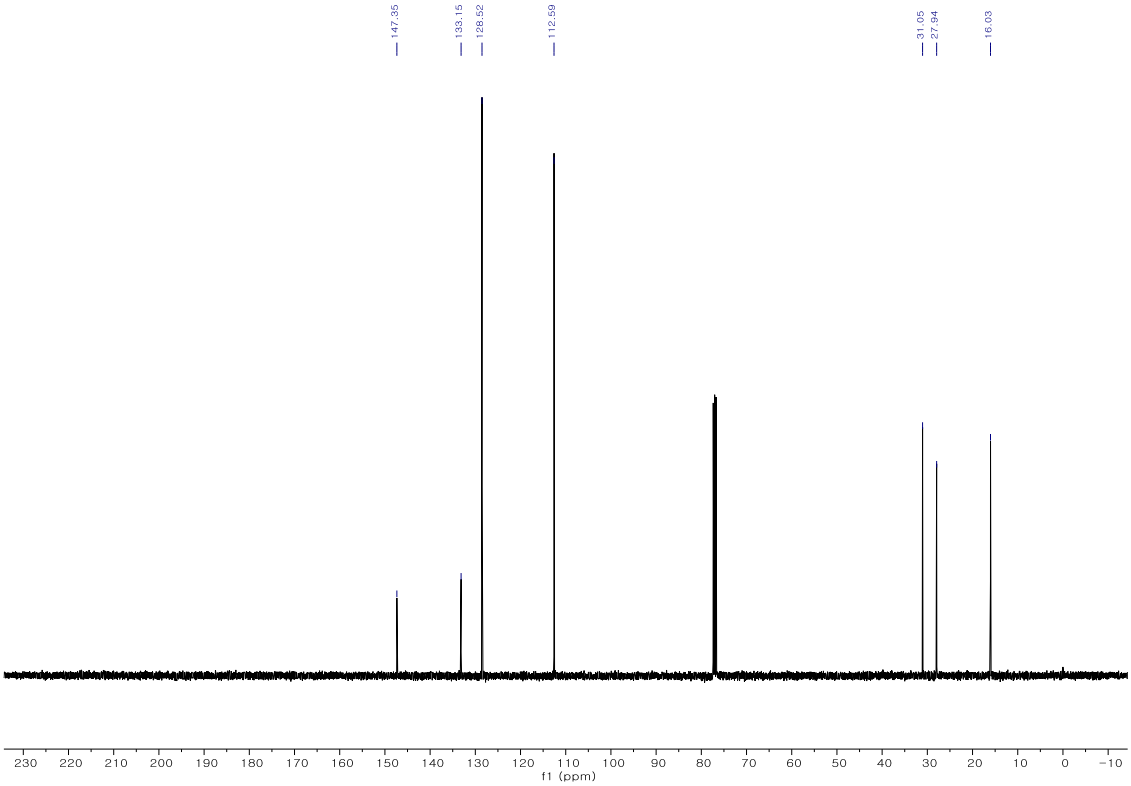

## *N*-Methyl-4-(propan-2-yl)aniline,[3] 2k

A yellow oil. $^{1}$H NMR (400 MHz, Chloroform-*d*) δ 7.07 (d, *J* = 8.4 Hz, 2H), 6.58 (d, *J* = 8.5 Hz, 2H), 2.83 (s, 4H), 1.22 (d, *J* = 6.9 Hz, 6H). $^{13}$C NMR (101 MHz, Chloroform-*d*) δ 147.40, 137.83, 127.04, 112.52, 33.16, 31.01, 24.26.

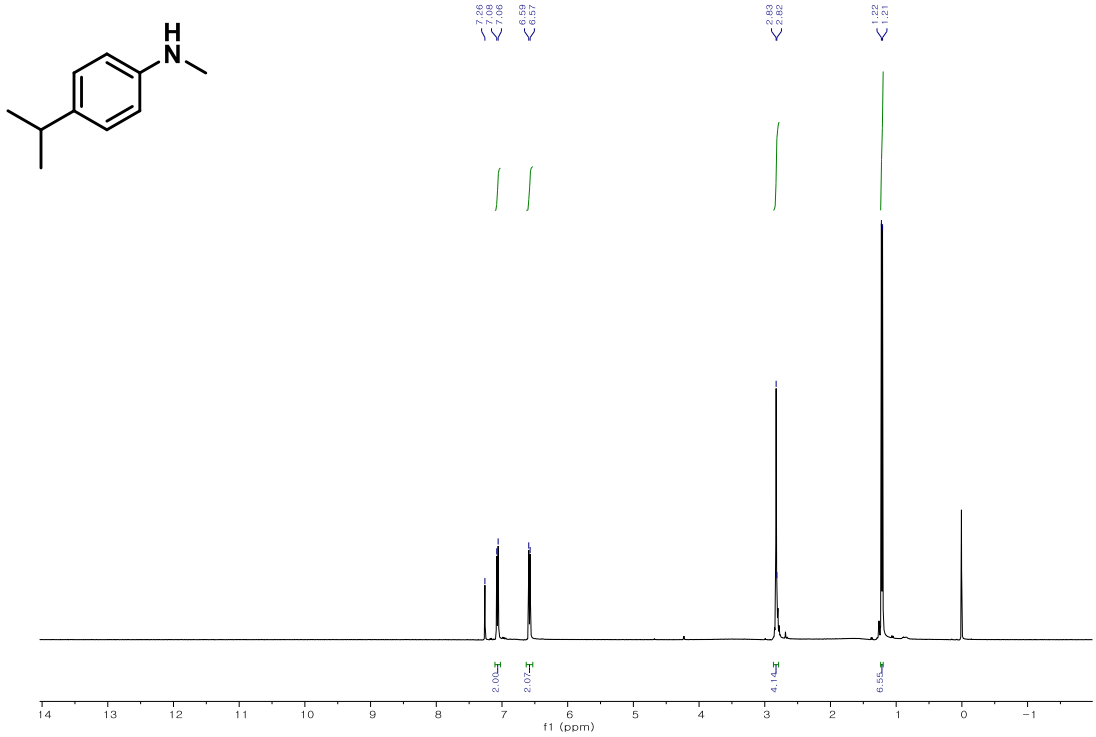


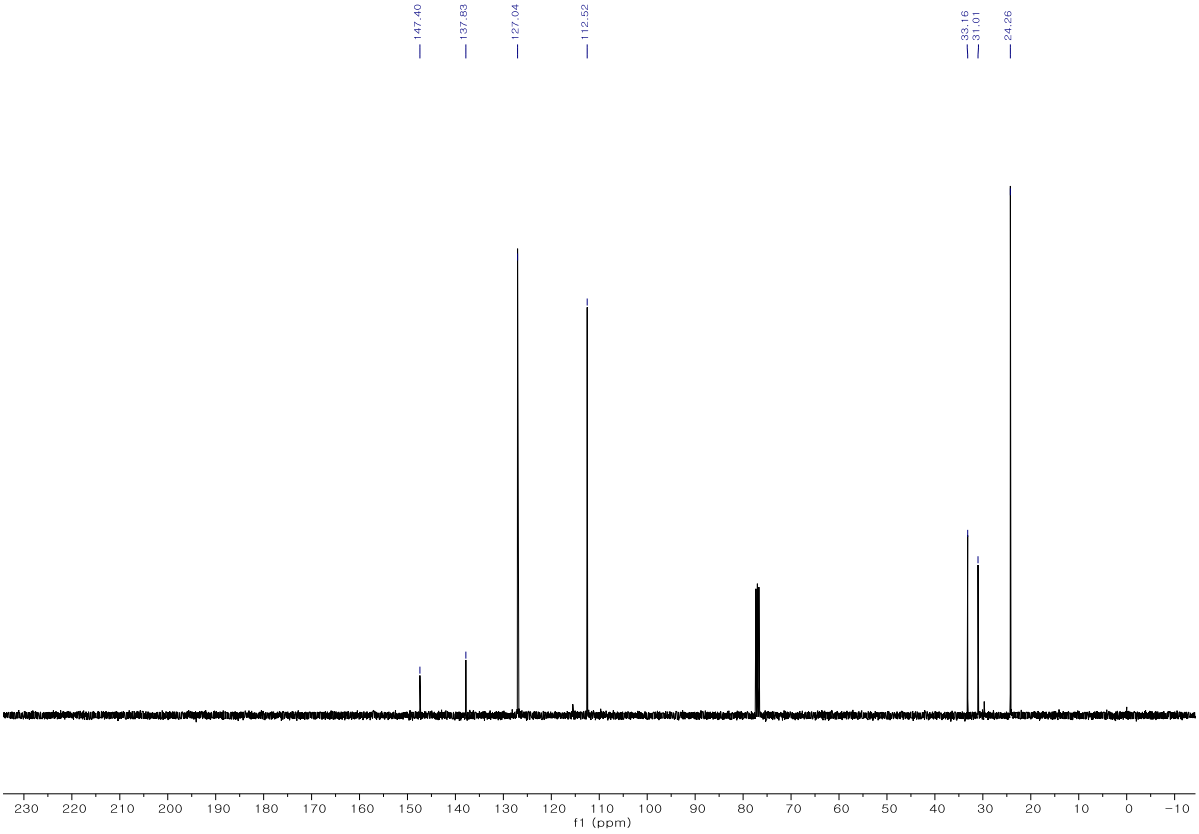

**4-Methylamino-benzamide,[13] 2l**

A brown solid. $^{1}$H NMR (400 MHz, DMSO-$d_6$) δ 7.66 (d, $J$ = 8.3 Hz, 2H), 7.55 (s, 1H), 6.85 (s, 1H), 6.50 (d, $J$ = 8.4 Hz, 2H), 6.17 (s, 1H), 2.70 (s, 3H). $^{13}$C NMR (101 MHz, DMSO-$d_6$) δ 168.52, 152.67, 129.50, 121.13, 110.72, 29.77.

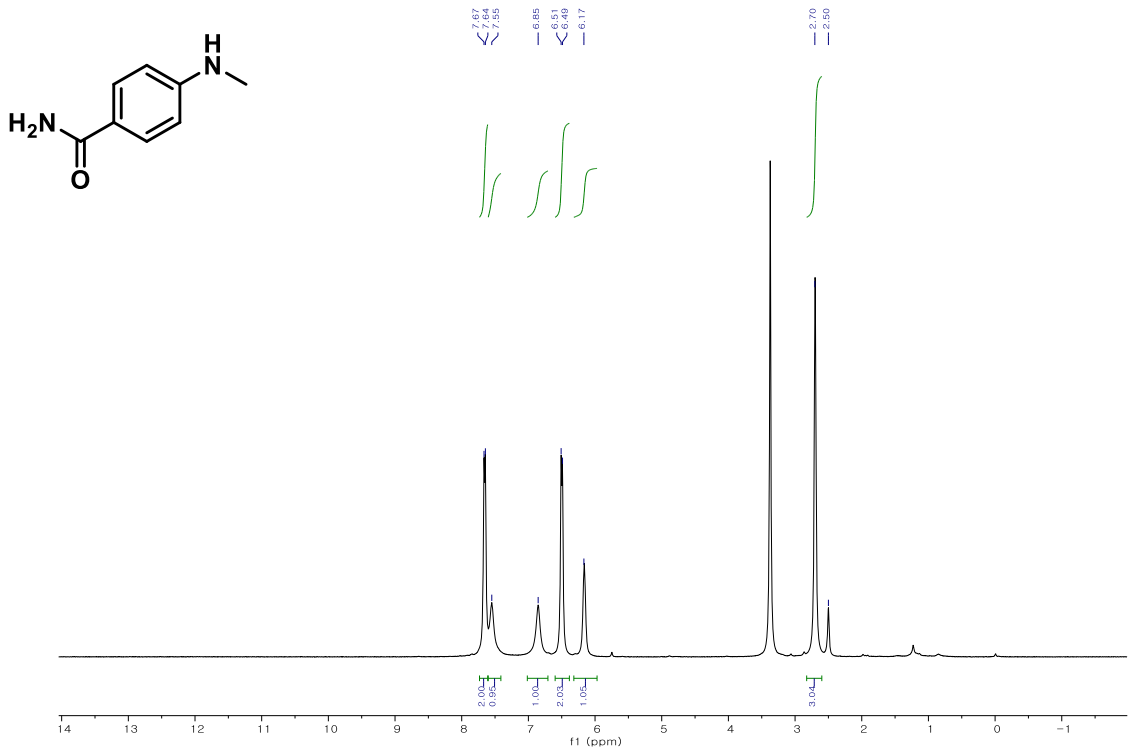


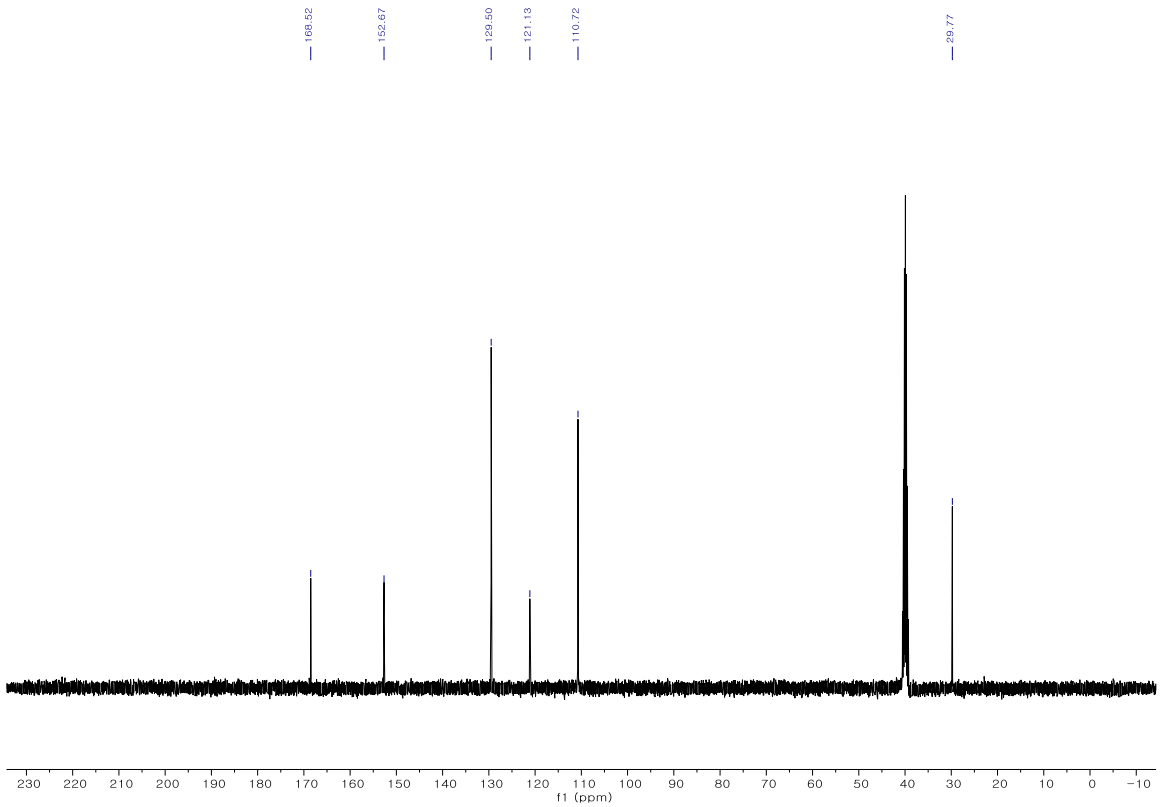

## *N*-Methyl-pyridin-3-amine,[2] 2m

A yellow oil. $^{1}$H NMR (400 MHz, Chloroform-*d*) δ 8.02 (d, *J* = 2.9 Hz, 1H), 7.95 (dd, *J* = 4.7, 1.4 Hz, 1H), 7.12–7.02 (m, 1H), 6.93–6.81 (m, 1H), 3.81 (s, 1H), 2.84 (s, 3H). $^{13}$C NMR (126 MHz, Chloroform-*d*) δ 145.17, 138.49, 135.67, 123.70, 118.03, 30.27.

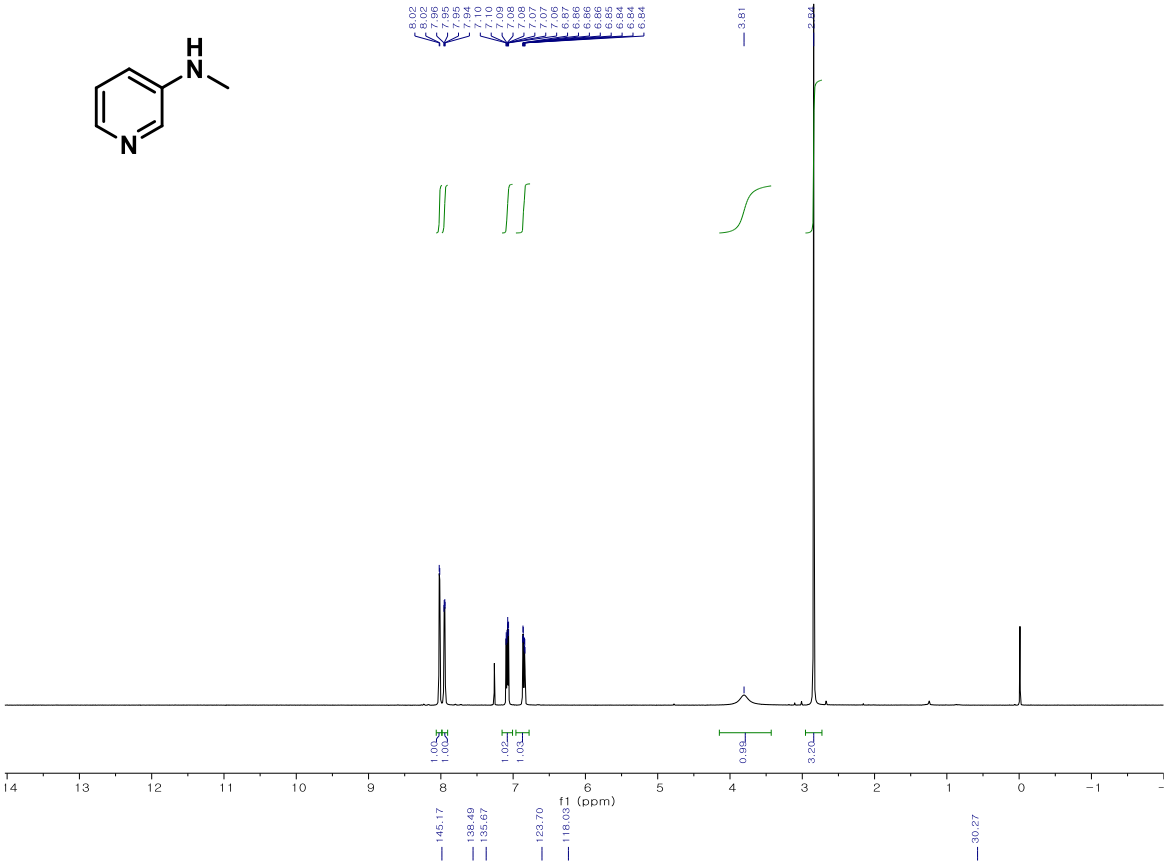


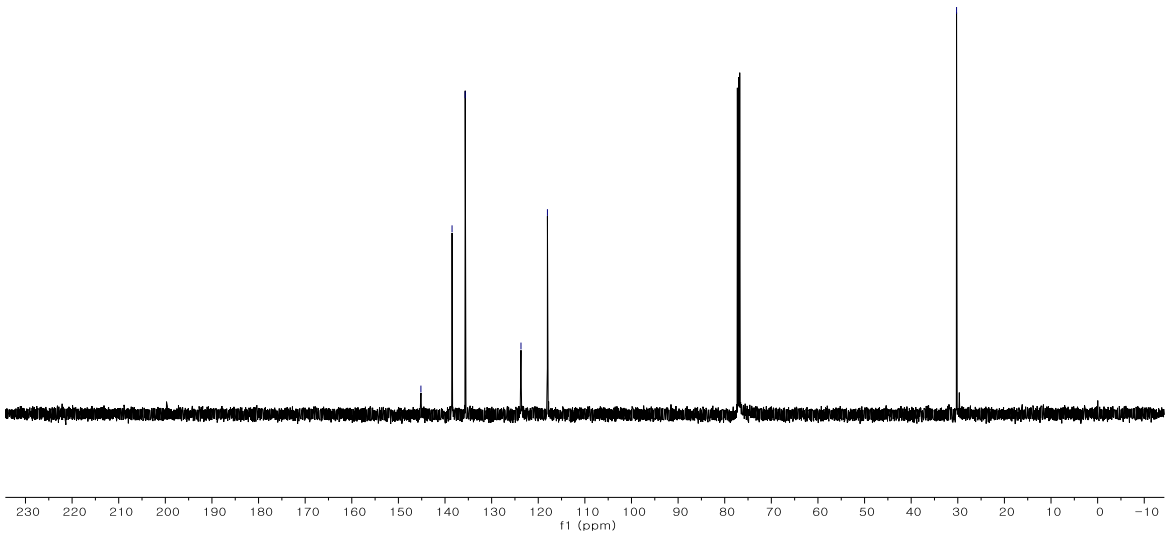

## *N*-Methylquinolin-5-amine,[14] 2n

A yellow liquid. $^{1}$H NMR (400 MHz, Chloroform-*d*) δ 8.90 – 8.80 (m, 1H), 8.14 (d, *J* = 8.6 Hz, 1H), 7.60 (t, *J* = 8.1 Hz, 1H), 7.49 (d, *J* = 8.5 Hz, 1H), 7.36 – 7.28 (m, 1H), 6.63 (d, *J* = 7.6 Hz, 1H), 4.46 (br, 1H), 3.02 (s, 3H). $^{13}$C NMR (101 MHz, Chloroform-*d*) δ 149.90, 149.15, 144.78, 130.45, 128.72, 119.22, 118.42, 118.15, 103.94, 30.89.

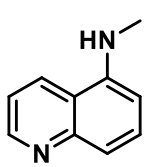


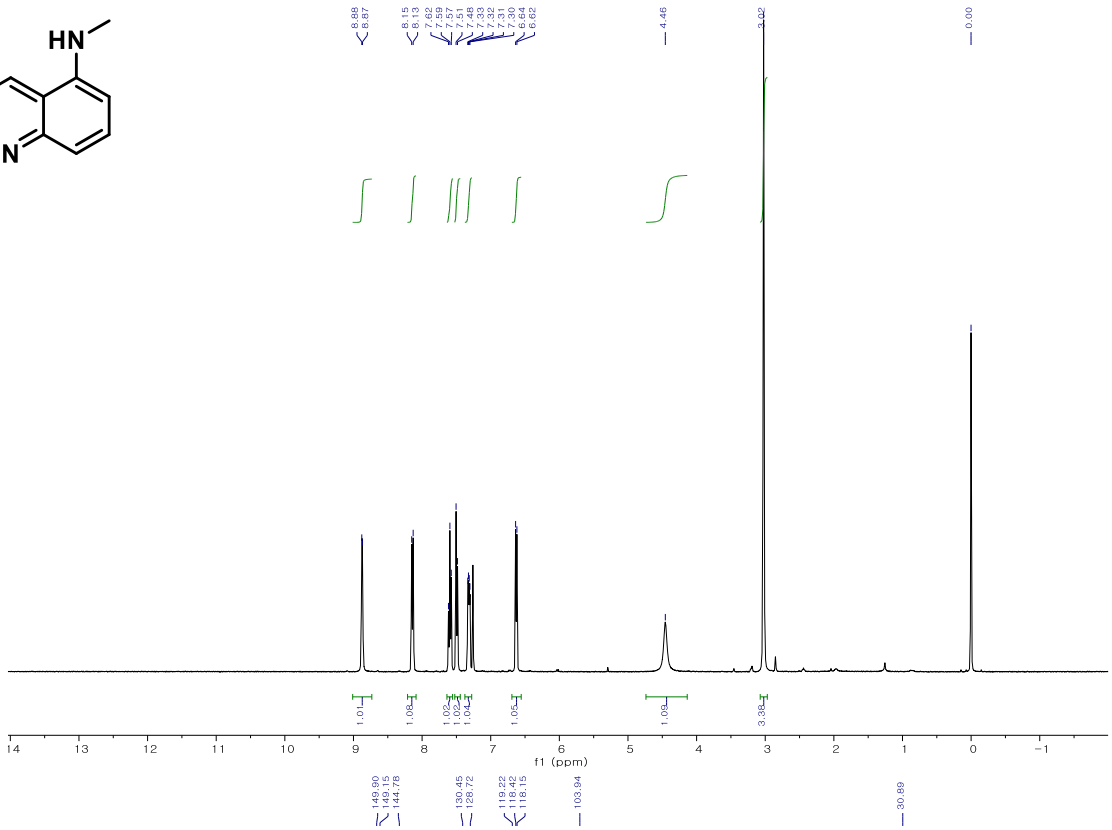


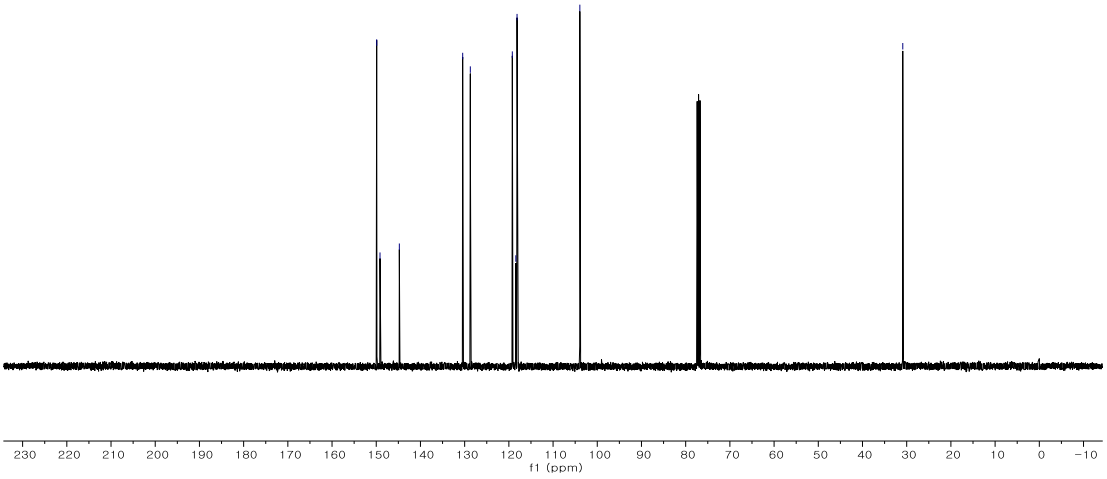

***N*-Methyl-1,3-benzodioxol-5-amine,[14] 2o**

A yellow solid. $^{1}$H NMR (400 MHz, Chloroform-*d*) δ 6.79 – 6.55 (m, 1H), 6.25 (d, *J* = 2.5 Hz, 1H), 6.04 (d, *J* = 8.3, 1H), 5.85 (s, 2H), 3.51 (br, 1H), 2.79 (s, 3H). $^{13}$C NMR (101 MHz, Chloroform-*d*) δ 148.32, 145.22, 139.50, 108.56, 103.75, 100.51, 95.55, 31.60.

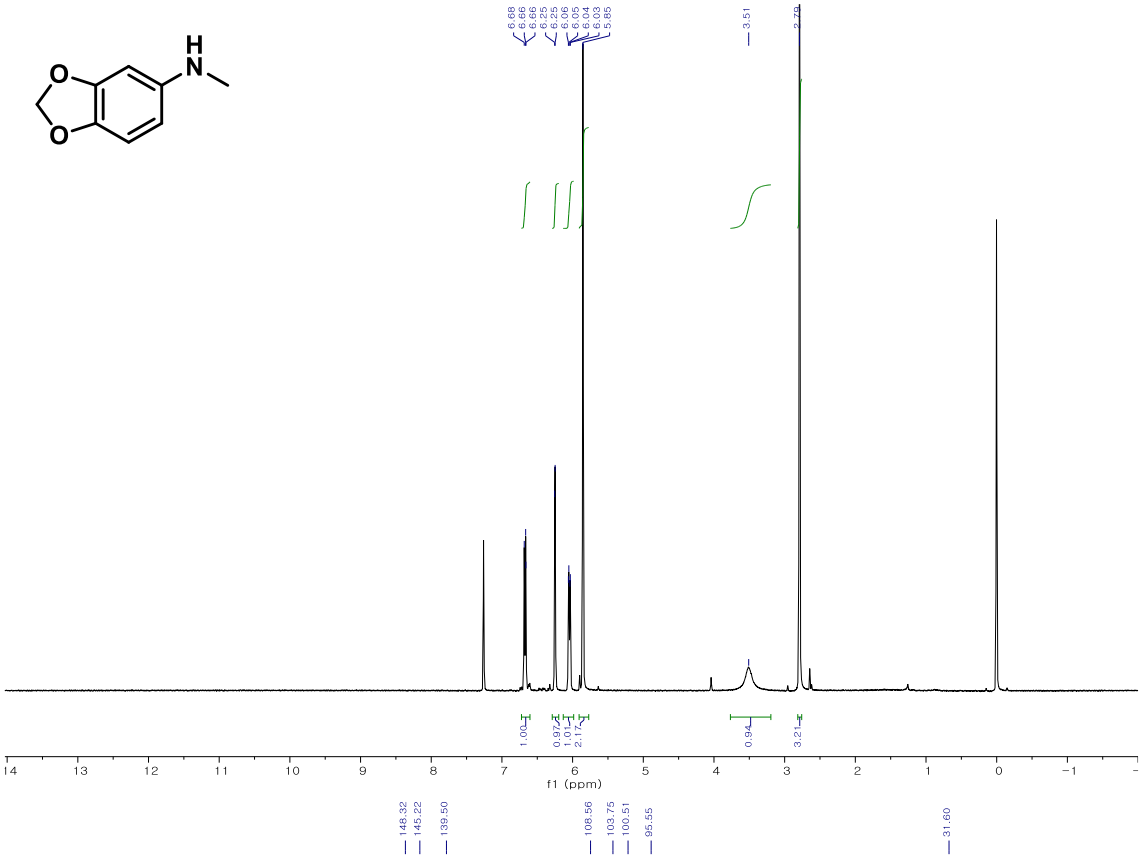


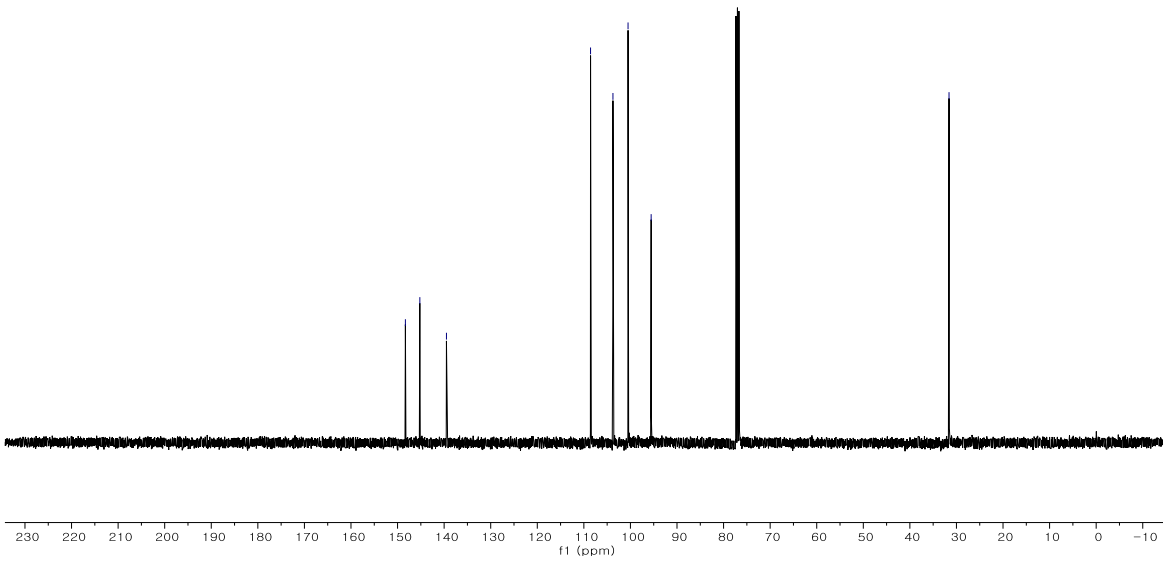

**4-Benzoyl-*N*-methylaniline,[15] 2p**

A yellow soild. $^{1}$H NMR (400 MHz, Chloroform-*d*) δ 7.77-7.17 (m, 4H), 7.53 (t, *J* = 7.4 Hz, 1H), 7.45 (t, *J* = 7.4 Hz, 2H), 6.59 (d, *J* = 8.8 Hz, 2H), 4.29 (s, 1H), 2.92 (d, *J* = 5.0 Hz, 3H). $^{13}$C NMR (101 MHz, Chloroform-*d*) δ 195.26, 153.09, 139.19, 132.95, 131.16, 129.41, 128.01, 125.81, 110.94, 30.04.

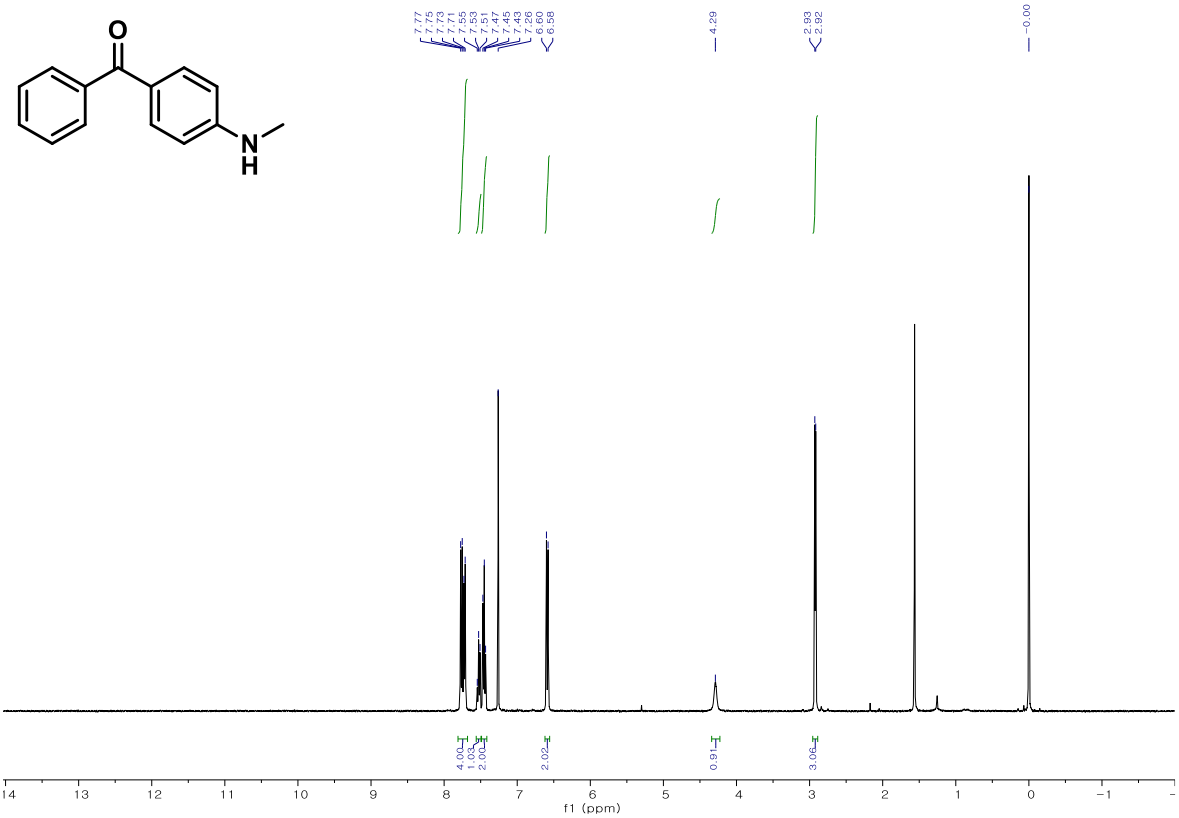


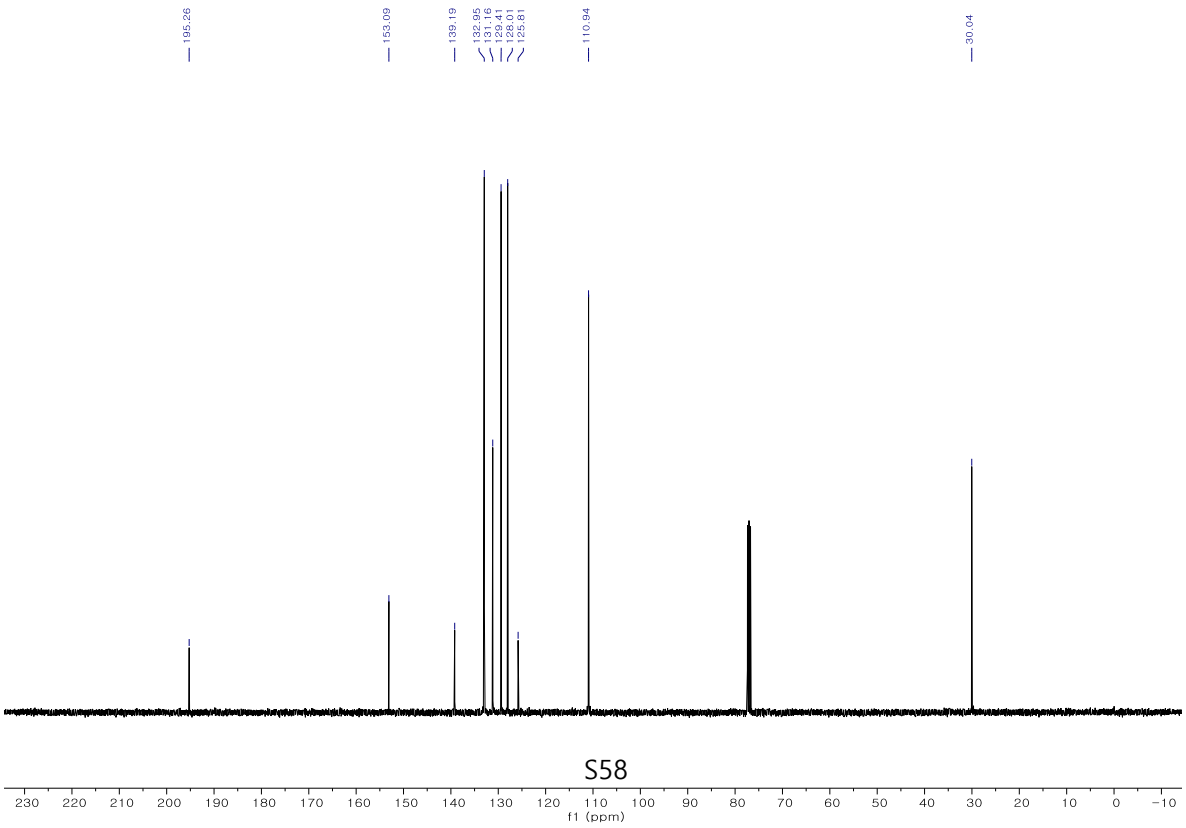

**1-Methyl-4-phenylpiperidine,[16] 2q**

A yellow oil. $^{1}$H NMR (400 MHz, Chloroform-*d*) δ 7.45 – 7.05 (m, 5H), 2.97 (d, *J* = 11.2 Hz, 2H), 2.56 – 2.39 (m, 1H), 2.32 (s, 3H), 2.15 – 1.95 (m, 2H), 1.92 – 1.73 (m, 4H). $^{13}$C NMR (101 MHz, Chloroform-*d*) δ 146.31, 128.40, 126.85, 126.11, 56.38, 46.49, 42.06, 33.50.

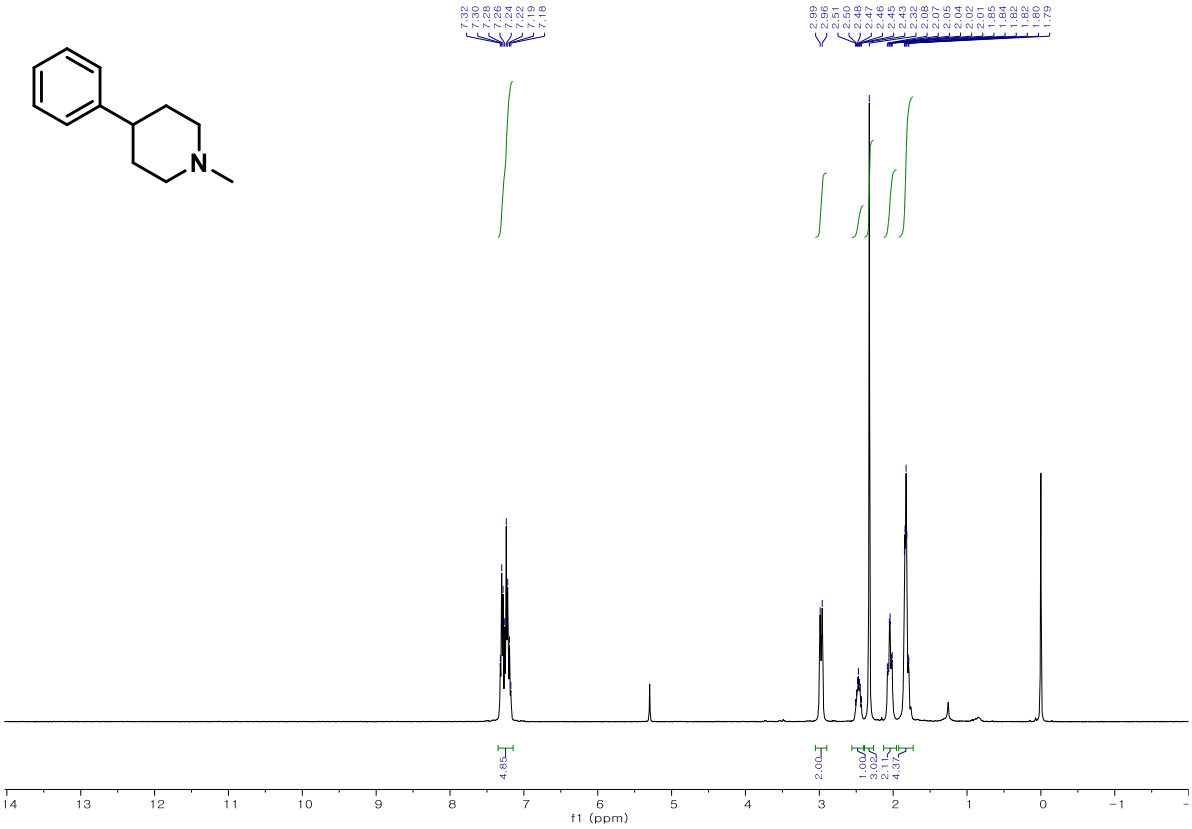


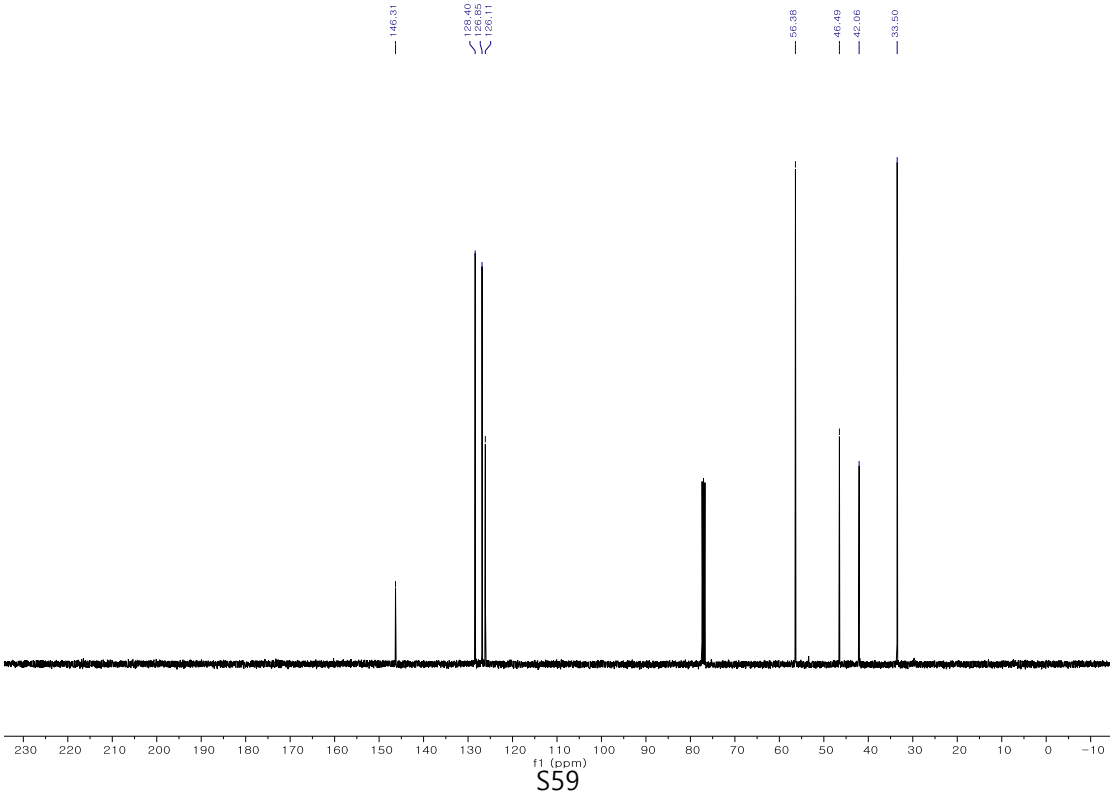

## 1-Methyl-4-phenylpiperazine,[16] 2r

A yellow oil. $^{1}$H NMR (400 MHz, Chloroform-*d*) δ 7.30 – 7.21 (m, 2H), 6.94 (d, *J* = 7.9 Hz, 2H), 6.86 (t, *J* = 7.4 Hz, 1H), 3.24 – 3.20 (m, 4H), 2.62 – 2.55 (m, 4H), 2.36 (s, 3H). $^{13}$C NMR (101 MHz, Chloroform-*d*) δ 151.25, 129.09, 119.69, 116.05, 55.12, 49.06, 46.12.

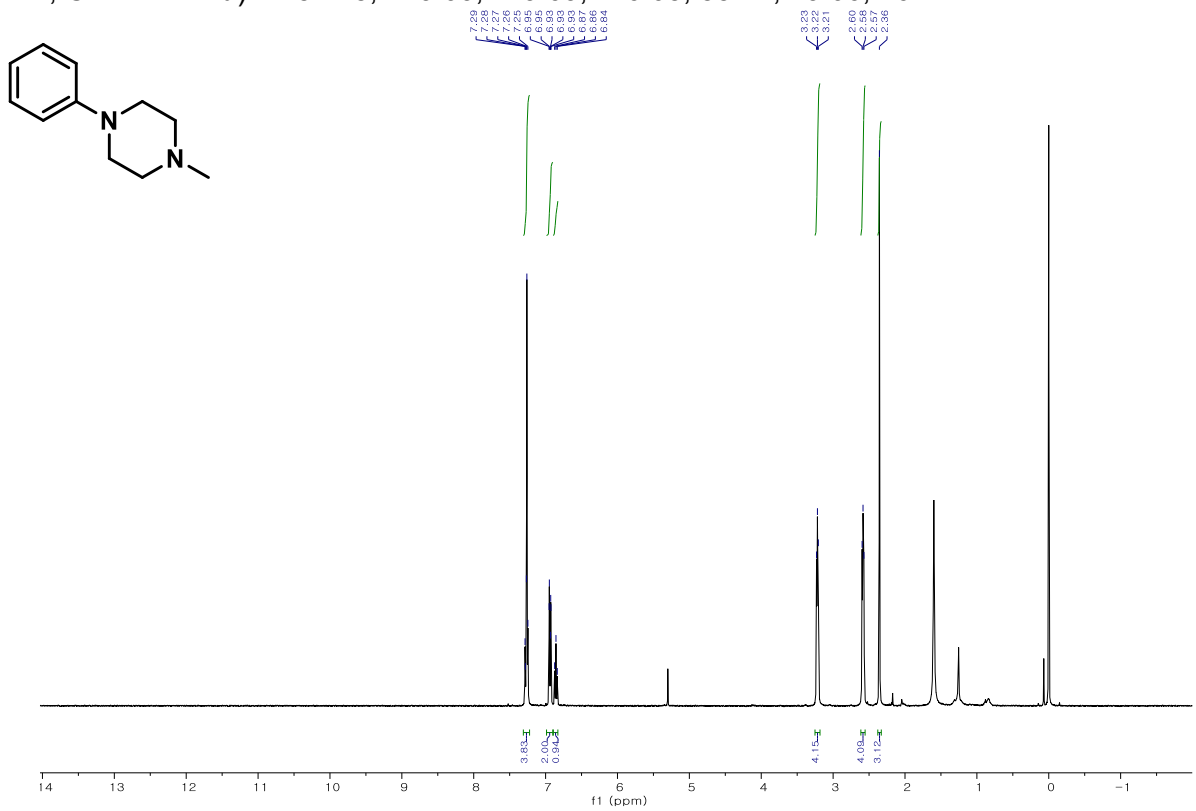


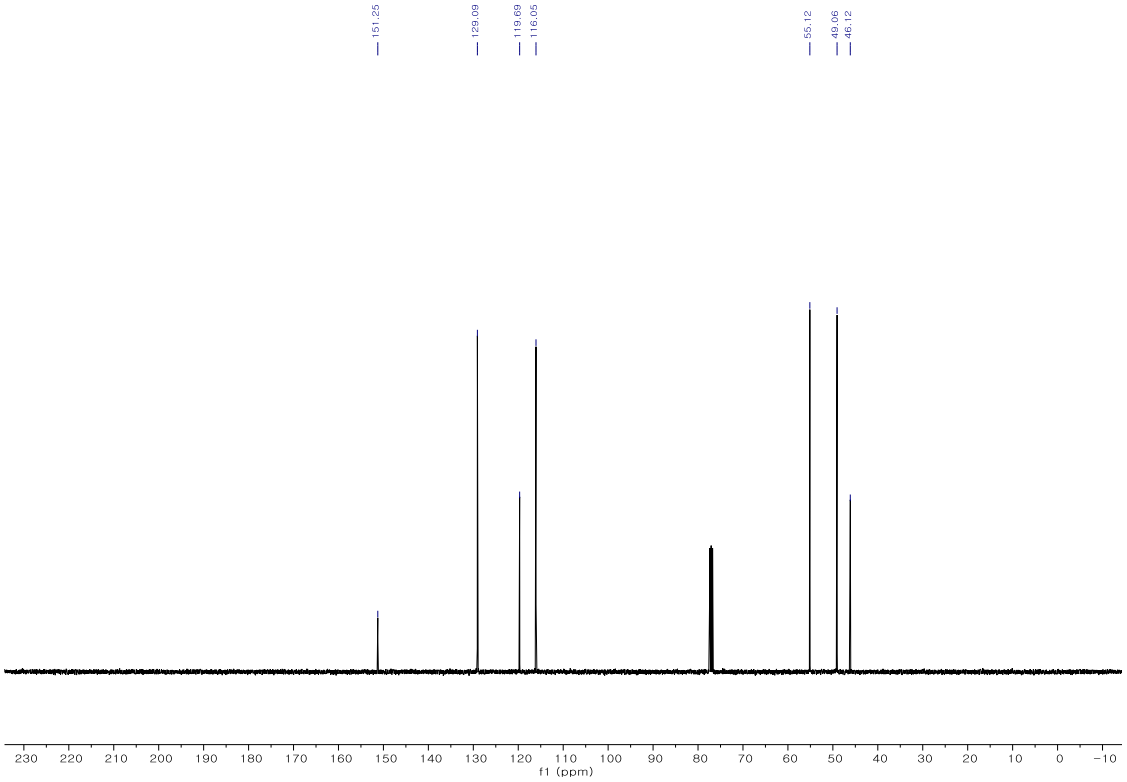

**3-(10,11-Dihydro-5*H*-dibenzo[*b,f*]azepin-5-yl)-*N*,*N*-dimethylpropan-1-amine (Imipramine),[17] 4a**

A yellow oil. $^{1}$H NMR (400 MHz, Chloroform-*d*) δ 7.15 – 7.00 (m, 6H), 6.93 – 6.85 (m, 2H), 3.76 (t, *J* = 6.9 Hz, 2H), 3.15 (s, 4H), 2.32 (t, *J* = 7.3 Hz, 2H), 2.23 – 2.05 (m, 6H), 1.73 (p, *J* = 7.1 Hz, 2H). $^{13}$C NMR (101 MHz, Chloroform-*d*) δ 148.29, 134.21, 129.77, 126.35, 122.39, 119.99, 57.63, 48.82, 45.44, 32.21, 26.09



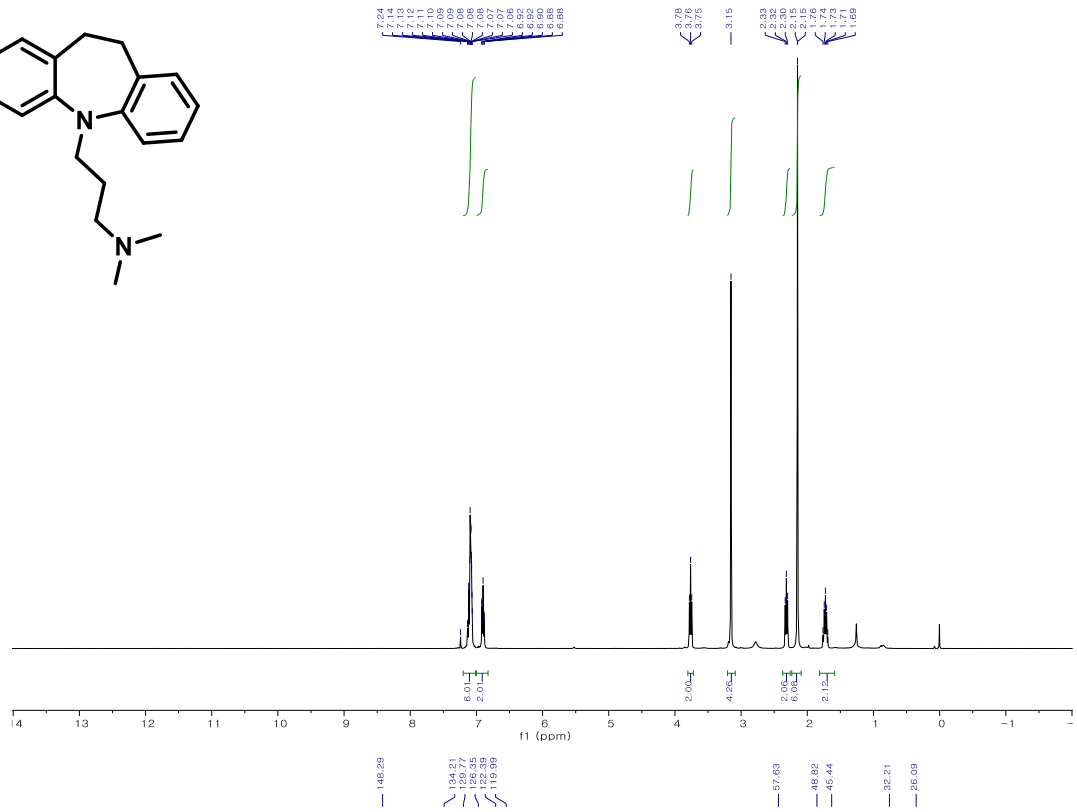


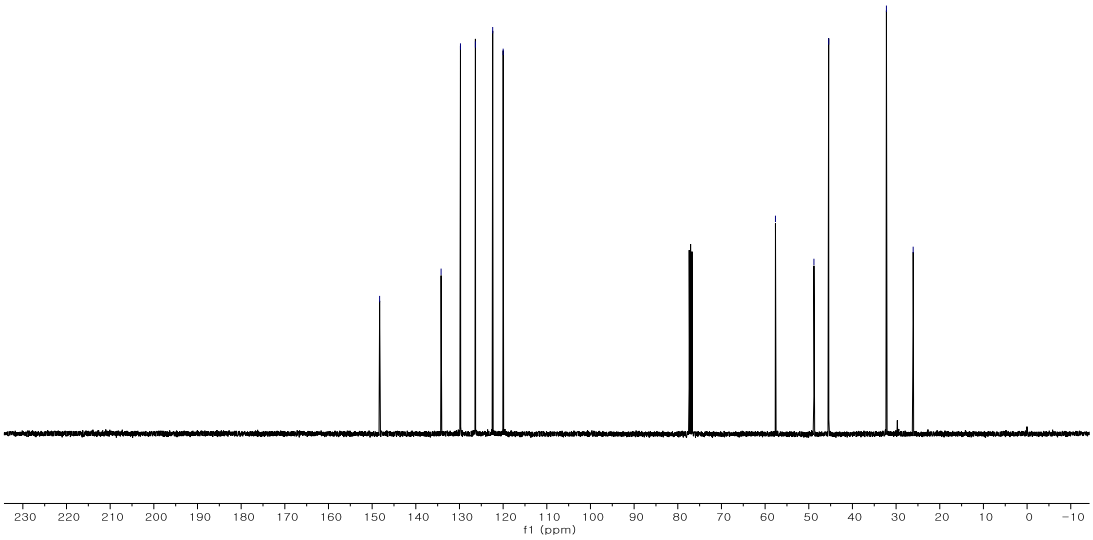

***N*-(Trideuteriomethyl)-aniline[18], 3a**

A yellow liquid. $^{1}$H NMR (400 MHz, Chloroform-*d*) δ 7.19 (t, *J* = 7.9 Hz, 2H), 6.71 (t, *J* = 7.3 Hz, 1H), 6.62 (d, *J* = 8.3 Hz, 2H). $^{13}$C NMR (101 MHz, Chloroform-*d*) δ 149.37, 129.20, 117.22, 112.41, 29.73




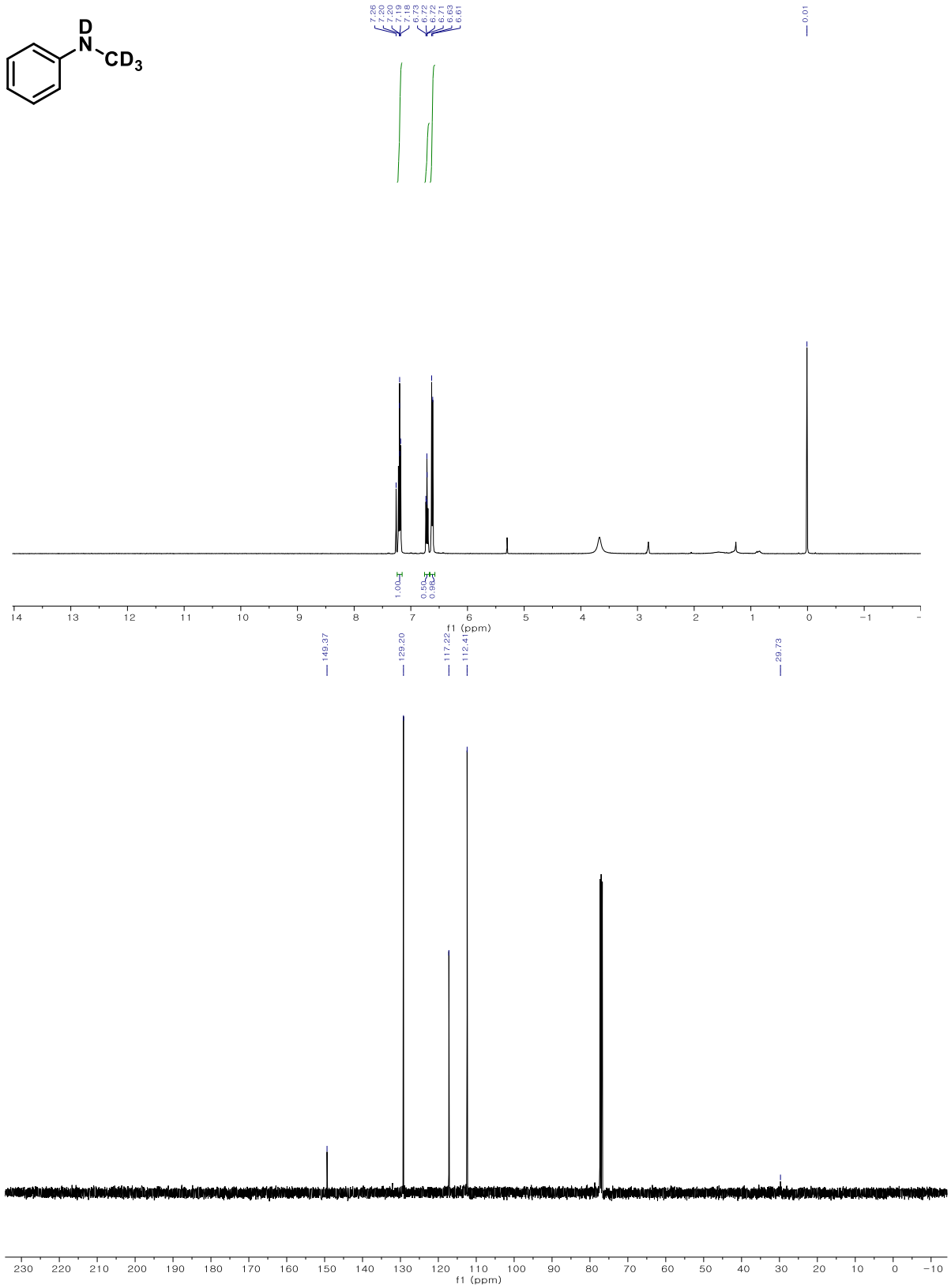

## 9. Reference


1. J. Wang, J. Wu, Z.-N. Chen, D. Wen, J. Chen, Q. Zheng, X. Xu, T. Tu, *J. Catal.,* **2020**, *389*, 337-344.
2. M. A. R. Jamil, A. S. Touchy, M. N. Rashed, K. W. Ting, S. M. A. H. Siddiki, T. Toyao, Z. Maeno and K.-i. Shimizu, *J. Catal.*, **2019**, *371*, 47-56.
3. L. Jiang, F. Guo, Y. Wang, J. Jiang, Y. Duan, Z. Hou, *Asian J. Org. Chem.* **2019**, *8*, 2046-2049.
4. P. Liu, J. Yang, Y. Ai, S. Hao, X. Chen, F. Li, *J. Catal.,* **2021**, *396*, 281-290
5. L. Jiang, X. Zhang, Y. Wang, F. Guo, Z. Hou, *Asian J. Org. Chem.* **2021**, *10*, 2165-2169.
6. G. Kresse, J. Furthmuller, *Phys. Rev. B Condens. Matter* **1996**, *54*, 11169-11186.
7. P. E. Blochl, *Phys. Rev. B Condens. Matter* **1994**, *50*, 17953-17979.
8. B. Hammer, L. B. Hansen, J. K. Nørskov, *Phys. Rev. B Condens. Matter* **1999**, *59*, 7413-7421.
9. P. E. Blochl, O. Jepsen, O. K. Andersen, *Phys. Rev. B Condens. Matter* **1994**, *49*, 16223.
10. (a) V. I. Anisimov, F. Aryasetiawan, A. I. Lichtenstein, *J. Condens. Matter Phys.* **1997**, *9*, 767-808.
    (b) S. L. Dudarev, G. A. Botton, S. Y. Savrasov, C. J. Humphreys, A. P. Sutton, *Phys. Rev. B* **1998**, *57*, 1505-1509.
    (c) M. Alexe, M. Ziese, D. Hesse, P. Esquinazi, K. Yamauchi, T. Fukushima, S. Picozzi, U. Gösele, *Adv. Mater.* **2009**, *21*, 4452-4455.
11. L. W. Finger, R. M. Hazen, A. M. Hofmeister, *Phys.Chem.Miner.,* **1986**, *13*, 215-220.
12. D. Wang, D. Kuang, F. Zhang, C. Yang, X. Zhu, *Adv. Synth. Catal.* **2015**, *357*, 714-718.
13. P. Piehl, R. Amuso, A. Spannenberg, B. Gabriele, H. Neumann, M. Beller, *Catal. Sci. Technol.* **2021**, *11*, 2512-2517.
14. J. Chen, J. Wu, T. Tu, *ACS Sustain. Chem. Eng.* **2017**, *5*, 11744-11751.
15. A. Lator, S. Gaillard, A. Poater, J. L. Renaud, *Org. Lett.* **2018**, *20*, 5985-5990.

16. K. Polidano, B. D. W. Allen, J. M. J. Williams, L. C. Morrill, *ACS Catal.* **2018**, *8*, 6440-6445.
17. K. Natte, H. Neumann, R. V. Jagadeesh, M. Beller, *Nat. Commun.* **2017**, *8*, 1344.
18. P. Liu, N. T. Tung, X. Xu, J. Yang, F. Li, *J .Org. Chem.,* **2021**, *86*, 2621-2631.